AALTO UNIVERSITY
School of Engineering
Department of Mechanical Engineering

Godwin Osezuwa Oamen

Uncertainties in simulation model for ice loads prediction in level ice with respect to structural reliability

Master's Thesis

Espoo, 07.01.2019

Supervisor: Prof. Pentti Kujala (Aalto University)
Advisers: Floris Goerlandt, D.Sc. (Aalto University)
Fang Li, M.Sc. (Aalto University)

Author Godwin Osezuwa Oamen

Title of thesis	Uncertainties in simulation model for ice load prediction in level ice with respect to structural reliability
Degree of programme	Mechanical Engineering
Major/minor	Marine Technology
Thesis supervisor:	Pentti Kujala, D.Sc.
Thesis advisers:	Floris Goerlandt, D.Sc. Fang Li, M.Sc

Date 30.07.2018 **Number of pages** 100 + 2 **Language** English

Abstract

Arctic shipping is increasingly in focus due to the diminishing ice cover due to the effects of climate change. With new shipping routes opening up, navigation in ice-covered waters receives increasing attention in industry and academia. One of the key issues in the design of ice-going vessels is the required plate thickness to withstand the ice loads. Several regulations have been developed, containing formulae for determining the place thickness for different ice classes. On the other hand, various engineering tools have been developed for simulating the ship performance in ice, with several of these tools explicitly aiming to determine the ice loads on the hull. Such tools in principle provide alternative means to determine the safety level of the hull elements based on first-principle modeling.

In this report, a risk-based design approach is taken as a starting point for contextualizing the determination of the required plate thickness based on a structural reliability analysis. The focus of the work is to analyze the importance of the uncertainties in the ice loads resulting from a ship performance in ice simulation model, in relation to the structural reliability as calculated based on the simulated ice load time series. The study centered on the influence of the applied empirical parameters in the model design on the predicted ice loads with respect to the long-term safety and reliability analysis of the ship. The various assumptions in the simulation model for ship performance in ice are systematically varied to quantify the uncertainty about the safety index and failure probability of a plate under ice loading.

The results showed that the predicted loads from the simulation model lead to some about of uncertainties across the investigated parameters, indicating the limited usefulness of the simulation model in a risk-based design context. The estimated uncertainties were however based on the relative variations of the simulated ice loads and the estimated safety index corresponding to each case studied. With these results, the suspicion for inherent uncertainties in the ice prediction model's performance associated with the applied parameters was justified. Hence, to obtain better or improved performance from the ice prediction model, the sources of uncertainties should be minimized or eliminated. Also, with the ultimate aim of developing models and tools for risk-based design of ships in Arctic and other ice-covered waters, areas of further research and development in context of the ship performance in ice simulation model are highlighted to reduce the uncertainties.

Keywords. Uncertainty, Structural reliability, Ice loads, Ship performance in ice, Risk-based ship design, Arctic

Acknowledgments

This project has received funding from the European Research Council (ERC) under the European Union's Horizon 2020 research and innovation programme (grant agreement n° 723526). Their financial support is deeply appreciated in the execution of this thesis. My profound gratitude to my supervisor in the person of Professor Pentti Kujala for the confidence showed in me and the consistent supports provided throughout the duration of this thesis. Also, with a heartfelt appreciation, I will like to specially thank my advisor in the person of D.Sc. Floris Goerlandt for initiating the topic and providing the required technical support and necessary guidance throughout the project. You will be missed by the Aalto family.

Furthermore, a huge appreciation goes to Fang Li, who provided the necessary code required for the commencement of the project as well as the technical support that aided the full utilization of the codes. More appreciation goes to Mihkel Kõrgesaar for his contributions across the entire project in terms of technical supports and provision of necessary materials. Finally, great appreciation to everyone who rendered supports in various capacity that lead to the successful completion of the thesis.

Table of Contents

List of figures

List of tables

1 Introduction

1.1 Background

Icebreaking is one of the frequent activities in the Arctic and Antarctica due to the all year appearance of ice which often impedes maritime activities in these regions. As such, the breaking of ice is of high maritime concern due to the need to maintain and enhance navigation in ice-infested water ways by commercial and industrial vessels in these regions and to ensure the continuous and smooth operations of oil and gas exploration and other related activities (Kujala, 2008). In addition, the continuous growing rate of research activities in these regions have necessitated the need for the continuous ice breaking operations in the Polar Regions. In respect of this, icebreakers are often used as escort convoys for one or more ships in order to ensure safe navigation and to support research and offshore related activities.

At the moment, extreme conditions and consequences such as loss of life, properties and environmental damages as well as severe structural damages on ship hull that often result from unexpected circumstances have been significantly minimized. This was achieved through the development of sophisticated navigation control systems such as the winter navigation system, traffic restriction systems and reasonable ice class rules (Kujala, 2008). Also, with the help of icebreakers, minimum damages are inflicted on ship hulls since the ice are broken and cleared before ship passage. But the hull damages resulting from the hull-ice interaction during ice breaking process remains a topic of interest because the consequence of the continuous ice-hull interaction is expected to have a long-term impact on the overall performance of the merchant vessel.

Many approaches have been employed to evaluate the long term impart of the gradual damage impose on the hull platen and frames of a typical icebreaker. A conventional approach applied in ice-hull interaction analysis are majorly experimental. However, drawbacks such as the limited insight into ice-hull interaction process, the nature of the ice loads and the cost intensiveness of the approach, alternative approaches such as the numerical and semi-empirical simulation have been developed (Lindqvist, 1989). Although experimental approaches have in time generated sufficient data for analysis but the limitation in understanding the interaction domain involving the ice loads dependencies (crushing, bending, submersion etc.) have not been sufficiently comprehended through the experimental approach. Also, the limitation in the repeatability of the experiment processes and available experimental data have made numerical modeling a more viable option. Based on this, since the advent of numerical and semi empirical approach, great insights into the ice-ship interaction and better analysis have since been achieved.

The numerical approach utilizes mathematical equations to model an ice-hull interaction in order to predict the induced ice loads and corresponding parameters. However, due to the complexity in the ice-ship interaction process, empirical parameters are often used to represent grey areas of the applied theory. A most recent example is the approach by Su. et. al. (2010) which was in line with the principles in (Wang , 2001). According to the Su's model, a number of empirical parameters have been utilized in formulating some aspects of the model such as the cusp size, the bending failure and the relative velocity of the interaction. In order to assign appropriate values for such empirical parameters, a number of studies have been carried out. However, the results from the investigations proved to vary and as such no specific values have been assigned for the empirical parameters, but a range of values were proposed.

For instance, Enkvist (1972) presented a range of values for the cusp size for different approaches (see Table 5.1) and based on these, Kuuliala (2015) in his thesis, carried out a sensitivity analysis on the empirical parameters to determine the appropriate range of values for them. Futhermore, in

other early work, Kastelyan proposed a value of 3.0 for the empirical parameter associated with the failure load, while Nguyen et al. (2009) applied a value of 4.5 with no justification (Nguyen, 2009). Also, a value of 2.2 was adopted by Quan et al. for same parameter based on series of sensitivity analysis made on some selected range values (Quan, et al., 2015). However, no two studies seem to provide a standard value for the empirical parameters, hence, given rise to suspected uncertainties associated with the choice of empirical values (Su, et al., 2010).

However, in an effort to minimize the sources of uncertainties and to propose a robust model, the model by Su et al. (2010) was investigated by Li et al. (2018). The Su's model which is an extension of the ice-structure model previously designed by Wang (2001) to predict ice loads on a conical structure, was extended to predict induced ice loads on an ice going vessel in a level ice field (Su, 2010) as well as under a random ice condition (Su, et al., 2014). However, due to the perceived uncertainties characterizing the model, efforts were made to modify certain branches of the model for better ice load prediction. Some of the modifications include; modification of the bearing capacity according to that proposed in (Tan, et al., 2014), introduction of the non-linear pressure-area relationship within the contact area and introduction of the random floe radius size to that proposed in Su et al. (2014) and Zhou et al. (2016).

However, since the model was still characterized with certain empirical parameters, it was necessary to extend its application to other related areas of interest within the marine technology sphere, for instance; the long-term reliability analysis of the ship hull, in order to ascertain the performance of the model. This direction of analysis was informed by the fact that the long-term reliability and safety of the ship hull is to a great extent, very important in the risk-based design. The idea is to quantify the reliability of the ship hull in terms of the safety index estimated from the induced ice loads and based on this, an uncertainty analysis will be carried out to quantify how much the estimated safety index of the model deviates from those of the full-scale data.

1.2 Aim of study

The partly improved version of the numerical and semi empirical ice load prediction model (Su, et al., 2010) as updated by Li, et al. (2018) has been applied in this thesis to investigate the uncertainties associated with the choice of empirical parameters characterizing the model with respect to reliability index using the S.A. Agulhas II ship hull model as a case study. Although, some studies suggest uncertainties may be important for transit modeling (ship performance), but the importance of the uncertainties in a ship design (risk-based) context are not well understood. Hence, the aim of the study is to investigate how much the choice of the empirical parameters' values influence the model predictions' by quantifying the uncertainties in the estimated safety index over the selected values.

In this study, an intensive analysis has been carried out to investigate the influence of the choice of empirical parameters with respect to the long-term reliability and safety of the S. A. Agulhas II ship hull. The idea is to investigate to what extent the empirical parameters influence the estimation of the ship hull reliability and safety using statistical approach. Also, considering the effect of the random nature of the ice condition, additional study was made to investigate uncertainties in the modelled ice field using the same approach. Finally, since the ship hull has been modelled and included in the simulation, uncertainties arising from the applied permanent deflection was carried out on the hull (Kujala, 2008). The result obtained were compared with corresponding results obtained from a full-scale experiment data.

The study presented in this report was discussed under eight chapters:

- Chapter one contains the introduction to the topic where a detailed background on the essence of the study has been established. In this chapter, the aim of the study as well as the applied approach were discussed. Also, the properties of the applied model in terms of its empirical characteristics were discussed.
- In chapter two, the fundamental principles employed by Wang and Su are described in detail. For each of the approach, the idealizations employed to model the ice-hull interaction, floe size and the force-motion relationship were clearly discussed.
- Chapter three presents the general principle of reliability and uncertainty analysis as applicable to the area of focus of this thesis. The necessary steps required for the estimation of the safety index and the corresponding failure probabilities were highlighted. Also, the approach employed in estimating the uncertainty characterizing the model was discussed.
- In chapter four, the reliability analysis for the full-scale data necessary for the validation of the model safety index estimation was presented.
- In chapter five, the process of selection of values for empirical parameters was presented. For all the empirical parameters, the basis for the selections were justified accordingly.
- Chapter six contains the reliability analysis of the ship model using the acquired ice load data from the simulation model. For each of the parameter and their respective values, corresponding reliability index and failure probabilities were estimated. The resulting reliability indices were analyzed against the typical values obtained from the literatures. Based on the analysis, comments on perceived uncertainties were provided.
- In chapter seven, a quantitative analysis of the uncertainty characterizing the model with respect to the estimated safety index, as provided in chapter seven, was presented and discussed. The uncertainties were quantified using a factor called coefficient of variation (COV). Also, the estimated uncertainties were discussed in terms of their variations across the studied cases.
- Finally, chapter eight contains the conclusion and recommendation.

2 Modeling of ice-ship Interaction

The capabilities of the ice-ship interaction modelled and proposed by Wang (2001) for a static conical structure was extended in predicting ice load for a continuous icebreaking model (Su, et al., 2010). In the original model by Wang, the interaction between a moving ice and a static conical structure was numerically idealized while in the later model by Su, et al. (2010), the induced ice loads resulting from an ice-ship interaction in a continuous ice breaking mode are predicted. In this section, the description of the Wang's model and Su's model are presented.

2.1 Wang's Model

The model was based on a stationary structure with an inclined surface (or conical) in a moving and level ice field. The stages of the modeling comprise of contact, crushing and bending. With regards to the vertical structures where the dominating failure mode is crushing, in an inclined structure as described here, the major failure mode is bending because the ice sheet rides up the structure surface and the failure occurs when the vertical force becomes equal or higher than the bearing failure capacity of the ice sheet. However, the failure mode depends on certain factors such as indentation velocity, temperature, ice thickness, width and inclination of structure (Timco 1986 & Sodhi 1988).

In order to fully comprehend the Wang's model for ice load prediction, it was important to understand the following concepts:

- Ice floe geometry
- The ice sheet driving forces
- The breaking pattern
- Force components of the structure

2.1.1 Ice floe geometry

The size of the ice floe resulting from the ice-structure interaction was first investigated by Enkvist (1972) and Varsta (1983). In these studies, it was established that the size of the ice floe was speed-dependent i.e. the higher the speed the smaller the ice floe. However, no significant explanation was provided regarding the geometry of the ice floe. As such, in an effort to describe the ice floe geometry, Wang idealized the ice floe geometry as part of a circle an assumption that was based on on-site visual observation. The idealized ice floe geometry was described with a single parameter called ice floe radius R and these was justified based on three major reasons:

1. During the ice-ship interaction, ice sheet is broken when the maximum bending stress exceeds the tensile strength of the ice sheet. Observations from full-scale and laboratory model proved that the ice floe assumes the shape of a sector.
2. The ship-ice interaction can also be idealized for an ice-cone interaction. The major differences are in the direction for which the ice floe breaks (up or down), the pattern of rubble accumulation and the effect of buoyancy.
3. The idealization of the ice floe as a sector of a circle provides the possibility of also idealizing the circumferential cracks and this further simplifies the process.

As mentioned above, the ice floe radius is considered linearly dependent on two major parameters (Equation 2.1):

- The relative velocity V, and
- The characteristic length l

$$R = C_l l(1 + C_v V) \tag{2. 1}$$

where

$$l = \left(\frac{E h_i^3}{12(1 - v^2)\rho g}\right)^{\frac{1}{4}} \tag{2. 2}$$

and E is the Young's modulus of ice, v Poison's ratio of ice, and ρ the density of water. The typical values for the constant parameters are $E = 5.40\ Gpa$, $v = 0.33\ and\ \rho$ =1010kg/m^3 $(g = 9.81 m/s^2)$. Also, the parameters $C_v\ and\ C_l$ are semi-empirical constants for which C_v value influences the velocity while C_l value influences the characteristic length of the ice floe. Based on experimental analysis, the values of C_v have always taken the negative signs while those of C_l are always positive.

2.1.2 Idealization of the force components

The driving forces are the conventional forces, comprising of wave force, current force, Coriolis force and thermal expansion force. However, due to the complexity in the simulation of these forces, a constant velocity V with which the ice sheet moves against the structure is assumed for the driving forces. In addition, it is assumed that there are sufficient forces enough to cause the failure of the idealized ice sheet.

2.1.3 The breaking pattern

Based on experimental observations during an ice-structure interaction, ice breaking was idealized as a discrete process in which new surfaces or boundary emerge after a bending failure. In order to model the ice breaking process, it was established by Wang that ice breaking only occur when there is a contact between the ice and the structure, and for each contact only one piece of ice is broken. Although, there could be several contact points, but they are treated as discrete points as each generates new edges.

In order to establish whether a contact occurs between the ice edge and the ship water line, two functions describing the ice edge and the ship waterline are defined respectively (Figure 2.1). The ice sheet edge is defined by $f_e(x)$ while the waterline is defined by $f_w(x)$. As the ice sheet approaches the structure, there are possibility of many contact points but to determine which of the ice edge will make a contact, a distance function D_{ew} is established as

$$D_{ew}(x) = f_e(x) - f_w(x) \tag{2. 3}$$

The contact point can then be determined as the value x_c which satisfies:

$$Min[D_{ew}(x)] = D_{ew}(x_c) \tag{2. 4}$$

After a bending failure has occurred, circular arcs are formed which helps to minimize the number of contact points to be checked thereby reducing the simulation time as well. Another condition for determining the contact points is that in the case where multiple but closed contact points are detected, it is assumed that those points are contained within a single broken ice floe. However, if there are various contact points with significantly large distances between the points, the total force for the duration of interaction is calculated as the sum total of the forces associated with the

individual contacts. The ice force is calculated using the two intersection points between the ice edge and the ice floe. Also, the ice floe radius is determined using the Equations (2.1 - 2.2).

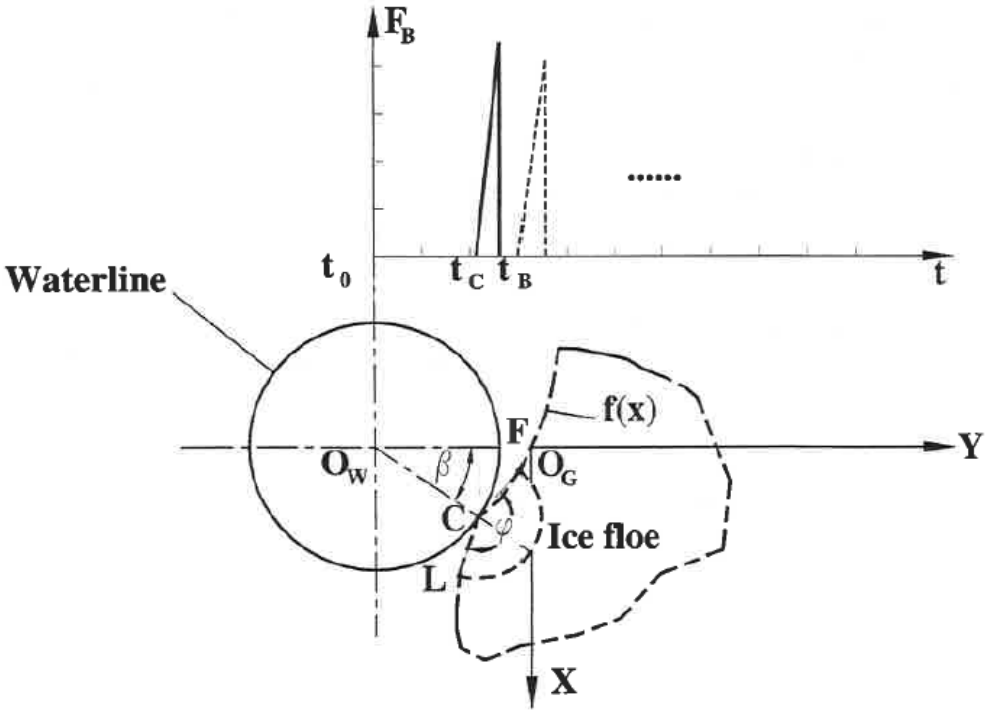

Figure 2. 1 Typical contact (Wang, 2001)

2.1.4 Force components of the structure

As mentioned earlier, there are two major stages involved in the ice breaking process; crushing and bending.

(a) Crushing

Ice crushing precedes the initial ice-ship contact. The crushing process continues until the minimum bending force P_f sufficient to cause an ice floe break up is reached. To calculate the time history of the crushing process, the time period in which the crushing took place is calculated based on two approaches:

1. Only the lower corner of the ice is crushed
2. The area required to generate the bending force is so large that the contact area reaches the top surface of the ice sheet.

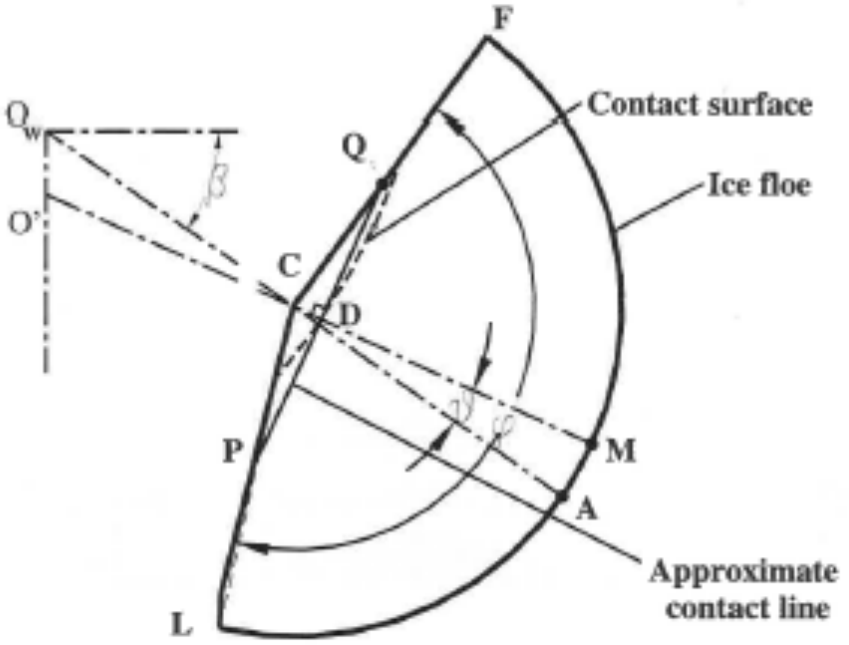

Figure 2. 2 Contact geometry (top view)

Trapezoidal contact 1

In this approach, the bending failure is assumed to occur at a height h_{ic} lower than the ice thickness h_i. Figure 2.2 describes the contact situation in the first approach. As the ice moves against the structure, the initial point contact changes into an area contact. The area established here lies at the lower corner of the ice under crushing. Figures 2.1 and 2.2 shows the front and side views of the ice-structure contact.

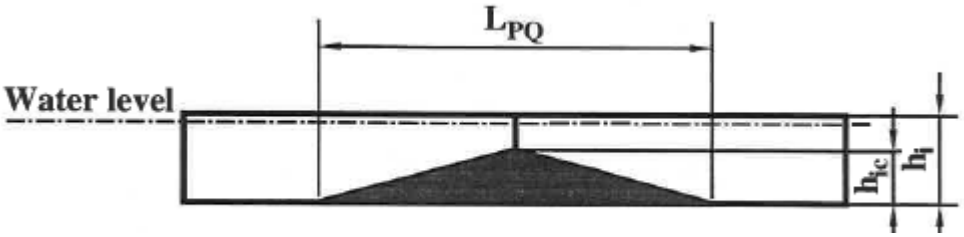

Figure 2. 3 Geometry of the contact (front view) (Wang, 2001)

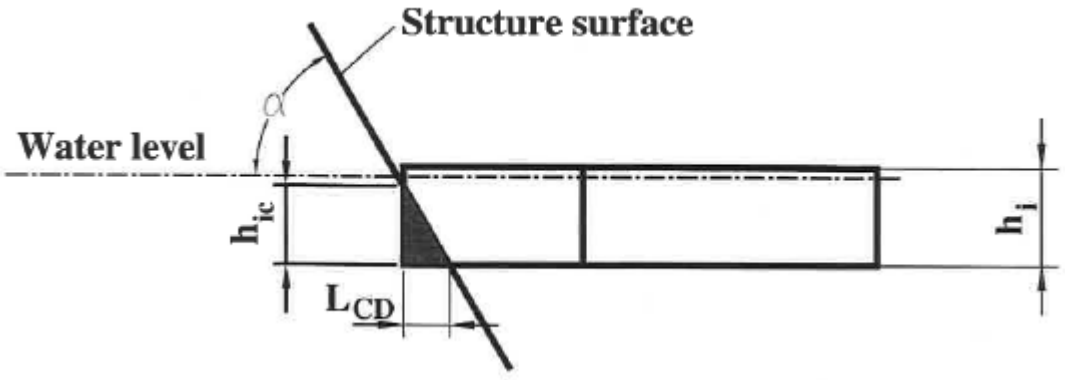

Figure 2. 4 Geometry of the contact along the centerline (side view) (Wang, 2001)

From the above geometries (Figures (2.2 – 2.4)), if the contact area is A_c and the contact pressure P_c then the force P_f required to cause bending failure will be

$$P_f = P_c A_c \tag{2. 5}$$

where

$$A_c = \frac{h_{ic}^2 \tan\frac{\varphi}{2}}{\sin\alpha \tan\alpha} \tag{2. 6}$$

$$h_{ic} = \tan\alpha \sqrt{\frac{C_F P_f}{\sigma_c \tan\frac{\varphi}{2}}} \tag{2. 7}$$

and C_F is a function of the structure inclination angle α and the coefficient of friction μ as defined in Equation 2.8.

$$C_F = \frac{1}{\cos\alpha - \mu \sin\alpha} \tag{2. 8}$$

Trapezoidal contact 2

The second approach to calculating the crushing force is depicted in Figures 2.9, 2.10 and 2.11. Here, the minimum bending force required to create a bending force is attained at a height h_{ic} equal to the ice thickness h_i. There is a change in the contact geometry compared to the first approach. The contact geometry transforms from a triangle to a truncated triangle or trapezium (Figure 2.10).

The crushing process in this case is divided into two stages (Figure 2.9):

- Crushing of the tip of the ice floe
- Widening of the contact width

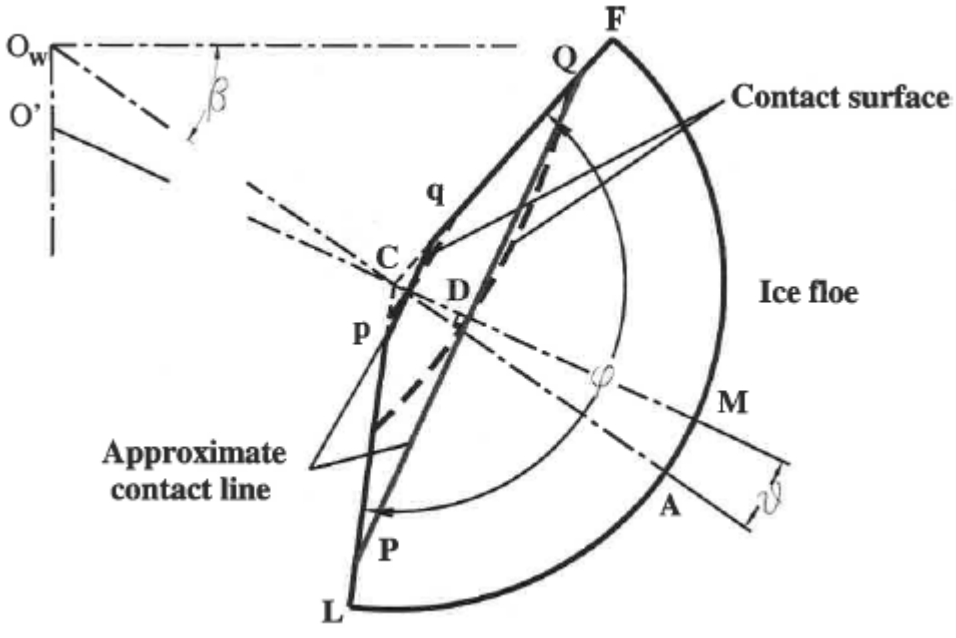

Figure 2. 5 Geometry of the contact, approach 2 (Wang, 2001)

The second stage indicates that the crushing area equivalent to the ice thickness is not sufficient enough to cause a bending failure as such further crushing in the direction normal to the contact surface is required. The consequence of this is that the bottom and top horizontal contact lines gets wider thereby increasing the contact area as well as the nominal pressure.

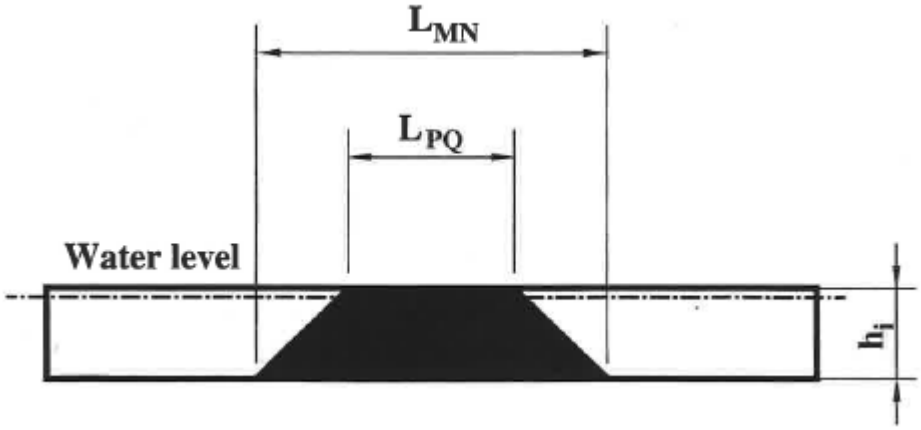

Figure 2. 6 Geometry of the contact (front view), approach 2 (Wang, 2001)

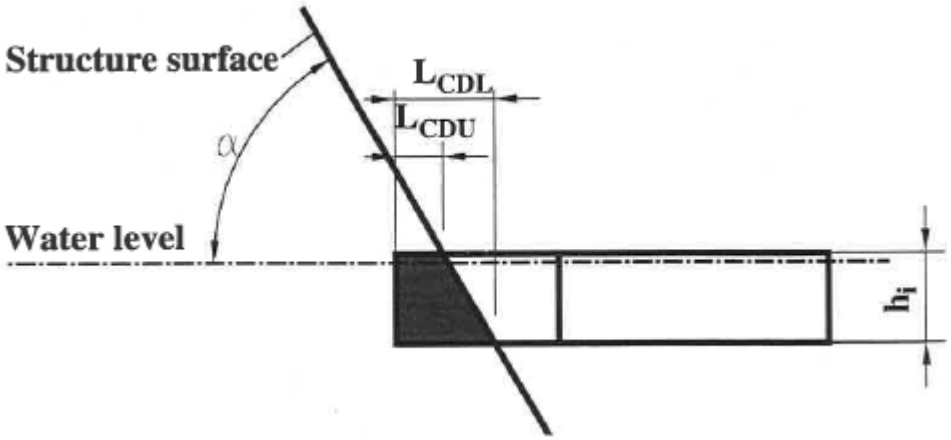

Figure 2. 7 Geometry of the contact (side view), approach 2 (Wang, 2001)

Although the same equation for the crushing force holds here but there are modifications for the contact area, and the length of bottom and top horizontal lines L_{PQ} and L_{MN} respectively as shown in Figure 2.6.

The resulting contact area is given as:

$$A_c = h_i \left[2L_{CDU} + \frac{h_i}{\tan \alpha} \right] \tan \frac{\varphi}{2} \qquad (2.\ 9)$$

The expressions for the L_{CDL} and L_{CDU} are given in Wang (2001).

(b) Bending

The global time of the bending failure is sum of the local crushing time period and the time of instant contact. Given the crushing time period as T_{cl} and the time of instant contact as t_C, then the global time of the bending failure will be

$$t_B = t_C + T_{cl} \tag{2. 10}$$

where

$$T_{cl} = \frac{L_{CC'Y-Y}}{V} \tag{2. 11}$$

In the above analysis by Wang, several assumptions where made in order to simplify the process but the major once are:

1. Neglect of friction. The influence of friction was balanced with the uncertainties in the contact pressure by assuming that lower pressure has the same effect. However, if friction was considered, there would have been a slight change in the direction of the resulted force.

Flat surface assumption. The structure was assumed a flat surface in order to eliminate the uncertainties associated with other assumptions.

2.2 Su's approach

In the previous model by Wang, a moving ice field against a stationary conical structure was considered. The analysis was however limited to a straight-line relative motion. To therefore extend the capabilities of the Wang's model, Su applied the principles as provided in Wang (2001) to predict ice loads resulting from the ice-ship interaction both for a straight movement and under a turning maneuverability condition (Su, et al., 2010).

In this approach, the following methodology and assumptions were used:

1) The ship was represented with a full-size waterline and the ice edge with set of wedges, both discretized with nodes.
2) The sway, surge and yaw motions are considered and assumed to act along the ship waterline
3) The contact zones, around the hull, the resulting forces and the breaking patterns are numerically determined based on the empirical estimates of the crushing force and ice breaking failure.
4) The ice forces induced (submersion and friction components) after the ice edge is broken are accounted for using the Lindqvist's ice resistance formula (Lindqvist, 1989).
5) The hydrodynamic effects (drag and added water) are predetermined numerically before the commencement of simulation in ice i.e. decoupling hydrodynamic and ice forces.
6) Other forces such as wave, wind and current forces were neglected as their effects were assumed to be minor.
7) The applied rigid body equations of motion are also numerically solved.
8) The balance between the motion and the contact forces is achieved through series of iterations.

2.2.1 Numerical model

In this approach, Su modeled the ice-hull interaction and the breaking process by applying the Newton's second law of motion. The model coupled the continuous ice forces and resulting ship motion using three degree-of-freedom equations for rigid body i.e. heave, sway and surge motions respectively. The applied equations were numerically solved to detect the icebreaking forces after the ice floe has been broken from the ice sheet.

The major aspects of the numerical model by Su are:

- Geometrical model for ice-hull interaction
- Ice crushing force
- Ice bending failure
- Submersion and friction forces
- Ship's motion
- Interdependence between the ship's motion and the ice loads

(a) Geometrical model for ice-hull interaction

The geometrical model for the ice-hull interaction is idealized such that a full-size waterline represents the ship hull while the ice edge is represented with a wedge (Figure 2.8). To simulate the interactions between the ice edge and the ship waterline, the ship waterline in discretized into a closed polygon while the ice edge is discretized into a polyline. Contacts are established when some ice nodes are inside the hull polygon based on some predetermined conditions.

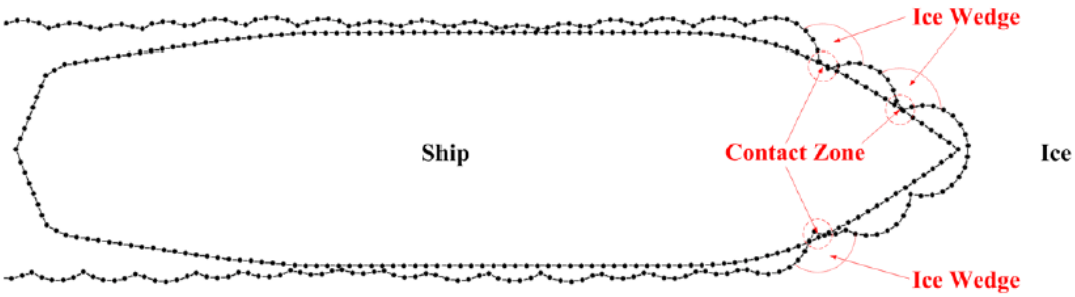

Figure 2. 8 Geometrical idealization of ice-hull interaction (Su, et al., 2010)

For simplicity purpose, the contact surface between the ice and the hull were assumed flat (Figures (2.9 - 2.10)). Similar to the Wang's approach, two cases were considered to calculate the contact area:

$$A_c = \begin{cases} \frac{1}{2} L_h \frac{L_d}{\cos\varphi}, & L_d \cdot tan\varphi \le h_i \\ \frac{1}{2}\left(L_h + L_h \frac{L_d - h_i/tan\varphi}{L_d}\right)\frac{h_i}{\sin\varphi}, & L_d \cdot tan\varphi > h_i \end{cases} \qquad (2.\ 12)$$

where h_i = ice thickness
φ = hull zone slope angle
L_h = contact length
L_d = Indentation depth

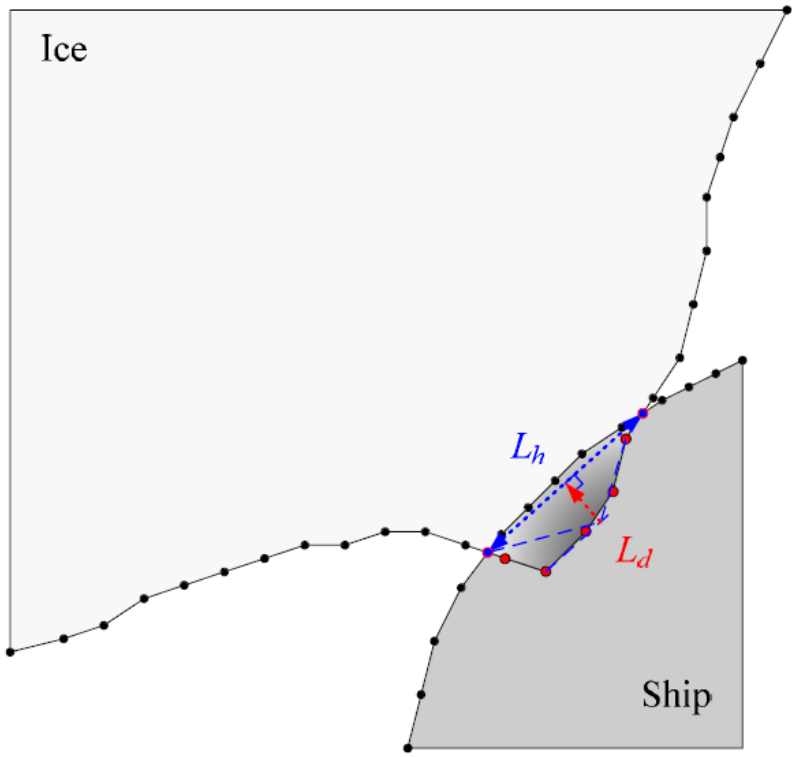

Figure 2. 9 contact length (L_h) and the indentation depth (L_d) at each contact zone (Su, et al., 2010)

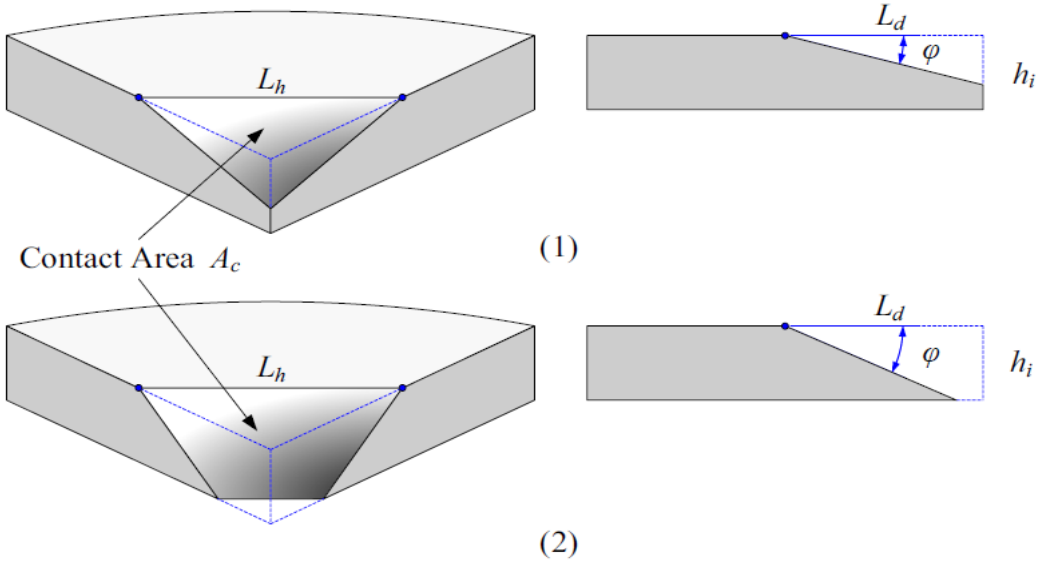

Figure 2. 10 Two cases of contact area (Su, et al., 2010)

(b) Ice crushing force

As shown in Figure 3.11, the crushing force F_{cr} is a product of the ice crushing strength σ_c and the contact area A_c (Eq. (2.13)).

$$F_{cr} = \sigma_c \cdot A_c \qquad (2.\ 13)$$

The effective ice crushing strength σ_c is realized from the measured crushing pressure on ship hull (Kujala, 1994). The frictional force components (horizontal component, f_H and vertical component f_v) resulting from the ice-hull interaction are given as (Figure 2.14 – 2.15):

$$f_H = \mu_i \cdot F_{cr} \cdot {v^{rel}}_t / \sqrt{(v_t^{rel})^2 + ({v^{rel}}_{n,1})^2} \qquad (2.\ 14)$$

$$f_v = \mu_i \cdot F_{cr} \cdot {v^{rel}}_{n,1} / \sqrt{(v_t^{rel})^2 + ({v^{rel}}_{n,1})^2} \qquad (2.\ 15)$$

where

μ_i = friction coefficient
v^{rel} = relative velocity between the ice and ship

Hence the horizontal and vertical components, F_H and F_v of the total contact force are calculated as (Figure 2.16 – 2.17):

$$F_H = F_{cr} \cdot \sin\varphi + f_H \cdot \cos\varphi \qquad (2.\ 16)$$

$$F_V = F_{cr} \cdot \cos\varphi - f_v \cdot \sin\varphi \qquad (2.\ 17)$$

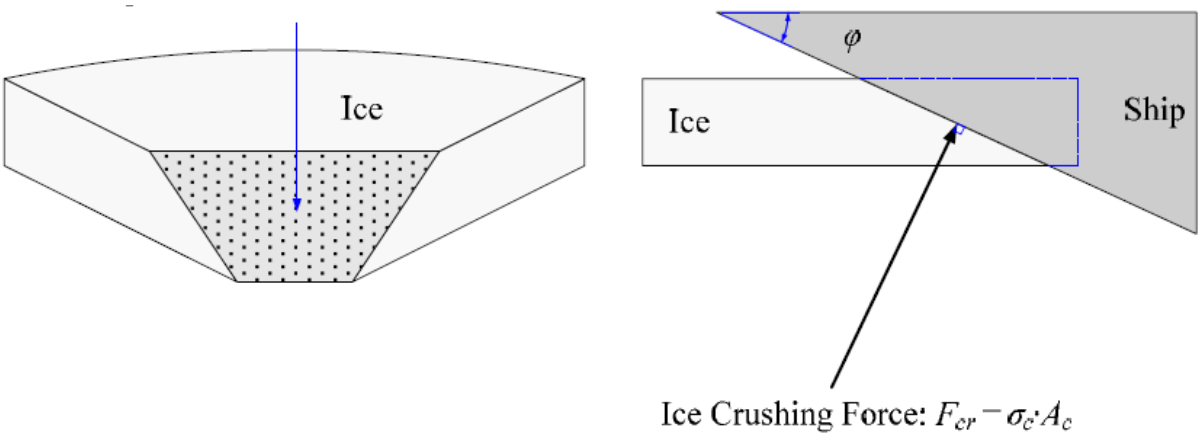

Figure 2. 11 Evaluation of the ice crushing force (Su, et al., 2010)

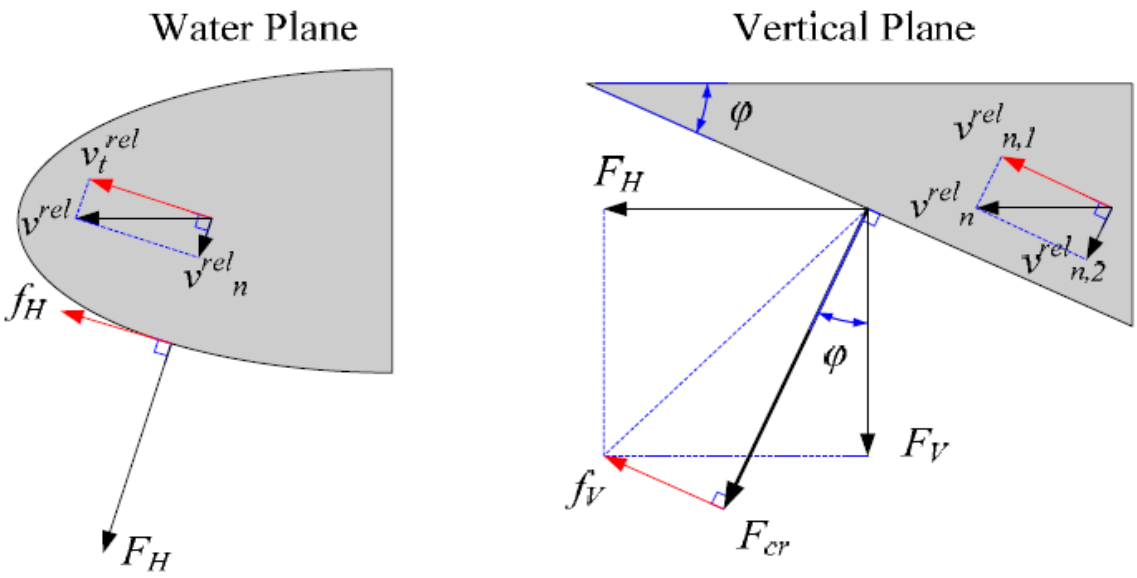

Figure 2. 12 Force and velocity components (Su, et al., 2010)

(c) Ice bending failure

Bending failure occurs when the vertical component of the total contact force F_V (Eq. (2.17)) exceeds the bending failure load, P_f of the ice cover. According to Kashtelyan (Kerr, 1975), the bending failure load P_f is calculated for a circular arc as:

$$P_f = C_f \left(\frac{\theta}{\pi}\right)^2 \sigma_f h_i^2 \qquad (2.18)$$

where

θ = opening angle of the ice wedge
σ_f = flexural strength of the ice
C_f = empirical parameter determined from measurements

The above bending failure equation is based on static failure criterion which according to (Tan, et al., 2014) was not proper as speed clearly influences the load. As such a formulation for the dependency of ice bending failure on loading rate was proposed (Equation 2.19)

$$P_f = (1.65 + 2.47 v_{rel}^{0.4}) \left(\frac{\theta}{\pi}\right)^2 \sigma_f h_i^2 \qquad (2.19)$$

Where v_{rel} = relative velocity

In addition, the bending crack is also determined by interpolating the icebreaking radii R (Equation 2.19) at the first and last contact nodes (i.e. R_f and R_l). Similar to Wang's, the icebreaking radius R is given as:

$$R = C_l \cdot l \cdot (1 + C_v \cdot v^{rel}{}_{n,2}) \qquad (2.\ 20)$$

From Equation 2.19, the empirical parameters C_l and C_v were obtained from measurements as against the Wang's approach in which the same parameters were a function of the inclination angles around the hull zone.

(d) Ship's motion

By applying Newton's law, the three degrees of freedom equation of motion is given as:

$$\begin{aligned} m \cdot \dot{u}_g &= FX_g \\ m \cdot \dot{v}_g &= FY_g \\ I_z \cdot \dot{r} &= N \end{aligned} \qquad (2.21)$$

where

$FX_g =$ forces in the surge directions
$FY_g =$ forces in the sway directions
$N =$ yaw moment
$I_z =$ moment of inertia
$u_g, v_g \ and \ r$ = velocities in surge, sway and yaw respectively.

The forces and velocities are translated into the same coordinates (X_g, Y_g) as given in Equation 2.21 (See Figure 2.13).

$$\begin{aligned} FX_g &= FX \cdot \cos\psi - FY \cdot \sin\psi \\ FY_g &= FX \cdot \sin\psi + FY \cdot \cos\psi \end{aligned} \qquad (2.\ 22)$$

$$\begin{aligned} u_g &= u \cdot \cos\psi - v \cdot \sin\psi \\ v_g &= u \cdot \sin\psi + v \cdot \cos\psi \end{aligned} \qquad (2.\ 23)$$

To obtain the corresponding accelerations, we differentiate Equation 2.22, which results into:

$$\begin{aligned} m \cdot \dot{u} &= FX + m \cdot v \cdot r \\ m.\dot{v} &= FY - m \cdot u.r \\ I_z \cdot \dot{r} &= N \end{aligned} \qquad (2.\ 24)$$

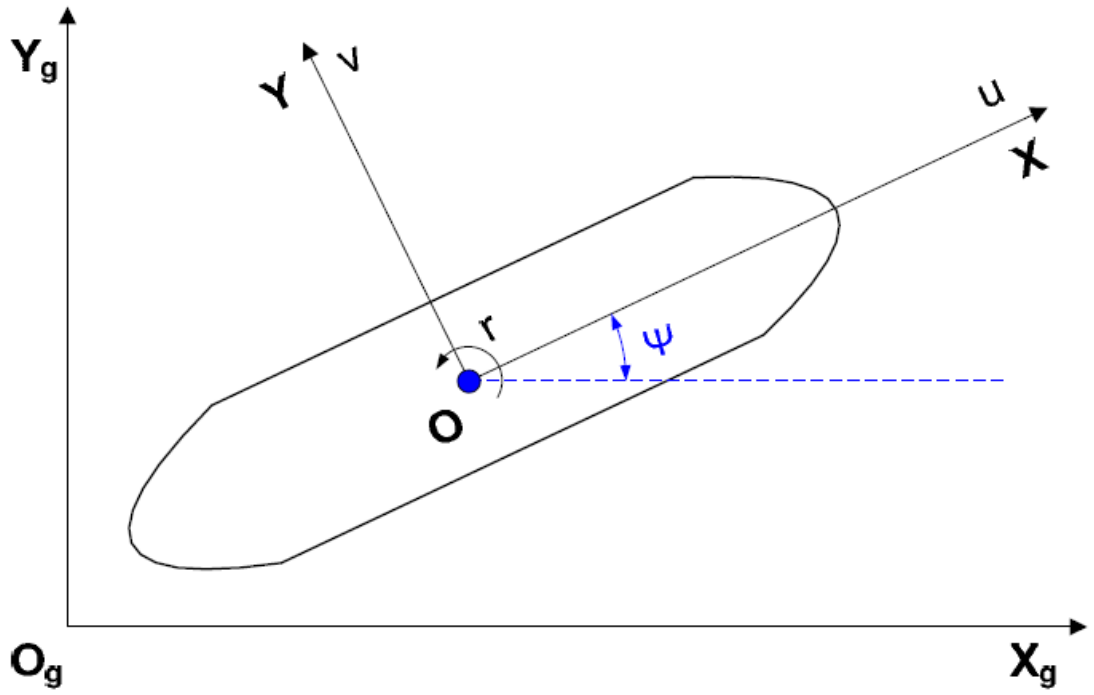

Figure 2. 13 Coordinate system for the ship motion (Su, 2011)

According to Newton's law as applied here, the general equation coupling the forces and moment terms is given as

$$(\mathbf{M}+\mathbf{A})\cdot\ddot{\mathbf{X}}(\mathrm{t})+\mathbf{B}\cdot\dot{\mathbf{X}}(\mathrm{t})+\mathbf{C}\cdot\mathbf{X}(\mathrm{t})=\mathbf{F}(\mathrm{t}) \qquad (2.\ 25)$$

Here, the added mass is determined based on the boundary element method while the damping and restoring terms are assumed zero values in the simulation. The force contributions from ice (i), propeller (p), rudder (r) and open water (ow) are decomposed in the directions of the surge (1), sway (2) and yaw (6) respectively:

$$\begin{aligned} F_1 &= F_1^i + F_1^p + F_1^r + F_1^{ow} + m\cdot v\cdot r \\ F_2 &= F_2^i + F_2^p + F_2^r + F_2^{ow} - m\cdot v\cdot r \\ F_6 &= F_6^i + F_6^p + F_6^r + F_6^{ow} \end{aligned} \qquad (2.\ 26)$$

The above equations are then solved using the step-by-step numerical integration method based on Newmark's approach:

$$\begin{aligned} \dot{\mathbf{X}}(t_{k+1}) &= \dot{\mathbf{X}}(t_k) + (1-\lambda)\cdot\ddot{\mathbf{X}}(t_k)\cdot\Delta t + \boldsymbol{\lambda}\cdot\ddot{\mathbf{X}}(t_{k+1})\cdot\Delta t \\ \mathbf{X}(t_{k+1}) &= \mathbf{X}(t_k) + \dot{\mathbf{X}}(t_k)\cdot\Delta t + \left(\frac{1}{2}-\beta\right)\cdot\ddot{\mathbf{X}}(t_k)\cdot\Delta t^2 + \beta\cdot\ddot{\mathbf{X}}(t_{k+1})\cdot\Delta t^2 \end{aligned} \qquad (2.\ 27)$$

where

$$\ddot{\mathbf{X}}(t_{k+1}) = (\mathbf{M}+\mathbf{A})^{-1}(\mathbf{F}(t_{k+1}) - \mathbf{B}\cdot\dot{\mathbf{X}}(t_{k+1}) - \mathbf{C}\cdot\mathbf{X}(t_{k+1})) \quad (2.28)$$

By combining Eq. (2.26 - 2.27), we obtain an explicit equation:

$$\mathbf{X}(t_{k+1}) = \left(\frac{6}{\Delta t^2}(\mathbf{M}+\mathbf{A}) + \frac{3}{\Delta t^2}\boldsymbol{B} + \boldsymbol{C}\right)^{-1}\cdot(\boldsymbol{F}(t_{k+1}) + (\boldsymbol{M}+\boldsymbol{A})\cdot\boldsymbol{a}_k + \boldsymbol{B}\cdot\boldsymbol{b}_k) \quad (2.29)$$

where

$$\boldsymbol{a}_k = \frac{6}{\Delta t^2}\mathrm{X}(t_k) + \frac{6}{\Delta t}\dot{\mathrm{X}}(t_k) + 2\ddot{\mathrm{X}}(t_k)$$
$$\boldsymbol{b}_k = \frac{3}{\Delta t}\mathrm{X}(t_k) + 2\dot{\mathrm{X}}(t_k) + \frac{1}{2}\ddot{\mathrm{X}}(t_k)\cdot\Delta t \quad (2.30)$$

2.2.2 Relationship between the ship's motion and ice loads

The forces and moments involved in the simulation at time step $k+1$ are unknown at time step t due to the nonlinear interdependence between the ice loads and the ship's motion; therefore, an iteration is performed base on a convergence criterion step $i+1$ (Eq. 2.30) to determine an acceptable value for the forces and moments.

$$\sqrt{(F_1^{I+1}-F_1^i)^2 + (F_2^{i+1}-F_2^i)^2 + (F_6^{I+1}-F_6^i)^2}\Big/\sqrt{(F_1^i)^2+(F_2^i)^2+(F_6^i)^2} < \varepsilon \quad (2.31)$$

where ε is a small positive number of the order 10^{-3}.

2.3 Discussion

To further establish the hypothesis on the floe geometry, an initial analysis was carried out to determine the condition for crushing and breaking of ice floe (Wang, 2001). According to the analysis, it was affirmed that ice crushing or breaking will only occur when some contact conditions between the ice floe and the structure are fulfilled. To model such contact points, a minimum distance function for detecting the minimum distance between the waterline of the structure and the contacting ice edge was determined based on the principle that 'the total force for the duration of ice-structure interaction is equal to the sum of the forces from the individual contacts acting simultaneously on the structure (Wang, 2001). The main parameter characterizing the established contact condition is the ice-breaking radius. This is expressed as a function of the critical length, inclination angle of the structure and the relative velocity (see Equation 2.1 – 2.2). However, the expression has been simplified using a number of empirical parameters or coefficients.

These empirical coefficients C_l and C_v accounts for the uncertainties in the estimation of the critical length and velocity dependences of the ice breaking process. As stated in Wang (2001) the coefficient C_l is a function of the critical length while C_v is a function of the inclination angle α of the conical structure and the angle β between the ice sheet motion and the horizontal normal to the cone. Since the Wang's model was developed for a static structure against a moving ice sheet, it was necessary to extend its capabilities in modeling a continuous-mode ice breaking so as to validate the already established values for the empirical parameters (Su, 2011).

For continuous-mode ice breaking, the Wang's model was extended by Su to predict ice loads during an ice-hull interaction. In his work, Su redefined the contact procedure under a uniform ice condition by representing the waterline with a discretized polygon while the ice edge was represented with a discretized polyline. According to the model, interaction occurs when the nodes of the ice wedge falls into the discretized waterline polygon. The ice wedges formed during the interaction are modelled by a parameter called *ice breaking radius*, similar to the Wang's model. The ice-breaking radius is a function of two major components, namely the characteristic length l of the ice sheet and the relative normal velocity V_n^{rel} between the ice and the hull nodes (see Equation 2.20). According to Su, crushing occurs once contact is established while bending failure is a function of the vertical force against the failure load i.e. ice will fail by bending when the vertical force becomes greater than the failure load. However, since the model is characterized with empirical parameters, the performance of the model is said to be characterized with certain uncertainties.

In order to present justifiable values for the empirical parameters so as to minimize the suspected uncertainties emanating from them, Quan (2015) carried out a sensitivity study on the empirical parameters C_f, C_v and C_l by investigating the effect of the parameters on the relationship between resistance and the relative velocity (Quan, 2015). Based on the study, it was established that there was consistency in the relationship between the resistance and the velocity for certain empirical parameter values. Based on this analysis and in line with the previous work by (Liu, et al., 2008) and (Wang, 2001) a value of 0.3 was selected for the C_l while a value of -0.5 was chosen for the C_v respectively. Also, a value of 2.2 for C_f gave the best match with experimental measurement values. However, since the parameters were established within the domain of values suggested in previous work, then there is a need for further validation in other to minimize the uncertainty characterizing the parameters.

In respect of this, Kuuliala carried out more sensitivity studies on the parameters as part of his final master's degree thesis. In his study the effect of C_v and C_l on the cusp size were investigated. The values of C_v and C_l selected for analysis were based on the Enkvist's result on the cusp size realized during ice-hull interaction (Enkvist, 1972). According to Eq. (2.2), the ratio R/l_c , which is a function of the cusp's size decreases with increasing relative velocity. To validate this, an initial sensitivity study using values of 0.8, 0.9 and 1.0 for C_l and -0.08, -0.09, -0.10, -0.11 and -0.12 for C_v was carried out by Kuuliala (Kurmiste, 2016). According to the result, there was a good agreement with the theoretical analysis as presented in Equation 2.2.

However, in more recent studies by Li (Li, et al., 2018) further improvements have been added to improve the model's performance on ice load prediction and analysis. Such improvements include: the modification of the bearing capacity to the dynamic form as defined in Tan et al., (2014), introduction of the non-linear pressure relationship within the contact area and finally the use of a random floe radius model Su et. al. (2014). Based on Using the improved model, assessment on the performance of model for ice load prediction was carried out and result compared to those obtained by Lindqvist and Riska's formula. Hence, for the study presented in this thesis, the improved model by Li (Li, 2016) have been applied in investigating the uncertainty associated with the model's parameter with regards to reliability and safety analysis.

3 Concept of reliability and uncertainty analysis

The general concept of reliability and uncertainty analysis is summarized in a flow chat as shown in Figure 3.1. According to the flow chat, the entire analysis begins with acquisition of necessary load and response data for the ice load and structure resistance respectively. The acquire data are thereafter processed into probability distributions from which the reliability index and probability of failure are estimated accordingly (Sipes, 1990). The resulting safety factors are then validated with the results obtained from a full-scale data analysis as well as the typical values obtained from literatures. Based on the information arrived from the comparative analysis, uncertainty characterizing the model is quantified and justifications are then drawn in respect to the magnitude of the uncertainty realized.

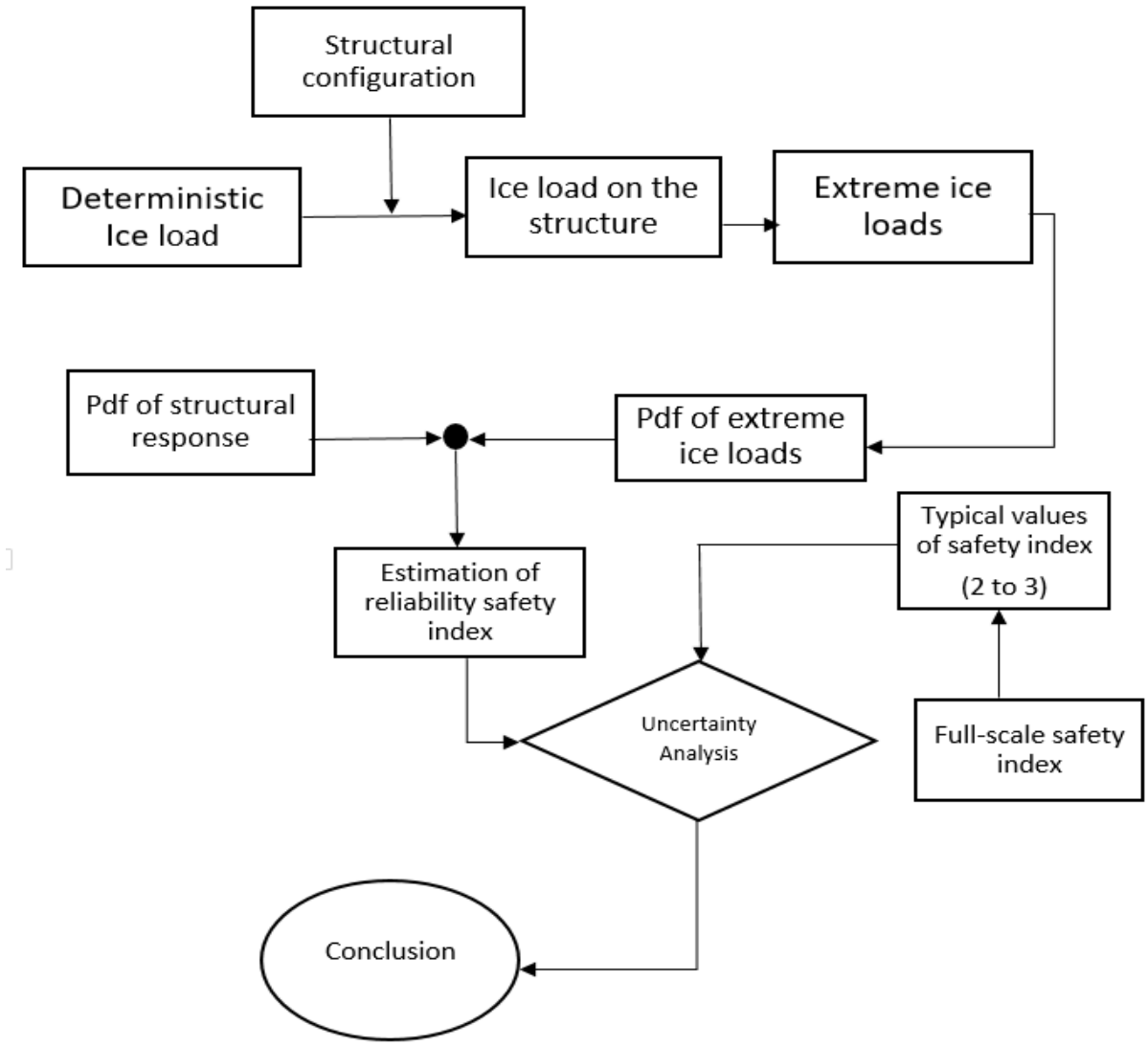

Figure 3. 1 Reliability and uncertainty analysis of S. A. Agulhas II ship hull

3.1 Reliability and safety analysis

The aim of reliability analysis is to predict the failure level P_f for a given marine structure. There are three levels of reliability analysis for which level three is the most difficult to apply in practice (Sipes, 1990). The challenges associated with the level three are in connection with the lack of

sufficient information to determine the joint probability density function of the design variables and the difficulties involved in evaluating the resulting multiple integrals (Kurmiste, 2016). Due to these reasons we have applied the level two approach for our reliability analysis.

As shown in Figure 3.1, the process starts with the mining of the required ice load data using the ice load prediction model for S. A. Agulhas II ship hull (Suominen, et al., 2012) based on some set conditions. The resulting ice loads are used to predict the extreme ice loads necessary for predicting the long-term ice load probability distribution. In addition, the associated structure responses are determined using the material parameters for the hull area under consideration. The realized structure responses are then used to calculate the necessary probability distribution for the structure responses (Goerlandt, 2017).

However, since the ship doesn't fail by short term loads, the short-term ice load prediction is not sufficient enough for reliability analysis (Faber, 2009). Therefore, we sort for the long-term extreme values and their respective statistical distributions (Figure 3.2) using the Gumbel's theory for long term extreme probability distributions. On comparing the distributions i.e., the ice loads and the structure response pdfs, the safety indices and probability of failure are estimated.

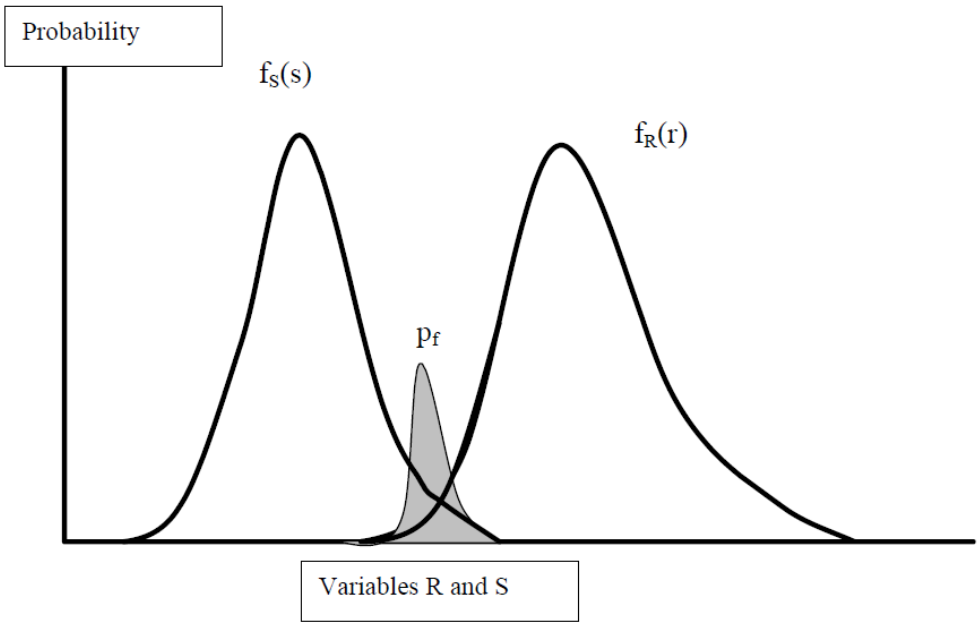

Figure 3. 2 Probability Distribution for Load and Hull Response (Kujala, 2008)

To estimate the safety index and the corresponding probability of failure, we develop a normal distribution for the load S and resistance R using the mean values μ_S and μ_R, and standard deviations of σ_S and σ_R respectively. We then evaluate the limit state function $g(s,z)$, which describes the safety margin or index β between the ship strength R and load S acting on it, i.e.

$$\beta = g(s,z) = S - R \qquad (3.\ 1)$$

The nature of the safety index depicts the state of reliability of the structure. There are three outcomes obtainable for the safety index.

(i) $\beta = g(s,r) < 0$ represents a failure condition since this indicates that the

load S exceeds the strength R

(ii) $\beta = g(s, r) > 0$ represents a safe state

(iii) $\beta = g(s, r) = 0$ represents the border line between the safe and failure state

The corresponding probability of failure is then given as:

$$\mathbf{P_f} = P[\beta = g(s, r) \leq 0] = \iint_{g(s,r) \leq 0} f_{S,Z}(s, r)\,ds\,dr \qquad (3.\ 2)$$

Where $f_{S,Z}(s, r)$ is the joint probability density function of S and R and the domain of integration is over all the values of s and z where the margin β is not positive, i.e. not in the safe state. Since S and R are statistically independent, then Equation 3.2 can be reduced to:

$$\mathbf{P_f} = \phi(-\beta) \qquad (3.\ 3)$$

Where ϕ (·) is the standard normal cumulative distribution function and **β** is called a safety index. To provide a simplified analysis, we assumed that the load and response are normally distributed. The safety index is then defined as:

$$\boldsymbol{\beta} = \frac{\mu_S - \mu_R}{\sqrt{\sigma_S^2 + \sigma_R^2}} \qquad (3.\ 4)$$

while the failure probability P_f becomes:

$$\mathbf{P_f} = \phi\left(\frac{\mu_S - \mu_R}{\sqrt{\sigma_S^2 + \sigma_R^2}}\right) \qquad (3.\ 5)$$

The safety index as shown in Figure 3.3 is the mean value of the safety margin from the origin relative to the standard deviation. According to Figure 3.2, the overlapping region of the distributions depicts the state of failure as expressed in Equation 3.5. The failure probability tends to zero as the overlapping diminishes (Kujala, 2008). However, since negative increase in the safety index β lead to increase in the probability of failure, we aim to have an increased value for β by obtaining a high difference between μ_S and μ_R or a decreasing sum for the standard deviations σ_S and σ_R (Sipes, 1990).

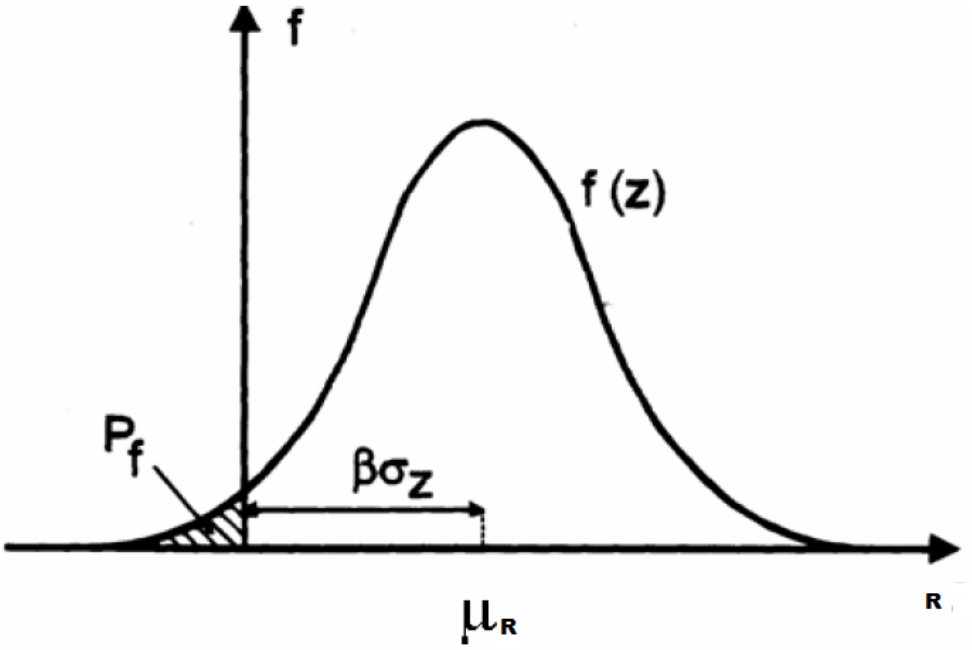

Figure 3. 3 Graphical Illustration of Safety Index (Kujala, 2008)

3.2 Structural Resistance R

Another major component in reliability analysis is the strength response of the structure and the respective failure mode. The structural response R corresponds to the load causing permanent deflection w_p on the plate section under consideration. In order to estimate the load causing permanent deflection in the plate, we apply an approach developed by Hayward (Hayward, 2001). The approach is based on the estimation of a correction factor considering the load level on the permanent deflection. The Hayward equations have the following forms:

When $w_p/t \leq 1$:

$$q = \frac{p_c h_c}{f_{DT}}\left[1 + \frac{w_p^2}{3t^2}\left(\frac{\zeta_o + (3-2\zeta_o)^2}{3-\zeta_o}\right)\right] \quad (3.\ 6)$$

And when $w_p/t \geq 1$:

$$q = \frac{2p_c h_c w_p}{t f_{DL}} \cdot \left[1 + \left(\frac{\zeta_0(2-\zeta_0)}{3-\zeta_0}\right)\left(\frac{t^2}{3 \cdot {w_p}^2} - 1\right)\right] \quad (3.\ 7)$$

Where t is the plate thickness, h_c is the load height and w_p is the permanent deflection in the hull plating. In addition, the threshold pressure p_c is given as

$$p_C = \frac{48M_p}{s^2\left(\sqrt{3 + (\frac{s}{l})^2} - \frac{s}{l}\right)^2} \quad (3.\ 8)$$

Where s is the frame spacing, l is the frame span, M_p is the plastic moment of the plating given as:

$$M_p = \sigma_y \frac{t^2}{4} \tag{3. 9}$$

Also, the shape parameter, ζ_o has the expression:

$$\zeta_o = \frac{s}{l}\left(\sqrt{3 + (\frac{s}{l})^2} - \frac{s}{l}\right) \tag{3. 10}$$

The correction factor f_{DL} is evaluated using the expression:

$$f_{DL} = -0.1330 \cdot {x_T}^2 + 0.6701 \cdot {x_T}^2 \tag{3. 11}$$

Where

$$x_T = \frac{h_c}{s} \cdot \left(\frac{s^2}{t \cdot l}\right)^{0.1} \tag{3. 12}$$

For our analysis, the values for the basic parameters are given in Table 3.1

Table 3. 1 Hull parameter

Parameters	**[m]**
Frame length l	1.2
Frame spacing s	0.4
Plate thickness t	See Table 3.2
Load height h_c	0.075

In this study, we have considered certain sections of the hull for our analysis. For each section of the hull i.e. the bow and shoulder, a plate section between two specific frames is selected. The hull plating response was determined by randomizing the yield strength average value μ_R relative to the standard deviation σ_R. The associated standard parameters of the hull plating under consideration are given in Table 3.2.

To calculate the value for the mean μ_R and standard deviation σ_R of the line load q, we made a normal distribution for the yield strength σ_y of the plate using the yield strength mean μ_{σ_y} and the standard deviation σ_{σ_y} of the applied material. We then calculate the line loads associated with these values of the yield strength by dividing with the frame span. For extra high strength steel, the following holds:

$$\begin{cases} \mu_{\sigma_y} = 441.1\ MPa \\ \sigma_{\sigma_y} = 34.25\ MPa \end{cases} \tag{3. 13}$$

Table 3. 2 Hull Plate Parameters (Suominen, et al., 2012)

	Steel Grade	Plate thickness [mm]	Mean (μ_R) (MPa)	Standard deviation (σ_R) (MPa)
Bow	NVE500	28	441.1	34.25
Bow shoulder	NVD500	26		

The steps applied for the determination of the hull response distribution are:

1. Determination of the statistical parameters of the steel material
2. Determination of the deflection level
3. Determination of strength associated with selected deflection
4. Determination of the mean and standard deviations associated with the resulting strength value.
5. Calculation of the probability density function and the associated cumulative frequency function
6. Plotting of the corresponding normal distribution.

For the determination of the safety index, the Pdfs associated with both loads and resistance are then plotted together to show the safety margin of the structure over the estimated life time of the structure (Figure 3.8).

The statistical parameters as given in Table 3.2 are associated with the material grades used for the hull areas under consideration. Since the steel grades are classed under the extra high strength steels, they have yield strengths as well as same statistical parameters except for the plate thickness. The deflection w_p applied in this study were extracted from a damage history data base (Appendix III) (Kujala, 2015).

3.3 Uncertainty analysis

In general, the design and construction of marine structures are often associated with varying degrees of uncertainties, especially in terms of the strength and the material properties of the structure (Sipes, 1990). Also, in predicting the performance of the ship in its proposed environment, certain assumptions are often made mostly because of the limited knowledge about the environment conditions. As such, in an attempt to develop an engineering tool for predicting the performance of an ice worthy ship such as S. A. Agulhas II ship in an ice infested water, significant amount of assumptions was often considered in the model design in other to accommodate any kind of complexity in the mathematical model (Su, et al., 2010). These assumptions however create in the model certain uncertainties that potentially reduce the model performance.

There are two major types of such uncertainties; objective and subjective uncertainties (Sipes,1990). While the former is associated with random variables for which statistical data can be obtained and analyzed, the latter is associated with lack of sufficient information and knowledge about the element to be modeled. Since the investigation carried out in this study is related to stochastic nature of the ship-ice interaction, the uncertainty analysis is this work is classified as 'objective uncertainty'.

In order to provide justifiable explanation on the suspected uncertainties, we have applied two major approaches; qualitative and quantitative approaches. For the qualitative approach, theoretical explanations based on visual inspection of the estimated safety indices are provided in each of the studied case while for the quantitative approach, coefficient of variation (COV) for the estimated safety index obtained for each studied case are calculated. The resulting COVs of the model safety indices are then analyzed and compared against the COV of the estimated safety indices of the full-scale measurements. Based on the disparities between the COV of both approaches, explanations are presented to justify the implications of the quantified uncertainties.

3.3.1 Analysis of model uncertainty

As mentioned above, the measuring factor for the uncertainty is the coefficient of variation (COV). For a given set of data, the COV (δ_X) is quantified as follows (Sipes, 1990):

$$\delta_X = \frac{\sigma}{\bar{x}} \qquad (3.14)$$

where

$\bar{x}$ = sample mean
σ = sample standard deviation

$$\begin{cases} \delta_X < 1 & Low\ variance \\ \delta_X > 1 & high\ variance \end{cases}$$

4 Full- scale data analysis

The full-scale ice load data measured during an on-site experiment with S. A. Agulhas II ship during voyages in December, 2013 and February, 2014 at Antarctic waters (Suominen, et al., 2013) respectively were applied to estimate the safety indices and failure probabilities of the ship over a 25years life time. The 10-minute maximum loads for bow and bow shoulder are studied in this thesis. The ice-induced loads were obtained by instrumenting certain frames at the bow, bow shoulder and stern areas of the ships. In order to ensure same ice conditions for the full-scale and the model for the purpose of validation, a preliminary check on the performance of the simulation model over a varying number of ice conditions from the full-scale data was carried out. From the result, it was established that four ice conditions were suitable for the optimum performance of the model as given in Table 4.1 (Kuuliala, 2015). As such the full-scale data associated with the selected ice conditions were then obtained and applied for validation.

Table 4.1 S.A. Agulhas II ship main particulars

Length, bpp.	121.8 m
Breath	21.7 m
Draught, design	7.65
Deadweight	5000 t
Displacement	13632 t
Open water Speed	14 kn
Propulsion power	9 MW

4.1 Short description of S. A. Agulhas II ship and the instrumentation

The S.A. Agulhas II ship was constructed in 2011/2012 and instrumented with strain gauges at certain areas of the hull to detect ice loads during voyages. The ship design is classed under the polar ice class PC5 while the hull was built in line with DNV ICE-10. The instrumentation of the hull area is such that two adjacent frames at the bow and two adjacent frames at the bow shoulder were instrumented (see also Appendix IV). The obtained maximum loads were at frames #134 and #134+400 at the bow and frames #112 - #113 at the bow shoulder. Based on the schematics of the S. A. Agulhas II ship (Appendix IV), the plate section between the frame #132 and #135 was considered for the bow section while the plate section between the frames #110 and #114 were considered for the shoulder section.

4.2 Comparison between short term measured and simulated ice loads

As a preliminary study to the uncertainty analysis presented in chapter 6 & 7, the short term measured and simulated ice loads for the bow plating were compared so as to establish qualitatively the uncertainties associated with the obtained short-term loads for both methods. However, the bow shoulder plating data were intentionally excluded due to insufficient number of peak loads for the considered ice condition. The measured ice load data as mentioned above are ice loads from frames obtained from an on-site ice load measured for S. A. Agulhas II ship during 2013/2014 voyages (Suominen, 2018). On the other hand, the simulated ice load data were numerically determined using a designed model of the same ship in a level ice field. The empirical parameters associated with the estimated ice loads were systematically selected such that $C_l =$

0.7 and $C_v = -0.10$ while $C_f = 1$ (dynamic bearing failure). The comparison between the simulated and measured short term loads are presented in Table 4.2 - 4.3 and Figures 4.1 - 4.2. The comparison was done based on the number of ice loads, maximum ice loads, mean value and the standard deviation. Two cases were considered for the bow with respect to the ice thickness while the bow shoulder was not considered due to insufficient data. At the bow, ice thicknesses 0.7m and 0.9m were considered.

Table 4.2 presents the mean value, standard deviation and maximum value obtained for the simulated and measured ice loads at the bow for ice thicknesses $h_i = 0.9$m and $h_i = 1.1$m respectively. The number of events obtained for the simulated loads were higher than those of the measured values. This is however expected as we assumed a level ice condition for the simulation, neglecting other ice features such as the ridges, snow covers etc. which sometimes characterize the actual ice. Hence, to ensure a proper comparison, other ice conditions influencing the measured ice loads must be well defined. Furthermore, Figures 4.1 – 4.2 compare the ice load distributions for the simulated and measured ice loads. As shown, on the average, the simulated ice loads were greater in terms of deviations and peaks than those of the measured ice loads.

Table 4. 2 Comparison of the measured and simulated ice load histograms at bow

		Measured	Simulated
$h_i = 0.9$m	Number of peaks	278	127
	Max (kN/m)	1027.2	894.83
	Mean (kN/m)	275.77	502.58
	Standard deviation (kN/m)	234.27	253.29
$h_i = 1.1$m	Number of peaks	305	146
	Max (kN/m)	1347.8	894.83
	Mean (kN/m)	274.91	791.13
	Standard deviation (kN/m)	199.37	304.67

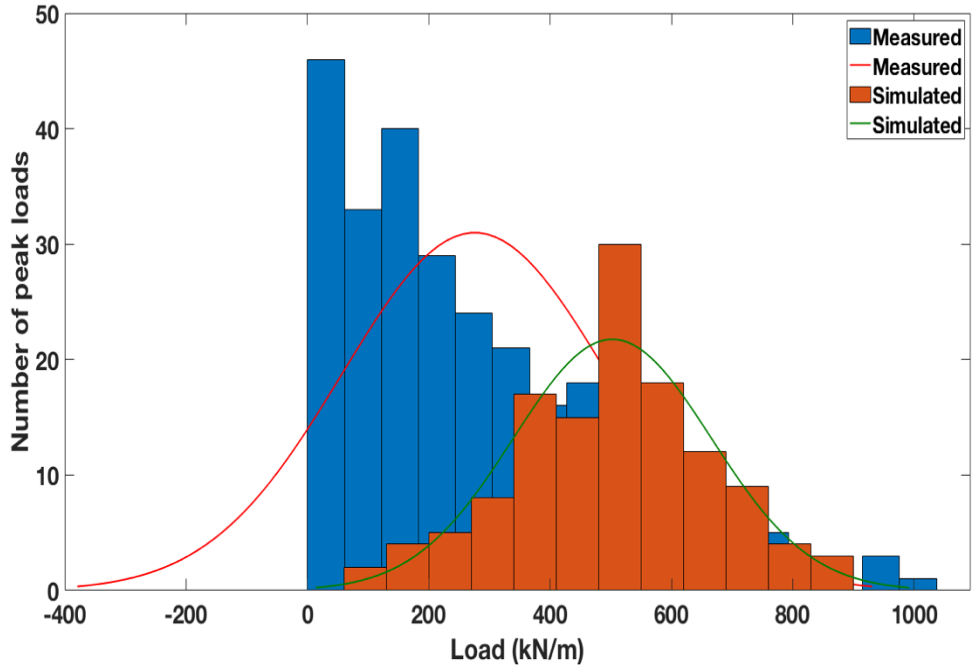

Figure 4. 1 Simulated and measured load histogram for $h_i = 0.9$m

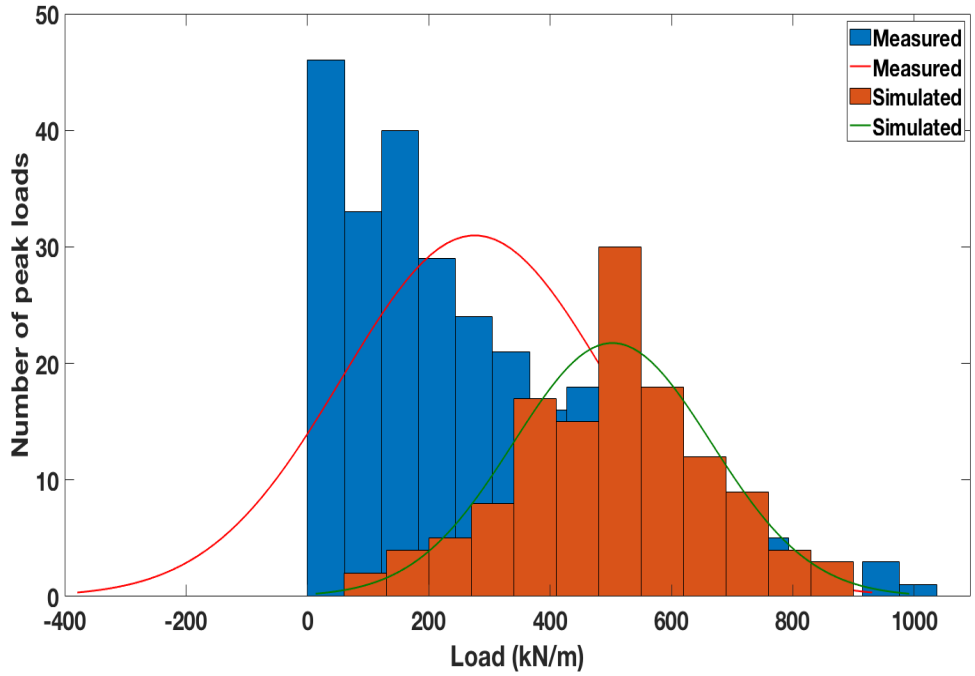

Figure 4. 2 Simulated and measured ice load for $h_i = 1.1m$

4.3 Ice Load and hull plate response distributions

As mentioned in section 3.1, the ice load data obtained from the simulation model are subjected to a selection protocol which was necessary to obtain the peak loads from the given ice load data. The procedure was necessary since most failures are propagated by peak loads over the lifetime period of the structure (Sipes, 1990). The peak load selection protocol employed in determining the required peak load was the *Rayleigh separation protocol* (Suominen, et al., 2012). The Rayleigh separation basically compares the maximum and minimum values and based on some pre-defined conditions, the peak loads are selected. The resulting peak loads are thereafter transformed into a short-term probability distribution (Figures 4.3).

However, since the failure of the structure is associated with continuous and long-term loading, the short-term peak loads are extrapolated into long-term peak loads (Faber, 2009) as given in Figure 4.4. In addition, the corresponding probability distribution for the hull plate response is obtained using a plate deflection $w_p = 25mm$.

4.3.1 Short-term probability distribution of the full-scale data and hull plate response

Figures 4.3 represents the probability distributions for the short-term peak loads and the corresponding hull plate response at the bow. From the figures, it was obvious that for short-term estimation, the structure was very safe based on the minimal overlaps between the ice loads pdf and the hull response pdf. However, this is not reliable since the failure of structures are associated with long-term loading. Hence, we need to obtain a long-term reliability distribution which will provide the required safety index; a measure of the ship reliability and safety.

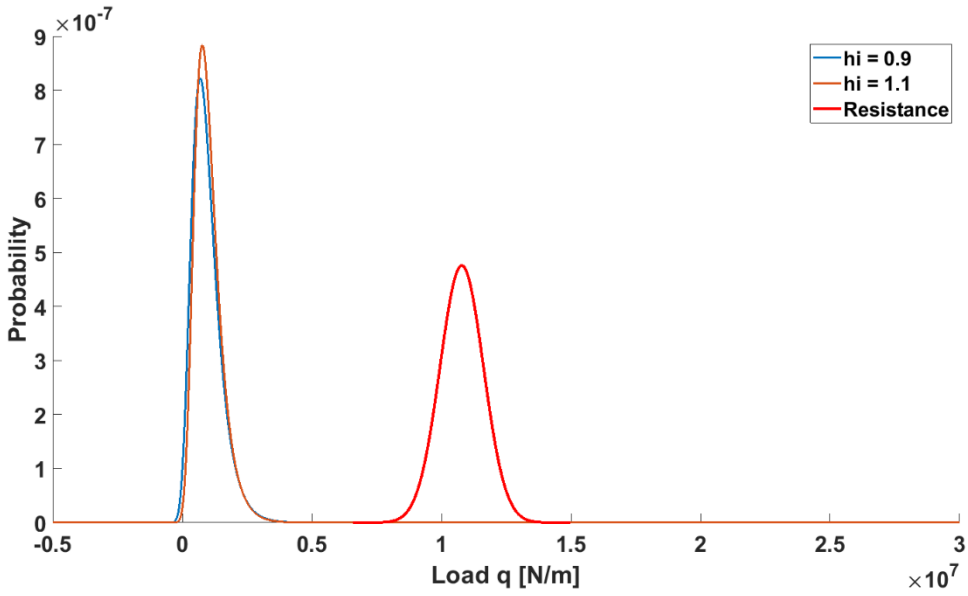

Figure 4. 3 Short-term probability distribution for full scale data (bow)

4.3.2 Long-term probability distribution of the full-scale data and the hull plate response

To obtain the long-time reliability and safety of the ship, we first determine the number of events expected for the ship during her estimated 25years life time. The amount of loading events is based on the amount of days per year in ice and the used time period for maximum loads. Hence, for S. A. Agulhas II ship, the estimated number of events is simply a product of the number of events per day which is a function of the realized 10-mins maxima, number of days in a year and the ship's life time. In this analysis, the ship is assumed to be in ice for an average of 20days in a year. For the various ice conditions considered for the bow and bow shoulder section, the expected number of events N are calculated as follows (Kurmiste, 2016):

$$N = events\ per\ day\ \times number\ of\ days\ in\ 1\ year \times ship\ lifetime$$

The number events associated with each ice condition for the bow and bow shoulders are presented in the Table 4.3. According the estimated N values, more events occur at the bow than the bow shoulder but observations have shown that effective crushing is more predominant at the bow shoulder and this gives rise to the lower safety index often obtained for the bow shoulder (Su, et al., 2014).

Table 4. 3 Number events for long time reliability estimation for the bow

	Number pf events per day	Number of days per year	N events
Bow			
$h_i = 0.9$m	47	25	23500
$h_i = 1.1$m	53		26500

Figures 4.1 - 4.2 represent the respective short-term probability distributions of the ice loads and hull plate responses for the bow and bow shoulder respectively. The overlaps between the ice load distribution and the hull response distribution are measures of the reliability and safety of the ship structure. The corresponding safety indices are provided in Table 4.4.

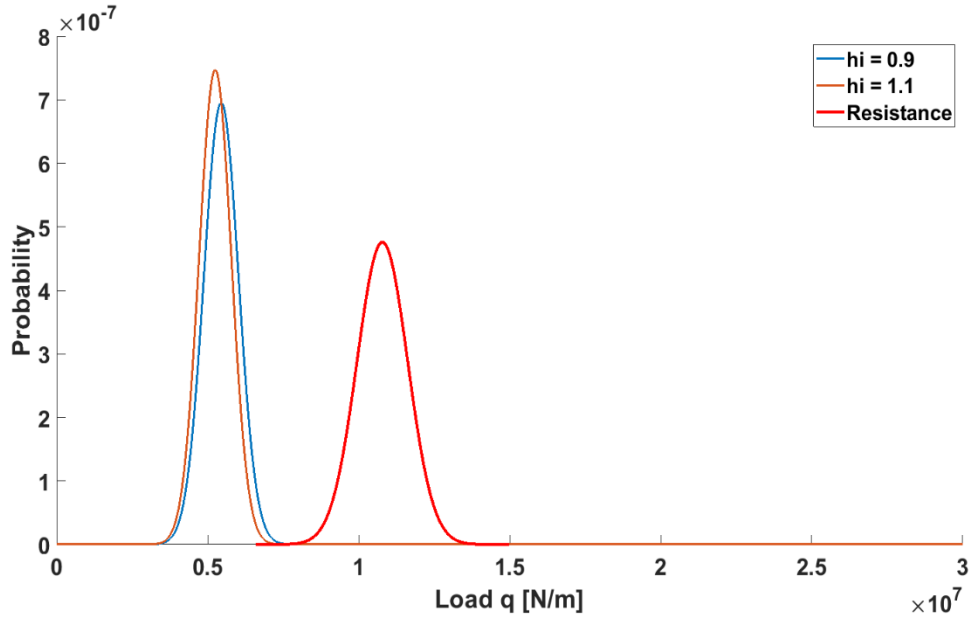

Figure 4. 4 Long-term probability distribution for full scale data (bow)

4.3.3 Safety index and probability of failure analysis of full-scale data

According to Table 4.4, the estimated safety indices for the bow plating showed direct correlation with the corresponding ice thicknesses i.e. higher ice loads resulted into higher safety indices. The result showed that for higher ice thicknesses, the bow plating proves to be more prone to failure than in the case of lower ice thickness. Also, the result suggests the possibilities of realizing varying peak loads with close or large variance under different ice conditions.

Table 4. 4 Safety indices and probability of failure (full scale)

h_i	Bow	
	β	P_f
0.9	5.25	7.46E-08
1.1	5.57	1.28E-08

5 Simulation model and parameters selection

The simulation model and the selected parameters for simulation are presented in this chapter. In section 5.1, the ice load prediction model for S. A. Agulhas II hull ship as compared with the full-scale ship is described. In section 5.2, the parameters selected for our analysis were described and justified in relation to our analysis. The simulation parameters being investigated in this report are the three empirical parameters C_v, C_l and C_f. The aim of the simulation with the empirical parameters is to verify the performance of the simulation model in estimating the long-term reliability of the ship based on the uncertainty analysis.

5.1 Simulation model

Figure 5.1 shows the planar motion of a ship in a level ice under a continuous ice breaking mode (Kuuliala, 2015). The interaction between the ship and the ice produces simulated time histories of the position, velocity and acceleration of the ship as well as magnitude and location of ice loads on the waterline. According to Su, et al. (2010), a 3-D equation of motion (Equation 2.24) comprising the directions of motion of the ship (surge, sway and yaw) and the respective ice forces are solved by the simulation program developed in MATLAB.

The ice field and the ship are modelled by discretized geometries of the ice edge and waterline of the ship (Figure 6.4). The responses are determined by the extent of the contact overlap of the polygons representing the ice field and the hull waterline. Also, the magnitude of the ice forces is determined as well as ice failure which includes bending and crushing respectively.

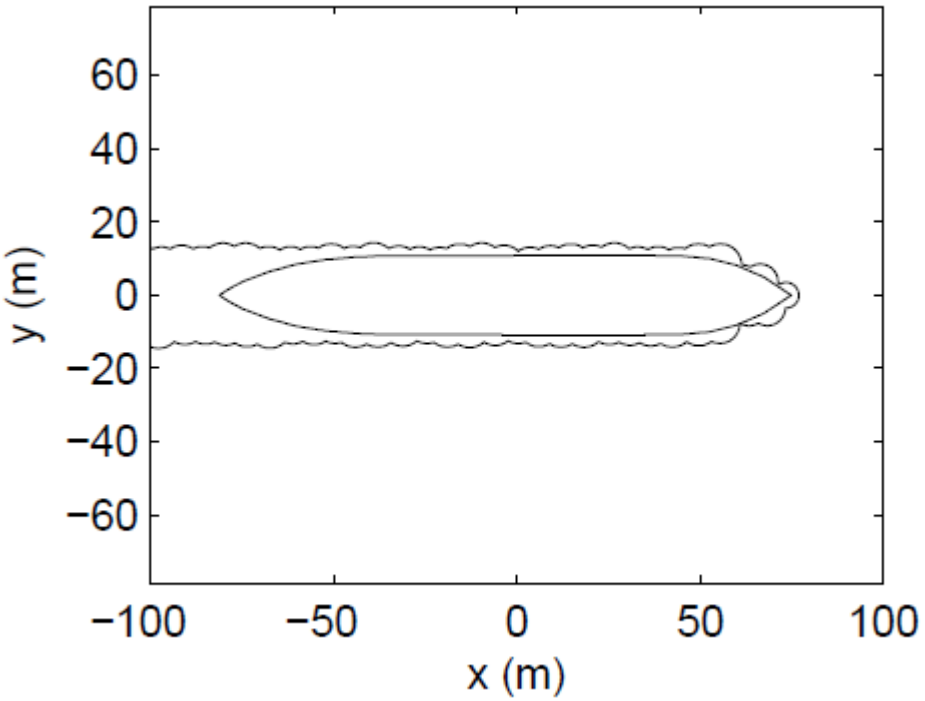

Figure 5.1 Interaction between the waterline of ship and edge of the ice field (Kuuliala, 2015)

5.2 Parameter selection for simulation

5.2.1 Empirical parameters

Three major empirical parameters have been selected for analysis: C_l, C_v and C_f. The three parameters are associated with the model design (Su, et al., 2010). Since these parameters were selected based on test analysis, they are said to be characterized with some level of uncertainties. In other to reduce the suspected uncertainties in the model, ongoing modifications are been made on the model. Currently, in his ongoing PhD research, Li et al. (2018) replaced the static form of ice bearing capacity with the dynamic form proposed in Tan et al. (2014) in order to take into consideration, the effect of relative velocity in the ice-hull interaction. However, for the sake of our investigation on the influence of the empirical parameters, the influence of C_f values on the model performance was considered in this study.

(a) Selection of values for C_l and C_v

The values of C_l and C_v selected for analysis were based on previous proposals by Wang (2001), Su et al. (2010) and Kuuliala (2015). By rearanging Equation 2.1 to obtain in Equation 5.1, we can investigate the effect of the empirical parameters on the cusp size in terms of the ice breaking radius. Since the product $C_l C_v$ gives a negative value, it simply shows that C_l is the upper limit of the relative cusp size R/l_c at realtive velocity of zero i.e. as the velocity increases , the cusp size decreases.

$$R/l_c = C_l C_v v_n^{rel} + C_l \qquad (5.1)$$

A plot (Figure 6.5) of the cusp size R/l_c against the relative velocity (Kuuliala, 2015) validates Eq. (5.1). The cusp size as proposed in Enkvist (1972) were studied (see Table 6.1).

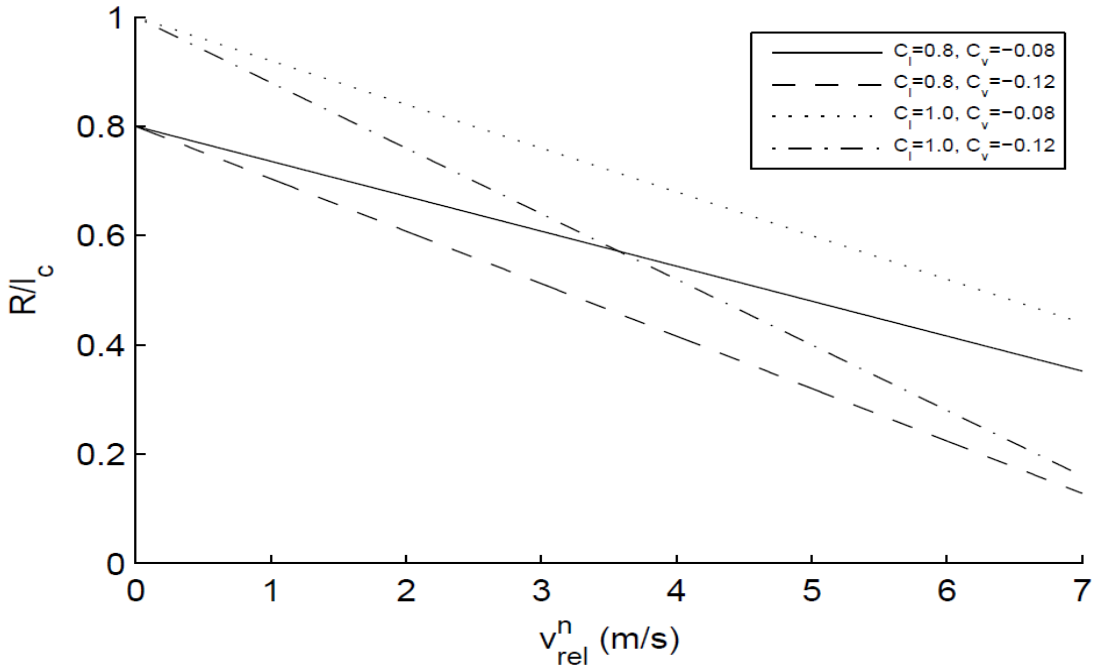

Figure 5.2 Dependency of cusp size on the relative velocity for varying values of C_l and C_v (Kuuliala, 2015)

Table 5. 1 Analytical and experimental values for the relative Cusp size (Enkvist, 1972)

R/l_c	Description
0.8	Analytical for cusp, plate theory
0.3 – 0.6	Cusp test
0.5 – 1.0	Model test
0.3 – 0.7	Full – scale test

From the simulation results by Kuuliala (2015) based on comparison with Enkvist (1972), the value of C_l should be in th vicinity of 1 in order to generate a cusp size close to know values as in Table (5.1). Although Wang (2001) had applied a combination of $C_l = 0.32$ and $C_v = -0.14$, but because the applied relative velocity was much lower and also the scenerio was ice against a conical structure, the combination could not be used for a continuous ice breaking case under consideration. In respect of this we have chosen the following values as presented in Table 5.2 for C_l and C_v.

Table 5. 2 Selected values for C_l and C_v

C_l	C_v
0.30	-0.09
0.32	-0.10
0.35	-0.12
0.37	-0.13
0.40	-0.14

(b) Selection of values for C_f

The value of parameter C_f influences the limit of the bending failure of the ice wedge based on the opening angle (Eq. (2.18). According to Kashtelian and Nguyen et al, values in the range of 1 to 4.5 were reported for C_f. Based on this range, Su (2011) applied a value of 3.2 for C_f while predicting ice loads in a continuous ice breaking in a level ice field. Therefore, in our analysis, we have chosen values in close proximity to that applied by Su (2011) for C_f (Table 5.3).

Table 5. 3 Selected values for C_f

C_f
1.5
2.0
2.2
2.5
3.0

5.3 Simulation with empirical parameters

The selected values for each parameter were sequentially simulated as shown in Table (5.4 – 5.6). For each run, the selected values of C_l were simulated for each value of C_v. The same order was applied for the case of C_v in which the C_v values were simulated for each value of C_l. However, for each simulation, the dynamic bending failure condition was applied such that $C_f = 1$ (Tan et al., 2014). Furthermore, the empirical parameter C_f was simulated over each value of C_l while keeping the $C_v = -0.10$ constant. The choice of $C_v = -0.10$ applied in this case was based on the result given in Quan (2015) in which -0.10 proved to be the most appropriate chooice for C_v.

5.3.1 Simulation with C_l

The selected values for the C_l parameter was sequentially simulated at each value of C_v in the order as shown in Table 5.4 at ice thickness of 0.5m.

Table 5. 4 Simulation with selected C_l values

C_l	C_v	h_i [m]
0.30		
0.32		
0.35	-0.09, -0.10, -0.12, -0.13, -0.14	0.5
0.35		
0.40		

5.3.2 Simulation with C_v

Similarly, the selected values for the C_v parameter were simulated at each value of C_l in the order as shown in Table 5.7 keeping the ice thickness at 0.5m.

Table 5. 5 Simulation with selected C_v values

C_v	C_l	h_i [m]
-0.09		
-0.10		
-0.12	0.30, 0.32, 0.35, 0.37, 0.40	0.5
-0.13		
-0.14		

As observed from the above tables (Table 5.4 - 5.5), the choice of values for both parameters are same and the same number of combinations will be obtained in both cases except for the order of arrangement, however, the results obtained for similar cases varies since the process is random.

5.3.3 Simulation with C_f

In order to investigate the effect of the empirical parameter C_f, the bearing capacity of the ice was switched to the static condition as in given in Equation 2.18. With respect to this, five ordered values in the range as proposed by Kashtelian and Nguyen et al. The values of C_l and C_v simulated with the C_f as given in Table 5.6.

Table 5.6 Simulation with selected values of C_f

C_f
1.5
2.0
2.2
2.5
3.0

(a)

C_l, C_v
0.30 ,-0.10
0.32, -0.10
0.35, -0.10
0.37, -0.10
0.40, -0.10

(b)

6 Results and discussion

The safety factors estimated for the bow and bow shoulder plating of the hull model for all tuning conditions of the empirical parameters are presented and discussed in this section. This chapter consists of three sections; with each section discussing the results obtained from each simulation mentioned in Chapter five. In order to ensure equal conditions were maintained for all the simulations, same distance in the ice field was maintained for each case study. The applied length of ice field depended on when a satisfactory result is attained.

Safety indices and probability of failure were estimated from the simulated ice loads and analyzed with respect to the applied empirical parameters as well as the typical values provided in literatures (Kujala, 2008). Typical values for the safety index β take a range of 2 to 3 while those of the failure probability takes a range between 10^{-2} and 10^{-3}. In each case study, the nature and trend of the resulting safety indices for the bow and shoulder were represented in Figures and Tables respectively so as to show the correlation between the estimated safety index and the choice of empirical parameter value.

The long-term probability density functions (PDF) associated with each case study are provided in Appendix I - II of this report but a step-by-step procedure for obtaining the safety indices and probability of failures are itemized in the following section.

6.1 Safety index β and probability of failure P_f estimation

Here, a preliminary description of how the safety indices and the corresponding probability of failures are estimated is presented. According to Sipes (1990), the safety index and probability of failure estimated from the long-term probability distributions of the ice loads and hull plate response are obtained as follows: First the short-term probability distributions (Figure 6.1.1) of the ice loads and hull plate response for a plate deflection of $w_p = 25$mm are obtained using the Gumbel I distribution (Equation 6.1).

$$G_t(x) = \frac{G(x) - G(x_t)}{1 - G(x_t)}, x_t \leq x \tag{6.1}$$

Secondly, the long-term probability distributions (Figure 6.1.2) for the ice loads and hull plating for the respective hull sections are estimated by extrapolating the short-term probability distributions according to Equation 6.2 using the number of events *N* over the ship estimated life time.

$$G_t(x) = \left[\frac{G(x) - G(x_t)}{1 - G(x_t)}\right]^N \tag{6.2}$$

Where N= Number of events or extrapolated peak loads over the estimated lifetime of the ship given as:

$$N = events\ per\ day\ \times number\ of\ days\ in\ 1\ year \times ship\ lifetime$$

The events per day is given by the number of simulated loads obtained from a single run of model simulation while the days in a year is synonymous to the number of voyages covered by S. A. Agulhas II ship in a year. In this thesis, 11 days in a year was applied (Kurmiste, 2016). Also, the ship estimated lifetime used was 25years. Finally, the safety index and probability of failure are then obtained as the statistical difference between the long-term distributions of the ice loads and the hull responses (Equation 3.1 – 3.4).

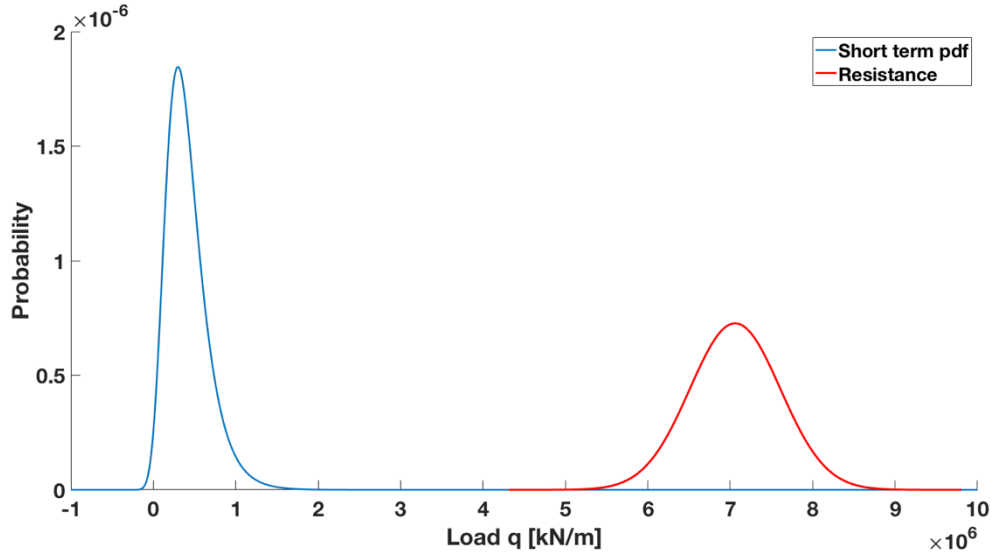

Figure 6.1.1 Short term ice load pdf vs hull resistance

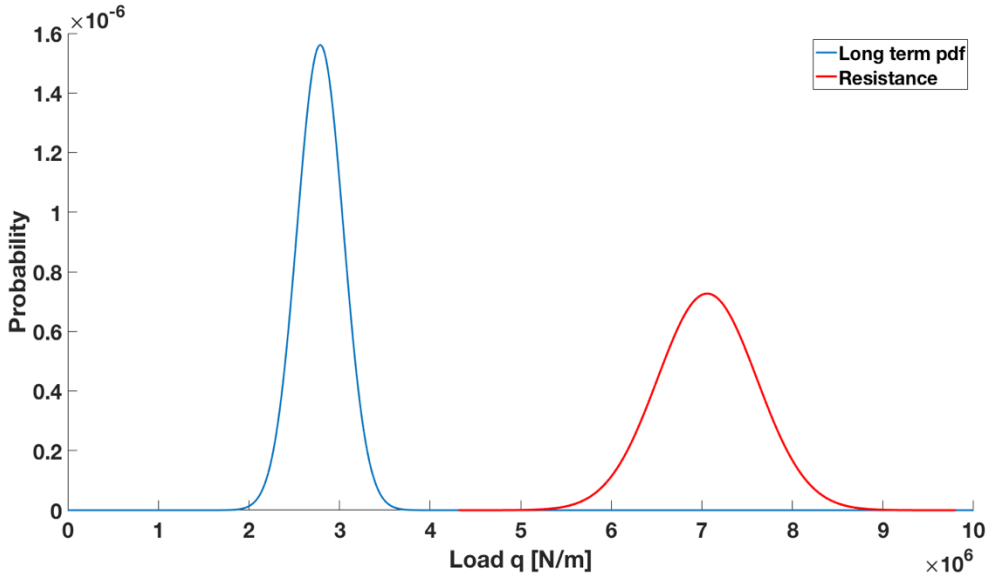

Figure 6.1.2 Long term ice load pdf vs hull resistance

6.1.1 Analysis of safety index and probability of failure for C_l values

Tables 6.1 – 6.5 and Figures 6.1 – 6.5 represents the estimated safety indices and failure probabilities for all the cases considered for the values for the empirical parameter C_l. In each case, the influence of the choice of values for empirical parameter C_l on the estimated safety indices and failure probabilities were discussed. Likewise, the correlations between the C_l values and the resulting safety indices were shown for both the bow and the bow shoulder. Additionally, the statistical parameter associated with the ice loads are presented in the tables to further substantiate the basis for the results obtained from the reliability and safety analysis.

Case 1: Influence of C_l parameters at $C_v = -0.09$

The resulting safety indices and failure probabilities obtained for each value of parameter C_l when the value of parameter C_v is -0.09 are presented in Table 6.1 and Figure 6.1. As given in table 6.1

(bow and shoulder), the number of realized peak loads and events decreases as the C_l value increases. Also, the average of the peak loads generally decreases for both sections of the hull. However, the estimated safety index correlates randomly with the selected C_l values with minimal variation in the results. As expected, as the value of C_l increases, the cusp size increases since the empirical parameter C_l directly influences the breaking radius R. As such, larger maximum peak loads are generated (Table 6.1) which makes the hull plating more susceptible to failure. However, since we are dealing with a random process, the safety indices were random with respect to the C_l values and vice versa (Figure 6.1). Comparing the results at both sections (bow and shoulder), the bow's safety index showed initial rise in value but declines later while the shoulder's result generally rises with increasing C_l value. Also, the safety index for the bow were obviously lower than those of the shoulder due to larger ice-hull interactions causes by larger contact surface for ice-hull interactions and larger inclination angles at the shoulder than the bow.

Table 6. 1 Safety indices and probability of failure for C_l parameters at C_v= -0.09

		Bow						
C_v = -0.09		No of peaks	N events	Max (kN/m)	Mean (kN/m)	Std. dev. (kN/N)	β	P_f
C_l	0.3	1253	344575	1017	825.11	241.76	6.39	8.50E-11
	0.32	1067	293425	1057.2	838.05	237.86	6.50	4.13E-11
	0.35	898	246950	993.74	820.42	233.26	6.67	1.25E-11
	0.37	777	213675	1032	821.47	248.06	6.41	7.07E-11
	0.4	633	174075	1038.8	814.09	250.35	6.45	5.72E-11

		Bow shoulder						
C_v = -0.09		No of peaks	N events	Max (kN/m)	Mean (kN/m)	Std. dev. (kN/N)	β	P_f
C_l	0.3	165	45375	910.99	546.05	267.93	6.31	1.37E-10
	0.32	162	44550	873.22	557.42	244.40	6.78	5.95E-12
	0.35	134	36850	967.2	556.11	235.93	7.02	1.08E-12
	0.37	110	30250	893.29	597.20	226.97	7.20	3.06E-13
	0.4	107	29425	897.88	571.48	243.46	6.92	2.27E-12

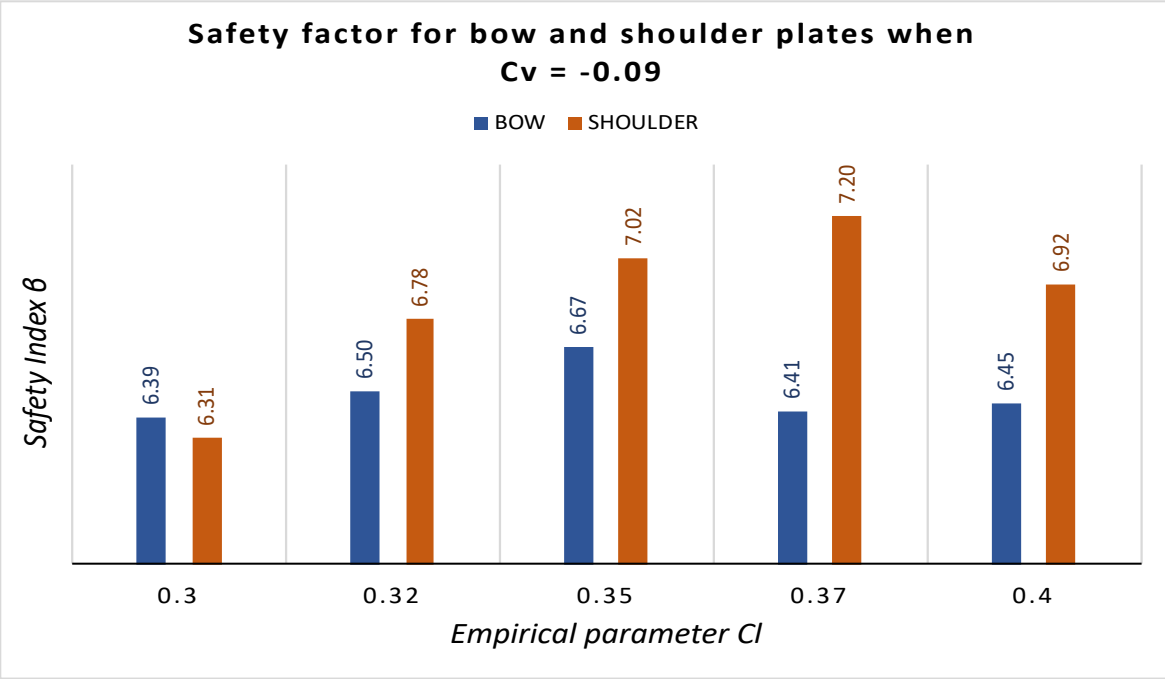

Figure 6. 1 Safety factors for bow and stern for C_l values at C_v = -0.09

Case 2: *Influence of C_l parameters at $C_v = -0.10$*

Table 6.2 and Figure 6.2 present the safety indices and failure probabilities corresponding to the selected values for parameters C_l when C_v is -0.10. As observed in the previous case ($C_v = -0.09$), the number of simulated peak loads decreases with increasing value of empirical parameter C_l. Also, the average of the peak loads decreases at the bow but random at the shoulder with increasing C_l value while the standard deviation over the C_l values are said to be very close with slight variations. In addition, as the C_l value rises, the resulting safety index changes slightly for the bow and shoulder sections with average values of 6.46 and 7.44 respectively. These results prove the relationship between the breaking radius and the empirical parameter C_l as expressed in equation 2.1. The greater the C_l value the higher the breaking radius which invariably signifies higher ice loads. The consequence of this should be a reducing safety index and increasing probability of failure (Figure 6.2). However, since the number of events decreases with increasing C_l values with minimal variations in the standard variations, the safety index showed slight variations for the bow and the shoulder. However, the bow plating was more susceptible to failure than the shoulder with respect to the safety index values.

Table 6. 2 Safety indices and probability of failure for C_l parameters at C_v = -0.10

		Bow						
C_v = -0.10		No of peaks	N events	Max (kN/m)	Mean (kN/m)	Std. dev. (kN/N)	β	P_f
C_l	0.3	1227	337425	1021.5	836.69	250.21	6.20	2.86E-10
	0.32	1149	315975	982.78	834.91	238.24	6.47	4.89E-11
	0.35	939	258225	1028.3	831.54	245.22	6.40	8.03E-11
	0.37	862	237050	1065.7	820.05	243.25	6.48	4.53E-11
	0.4	685	188375	1008.5	803.16	233.89	6.77	6.34E-12

		Bow shoulder						
C_v = -0.10		No of peaks	N events	Max (kN/m)	Mean (kN/m)	Std. dev. (kN/N)	β	P_f
C_l	0.3	476	344575	883.18	464.22	205.76	7.44	4.96E-14
	0.32	428	293425	997.51	507.34	219.31	7.09	6.71E-13
	0.35	358	246950	864.62	512.53	192.18	7.74	4.98E-15
	0.37	219	213675	912.32	515.78	221.46	7.24	2.23E-13
	0.4	224	174075	857.37	493.04	203.31	7.67	8.73E-15

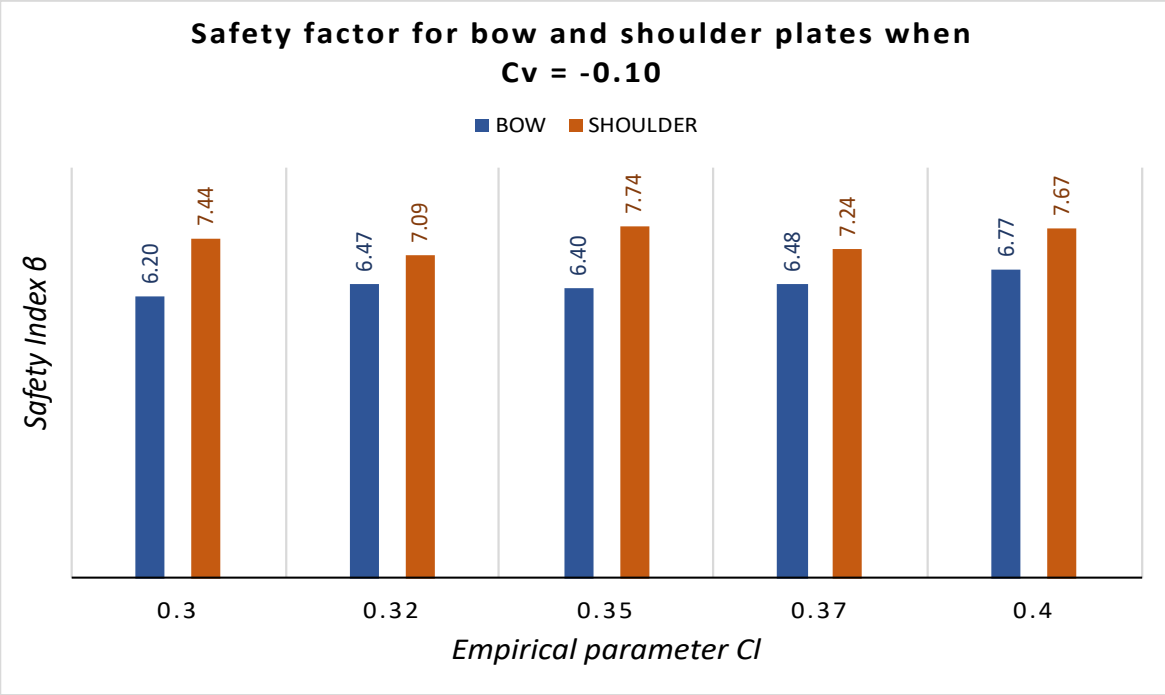

Figure 6. 2 Safety factors for bow and shoulder for C_l values at C_v = -0.10

Case 3: *Influence of C_l parameters at $C_v = -0.12$*

Table 6.3 and Figure 6.3 present the respective safety indices and corresponding probability of failures associated with the selected values for the parameter C_l when $C_v = -0.09$. For the bow and the bow shoulder, the simulated number of events decreases with increasing C_l value. Other

quantities such as the average peak loads and the maximum simulated ice loads varies moderately while the standard deviations were somewhat close with minimal variations across the C_l value. The decreasing number of events are simply a consequence of the larger breaking radius causes by increasing C_l value. However, the estimated safety indices were very close for both the bow and shoulder with minimal variations reflected by the trend shown by the standard deviations (Figure 6.3). Between the bow and shoulder, there were some observable differences in the simulated statistical data and the estimated safety indices. Although the results were similar in terms of their variations but relatively lower safety indices at the bow showed that the bow were more susceptible to failure than the bow shoulder.

Table 6. 3 Safety indices and probability of failure for C_l parameters at $C_v = -0.12$

		Bow						
C_v = -0.12		No of peaks	N events	Max (kN/m)	Mean (kN/m)	Std. dev. (kN/N)	β	P_f
C_l	0.3	1308	359700	1051.6	823.11	245.34	6.30	1.48E-10
	0.32	1194	328350	1109.5	835.45	253.35	6.14	4.03E-10
	0.35	1001	275275	1009.8	833.22	245.60	6.36	9.82E-11
	0.37	897	246675	1068.7	817.51	240.34	6.53	3.22E-11
	0.4	762	209550	1043.7	831.19	236.69	6.64	1.62E-11

		Bow shoulder						
C_v = -0.12		No of peaks	N events	Max (kN/m)	Mean (kN/m)	Std. dev. (kN/N)	β	P_f
C_l	0.3	526	144650	1008.4	516.17	234.14	6.68	1.23E-11
	0.32	469	128975	872.34	503.83	206.53	7.35	9.57E-14
	0.35	338	92950	870.62	510.39	218.91	7.17	3.80E-13
	0.37	255	70125	870.38	505.53	183.76	8.03	4.72E-16
	0.4	240	66000	910.81	499.83	211.47	7.46	4.41E-14

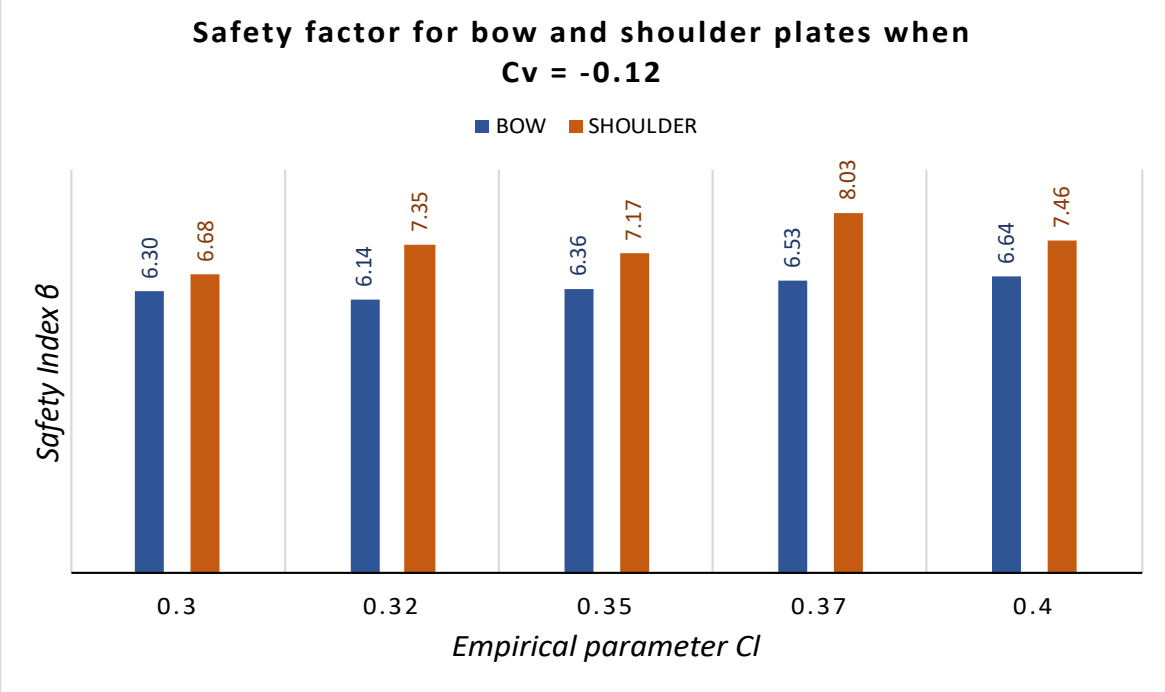

Figure 6. 3 Safety factors for bow and shoulder for C_l values at C_v = -0.13

Case 4: *Influence of C_l parameters at $C_v = -0.13$*

According to Table 6.4, bow and shoulder, the number of simulated events decreases with increasing C_l values while the obtained maximum and mean peak loads fluctuates minimally across the C_l values. Also, the standard deviations were very close with very minimal variations and these are reflected in the nature of the estimated safety indices which were very close and predictably could convergence with much higher simulated number of events. Comparing the results for the two hull sections (bow and shoulder), the safety index showed similar trends but with higher values obtained at the shoulder than the bow (Figure 6.4), implying the bow to be more prone to failure than the bow shoulder. Also, relatively higher number of events were simulated at the bow than the bow shoulder as a result of higher hull angles at the shoulder as well as greater ice-hull contact area at the bow.

Table 6. 4 Safety indices and probability of failure for C_l parameters at C_v = -0.13

		Bow						
C_v = -0.13		No of peaks	N events	Max (kN/m)	Mean (kN/m)	Std. dev. (kN/N)	β	P_f
C_l	0.3	1367	375925	1067.1	827.40	251.21	6.16	3.70E-10
	0.32	1202	330550	1010.6	833.34	242.27	6.37	9.15E-11
	0.35	1063	292325	1117.9	835.66	242.45	6.41	7.47E-11
	0.37	939	258225	1064.8	826.29	242.63	6.46	5.34E-11
	0.4	765	210375	1044.3	824.80	246.64	6.44	5.87E-11

		Bow shoulder						
C_v = -0.13		No of peaks	N events	Max (kN/m)	Mean (kN/m)	Std. dev. (kN/N)	β	P_f
C_l	0.3	570	156750	885.34	482.73	208.74	7.28	1.61E-13
	0.32	516	141900	1011.7	486.82	216.95	7.12	5.33E-13
	0.35	411	113025	871.85	491.98	204.88	7.45	4.53E-14
	0.37	290	79750	935.96	492.14	228.65	7.04	9.88E-13
	0.4	289	79475	967.78	506.56	226.38	7.06	8.20E-13

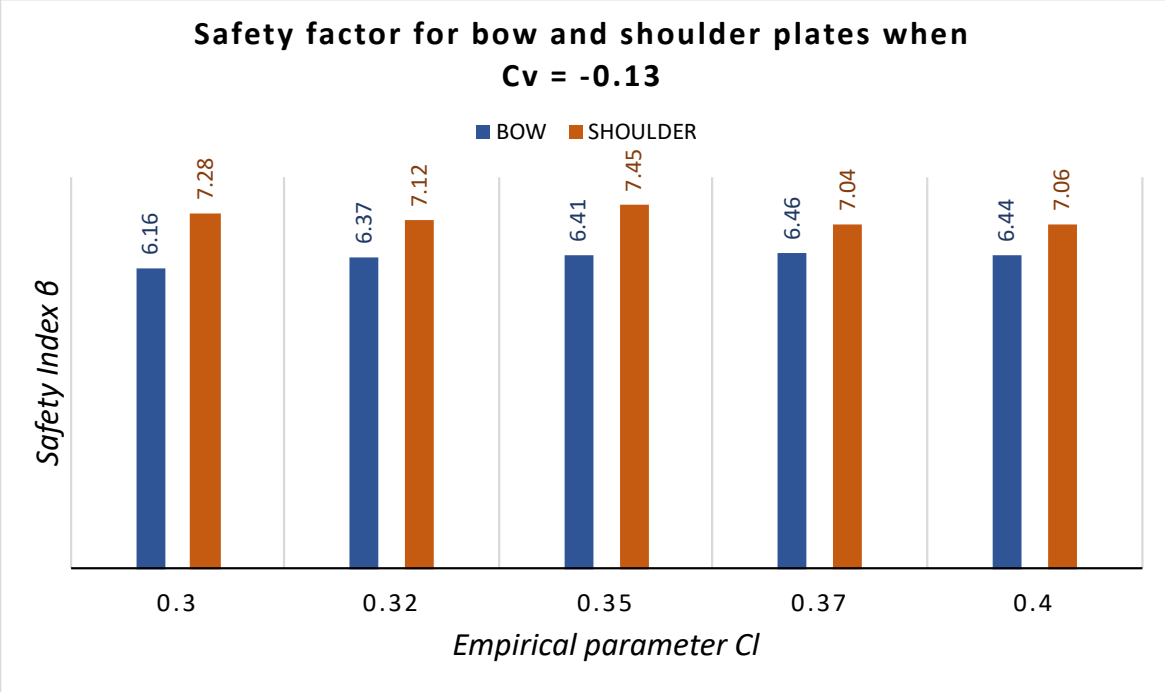

Figure 6. 4 Safety factors for bow and shoulder for C_l values at C_v = -0.13

Case 5: *Influence of C_l parameters at $C_v = -0.14$*

From Table 6.5, the number of simulated events over the ship lifetime decreases with increasing value of parameter C_l. The maximum peak load and average peak load showed random correlation with slight variations with respect to the C_l values for both hull sections. Consequently, the standard deviation for the bow and shoulder showed minimal variations which are reflected in the nature and trend of the estimated safety indices. The safety indices for both hull sections proved that at constant C_v, minimal variations will emerge in the results for sufficient number of simulations. However, the clear variations in the number of events were simply direct consequence of increasing ice loads due to larger ice breaking radius and ice cusp.

Furthermore, between the bow and shoulder, similar trends in the results were observed, although with larger variations at the bow (Figure 6.5). Also, it was obvious that the bow plating was more susceptible to failure than the bow shoulder in terms of the magnitude of their safety indices. Again, the observed differences in the results are associated with the number of events and ice-hull contact area.

Table 6. 5 Safety indices and probability of failure for C_l parameters at C_v = -0.14

		Bow						
C_v = -0.14		No of peaks	N events	Max (kN/m)	Mean (kN/m)	Std. dev. (kN/N)	β	P_f
C_l	0.3	1460	401500	994.31	816.93	241.69	6.35	1.05E-10
	0.32	1279	351725	1019.6	827.07	242.84	6.35	1.05E-10
	0.35	1085	298375	1044.9	820.23	252.95	6.21	2.67E-10
	0.37	961	264275	1086.8	829.94	253.41	6.22	2.44E-10
	0.4	808	222200	1039.9	826.33	242.23	6.51	3.70E-11

		Bow shoulder						
C_v = -0.14		No of peaks	N events	Max (kN/m)	Mean (kN/m)	Std. dev. (kN/N)	β	P_f
C_l	0.3	504	138600	1149.2	482.71	226.89	6.91	2.37E-12
	0.32	481	132275	992.95	511.94	221.39	7.00	1.30E-12
	0.35	383	105325	894.26	464.88	200.81	7.62	1.30E-14
	0.37	341	93775	904.89	486.09	213.06	7.34	1.07E-13
	0.4	287	78925	890.62	468.15	204.22	7.62	1.26E-14

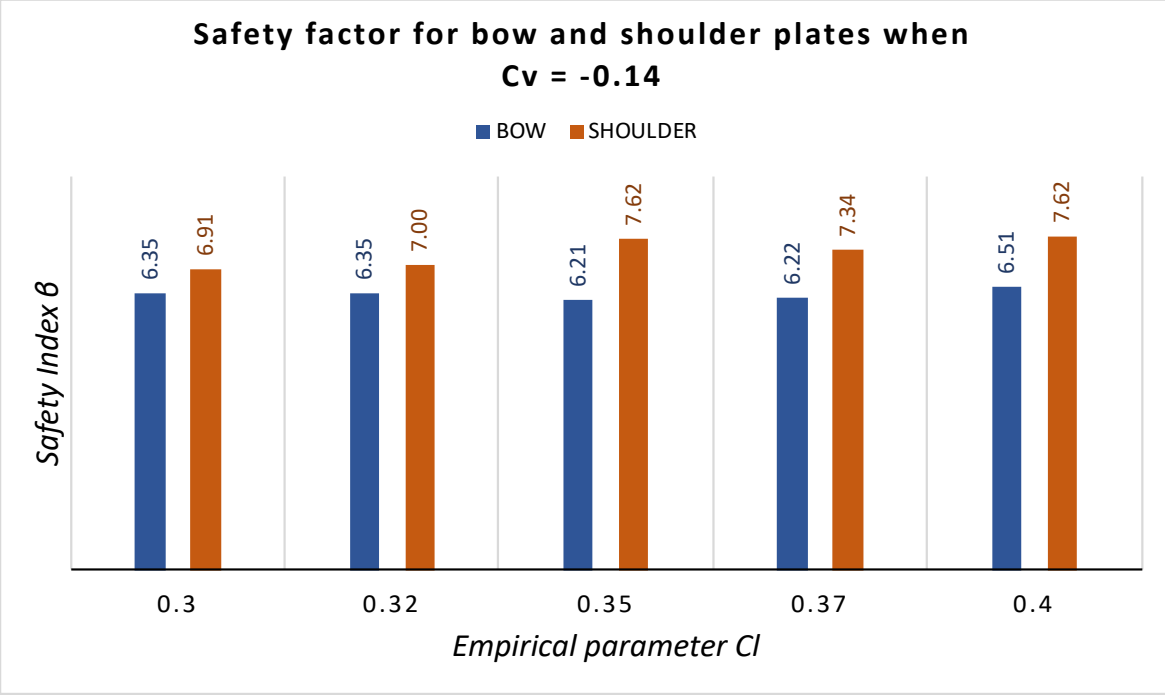

Figure 6. 5 Safety factors for bow and shoulder for C_l values at C_v = -0.14

Summary

In summary, for the results obtained from the cases studied for the C_l parameter proves to be reliable to great extent when compared with the processes involved with continuous ice-hull interaction during ice breaking process. At both sections of the hull (bow and shoulder), consistently high number of events decreasing with increasing C_l values were obtained across all the cases as well as minimally varying safety indices that correlated randomly with the selected C_l values. Across all the cases considered in this section, the estimated safety indices were very close in each case with minimal variations. Although random trends were consistently shown in the results, but these were simply consequences of the stochastic nature of the ice-hull interaction and ice breaking process. Also, for all the cases, the standard deviation of the simulated ice loads was consistently very close with minimal variations in each case study. The implication of these are that there are minimal uncertainties in the simulation results.

Furthermore, the influence of changing C_v across the cases as shown in Figure 6.6 – 6.7 proves the influence of varying the C_v value on the estimated safety index across the cases. For the bow, the result showed that as the value of C_v decreases, the safety and reliability of the hull simply reduces even though the result associated with $C_v = -0.09$ deviated from the trend as the C_l appreciates. On the other hand, for the shoulder, the results were obviously random. Likewise, higher number of simulated events were obtained at the bow than the shoulder which were reflected in the respective results. The result at the bow section proves the bow to be more prone to failure than the corresponding shoulder plating as a result of greater number of ice-hull interaction and larger ice-hull contact area obtainable at the bow.

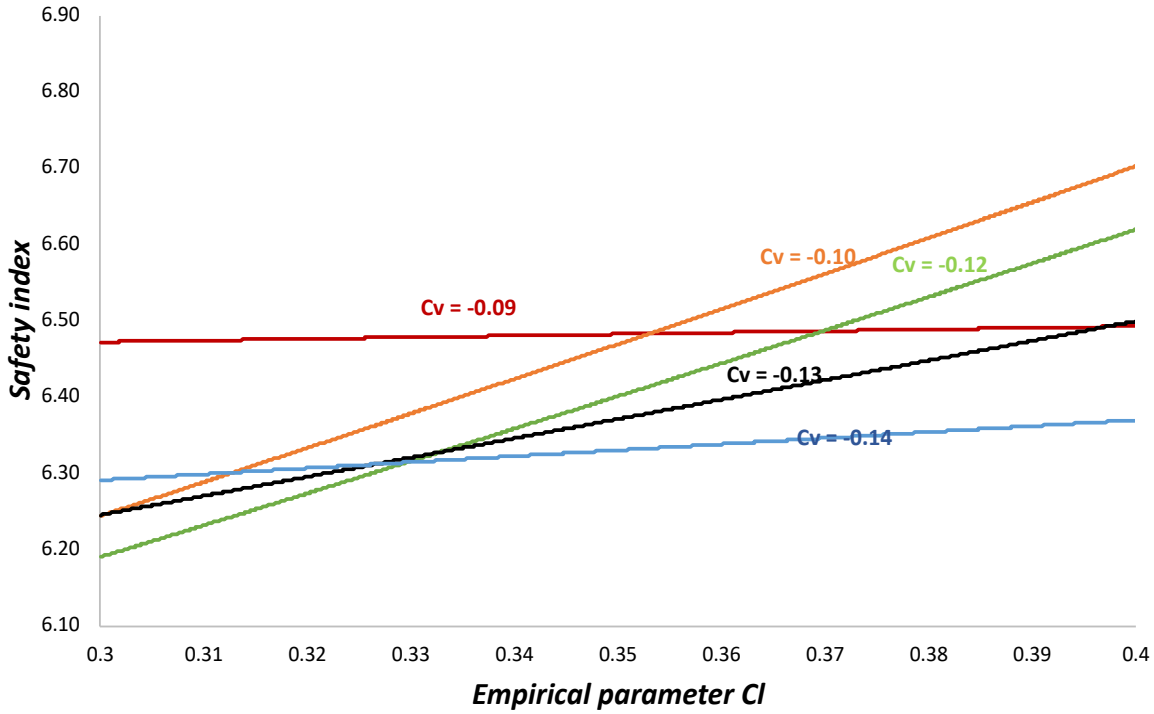

Figure 6. 6 Influence of empirical parameter C_v on the simulation with empirical parameter C_l (Bow)

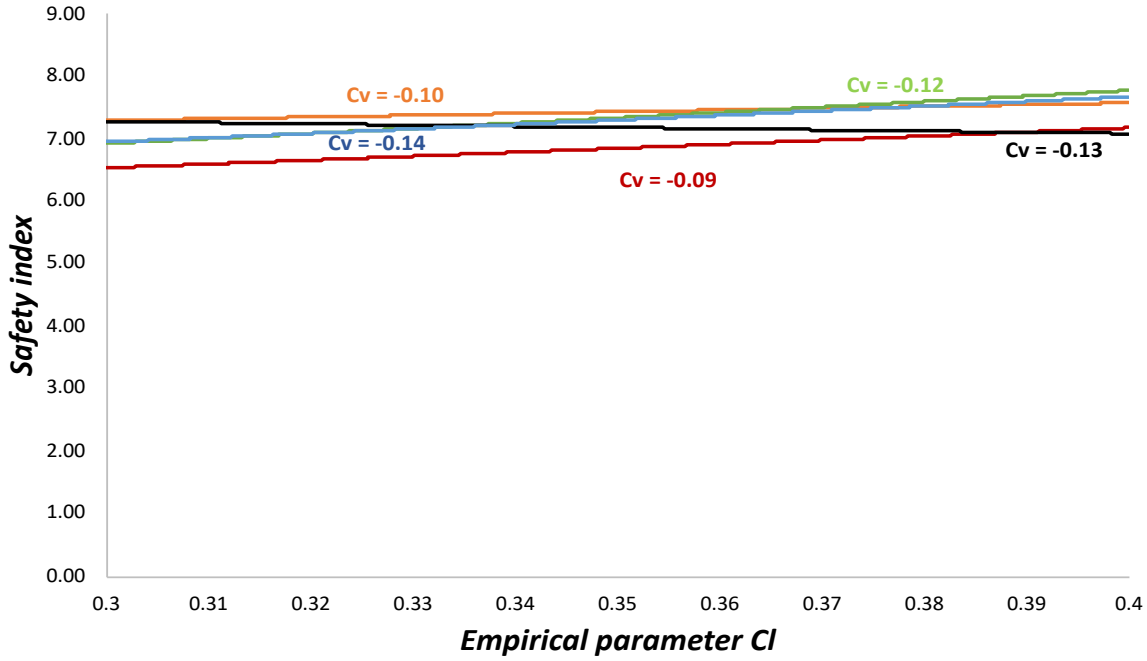

Figure 6. 7 Influence of empirical parameter C_v on the simulation with empirical parameter C_l (Shoulder)

6.1.2 Analysis of safety index and probability of failure for C_v values

Tables 6.8 – 6.12 and Figures 6.8 – 6.12 presents the simulation results corresponding to the five (5) selected values for the empirical parameter C_v. In each case, the results consist of the number of events, simulated statistical data and the respective reliability index for the bow and shoulder of the hull. Analysis of the results were also given for each case study to establish the influence of the choice of values for the parameter C_v in relation the ice breaking radius leading to the eventual nature of the estimated safety indices and probability of failure. Also, the observed uncertainties associated with the results in each case are mentioned. The respective probability distributions for each case studied are presented in Appendix I-II.

Case 1: *Influence of C_v parameters at $C_l = 0.30$*

In this case, the simulated statistical data and reliability indices associated with the choice of values for C_v when $C_l = 0.30$ are presented and analyzed accordingly. From Table 6.6, the simulated number of event and the maximum peak loads generally rises as the value of C_v decreases. However, the mean values and the standard deviations clearly showed randomly correlations and minimal variations as the C_v values decrease. Also, the estimated safety index for the bow and shoulder showed clearly minimal variations with respect to the C_v values. As the number of simulated events increases, the estimated safety index fluctuates about an average value of 6.38 for the bow and 7.13 for the shoulder. According to equation 2.1, it is expected that as the C_v decreases from -0.09 to -0.14, the relative velocity increases negatively which invariably causes a decrease in the breaking radius R, leading to more simulated events.

Comparing the results simulated for the bow and shoulder of the ship hull, the estimated safety index shows same trends for both hull sections as the C_v value decreases (Figure 6.8). However, the results for the bow were again lower than those of the shoulder which simply means that the bow plating were more prone to failure as compared to the shoulder. The reasons are that there

are more ice-hull activities at the bow than the shoulder (Table 6.6) as well as the hull plate area for ice-hull interaction is often greater than those at the shoulder.

Table 6. 6 Safety indices and probability of failure for C_v parameters at $C_l = 0.30$

		Bow						
C_l = 0.30		No of peaks	N events	Max (kN/m)	Mean (kN/m)	Std. dev. (kN/N)	β	P_f
C_v	-0.09	1253	344575	1017	825.11	241.76	6.39	8.50E-11
	-0.1	1227	337425	1021.5	836.69	250.21	6.20	2.86E-10
	-0.12	1308	359700	1051.6	823.11	245.34	6.30	1.48E-10
	-0.13	1368	376200	1067.1	827.44	251.12	6.16	3.66E-10
	-0.14	1460	401500	994.31	816.93	241.69	6.35	1.05E-10

		Bow shoulder						
C_l = 0.30		No of peaks	N events	Max (kN/m)	Mean (kN/m)	Std. dev. (kN/N)	β	P_f
C_v	-0.09	475	130625	910.99	476.88	209.90	7.33	1.19E-13
	-0.1	476	130900	883.18	464.22	205.76	7.44	4.96E-14
	-0.12	526	144650	1008.4	516.17	234.14	6.68	1.23E-11
	-0.13	570	156750	885.34	482.73	208.74	7.28	1.61E-13
	-0.14	505	138875	1149.2	482.75	226.67	6.92	2.29E-12

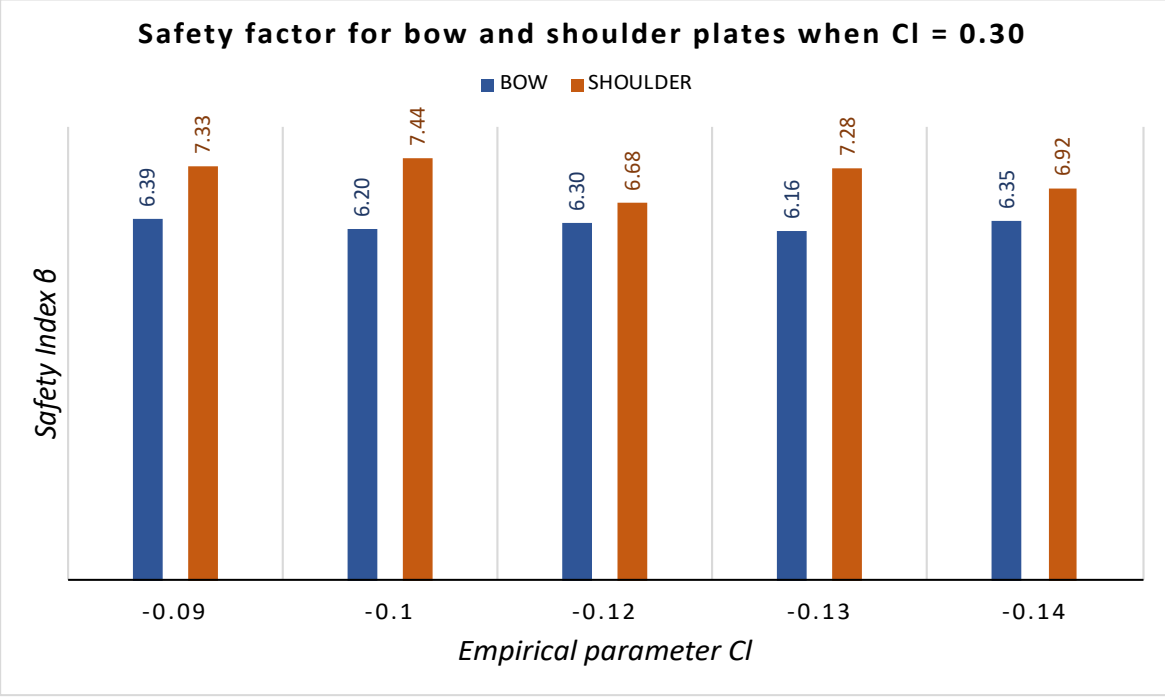

Figure 6. 8 Safety factors for bow and shoulder for C_v values at $C_l = 0.30$

Case 2: *Influence of C_v parameters at $C_l = 0.32$*

Table 6.7 contain the simulated statistical data and reliability indices associated with parameter C_v values at $C_l = 0.32$. The simulated number of events increases as the values of C_v decreases. However, the maximum peak load and the standard values showed random trend with decreasing C_v value while the mean obviously decreases with decreasing C_v values. The safety index on the other hand, fluctuates around average values of 6.37 and 7.12 for the bow and shoulder respectively. The minimal variations observed in the safety index is reflected in the standard deviation values which showed the closeness in the results of the simulation. In addition, the relationship between the C_v and the ice breaking radius is also reflected in the result. As the C_v decreases, the breaking radius or ice cusp reduces (Equation 2.1), giving rise to reduced ice loads (Table 6.7).

The combined results for the bow and shoulder (Figure 6.9) showed that the safety indices randomize with minimal variation for both hull sections with lower values obtained for the bow plating. Also, greater number of simulated ice loads were achieved at the bow compared to the shoulder due to larger contact area available for ice-hull interaction.

Table 6. 7 Safety indices and probability of failure for C_v parameters at $C_l = 0.32$

		Bow						
C_l = 0.32		No of peaks	N events	Max (kN/m)	Mean (kN/m)	Std. dev. (kN/N)	β	P_f
C_v	-0.09	1067	293425	1057.2	838.05	237.86	6.50	4.13E-11
	-0.1	1149	315975	982.78	834.91	238.24	6.47	4.89E-11
	-0.12	1194	328350	1109.5	835.45	253.35	6.14	4.03E-10
	-0.13	1202	330550	1010.6	833.34	242.27	6.37	9.15E-11
	-0.14	1278	351450	1019.6	826.94	242.89	6.35	1.05E-10

		Bow shoulder						
C_l = 0.32		No of peaks	N events	Max (kN/m)	Mean (kN/m)	Std. dev. (kN/N)	β	P_f
C_v	-0.09	415	114125	873.22	477.21	224.53	7.04	9.65E-13
	-0.1	428	117700	997.51	507.34	219.31	7.09	6.71E-13
	-0.12	469	128975	872.34	503.83	206.53	7.35	9.57E-14
	-0.13	516	141900	1011.7	486.82	216.95	7.12	5.33E-13
	-0.14	481	132275	992.95	511.94	221.39	7.00	1.30E-12

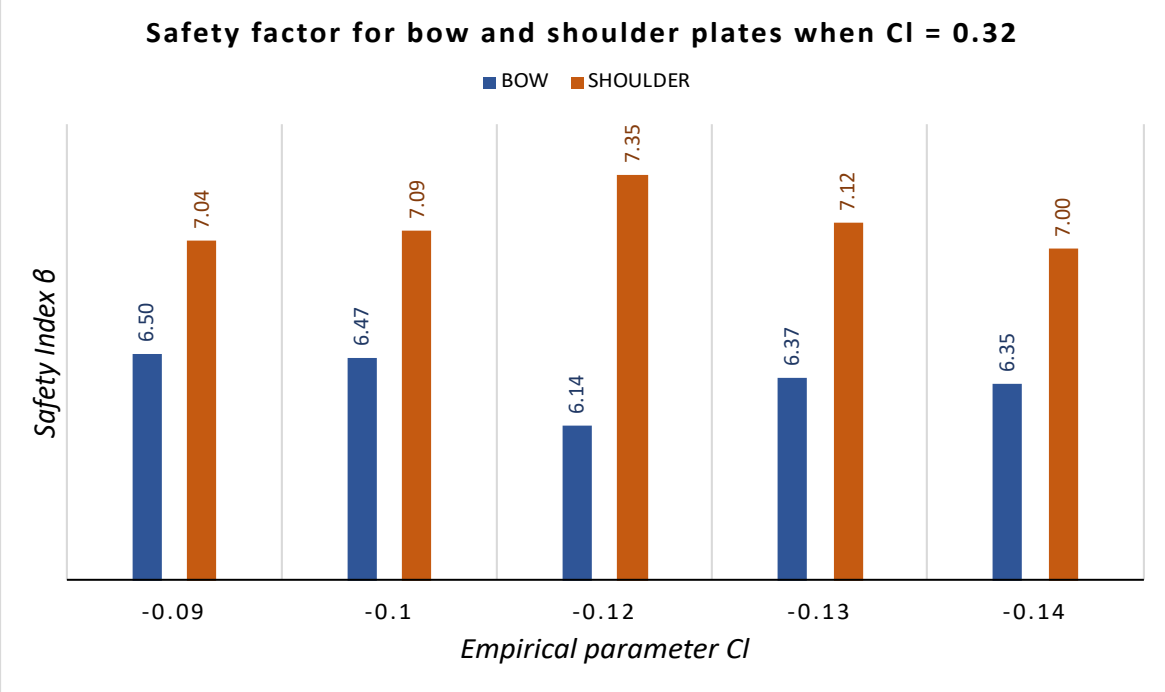

Figure 6. 9 Safety factors for bow and shoulder for C_v values at C_l = 0.32

Case 3: *Influence of C_v parameters at $C_l = 0.35$*

Table 6.8 contains the simulated statistical data and reliability index corresponding to the simulated values of C_v when $C_l = 0.35$ for the bow and shoulder of the ship hull. The result proves that the number of events increased at the bow but fluctuates at the shoulder as the C_v value decreases. The mean of the peak loads and the corresponding standard deviation showed gradual increase in value with minimal variations as the C_v values fall. These are reflected in the nature of the resulting safety index in which the values were very close and with minimal variations. The implication of this is that the variations in the empirical parameter value introduced minimal disparities in the result. Additionally, according to equation 2.1, as the C_v value decreases, the breaking radius is expected to decrease which should invariably reduce the average peak load, but this impact is minimized by the corresponding increase in number of peak loads.

Comparatively, the estimated safety indices for the bow and shoulder plating of the hull as given in Figure 6.10 shows that both hull sections produced same trend of result for the safety index estimation with greater fluctuation observed in the shoulder's result. Also, higher values were obtained with respect to the shoulder which implied lesser susceptibility to failure.

Table 6. 8 Safety indices and probability of failure for C_v parameters at $C_l = 0.35$

		Bow						
C_l = 0.35		No of peaks	N events	Max (kN/m)	Mean (kN/m)	Std. dev. (kN/N)	β	P_f
C_v	-0.09	894	245850	1053.9	820.42	233.26	6.67	1.25E-11
	-0.1	924	254100	1049.6	831.54	245.22	6.40	8.03E-11
	-0.12	1015	279125	1113.7	833.22	245.60	6.36	9.82E-11
	-0.13	1063	292325	1036.7	835.74	242.55	6.40	7.57E-11
	-0.14	1083	297825	1053.9	820.23	252.95	6.21	2.67E-10

		Bow shoulder						
C_l = 0.35		No of peaks	N events	Max (kN/m)	Mean (kN/m)	Std. dev. (kN/N)	β	P_f
C_v	-0.09	331	91025	967.2	485.47	201.57	7.60	1.43E-14
	-0.1	358	98450	864.62	512.53	192.18	7.74	4.98E-15
	-0.12	338	92950	870.62	510.39	218.91	7.17	3.80E-13
	-0.13	410	112750	871.85	492.19	205.09	7.45	4.68E-14
	-0.14	383	105325	894.26	464.88	200.81	7.62	1.30E-14

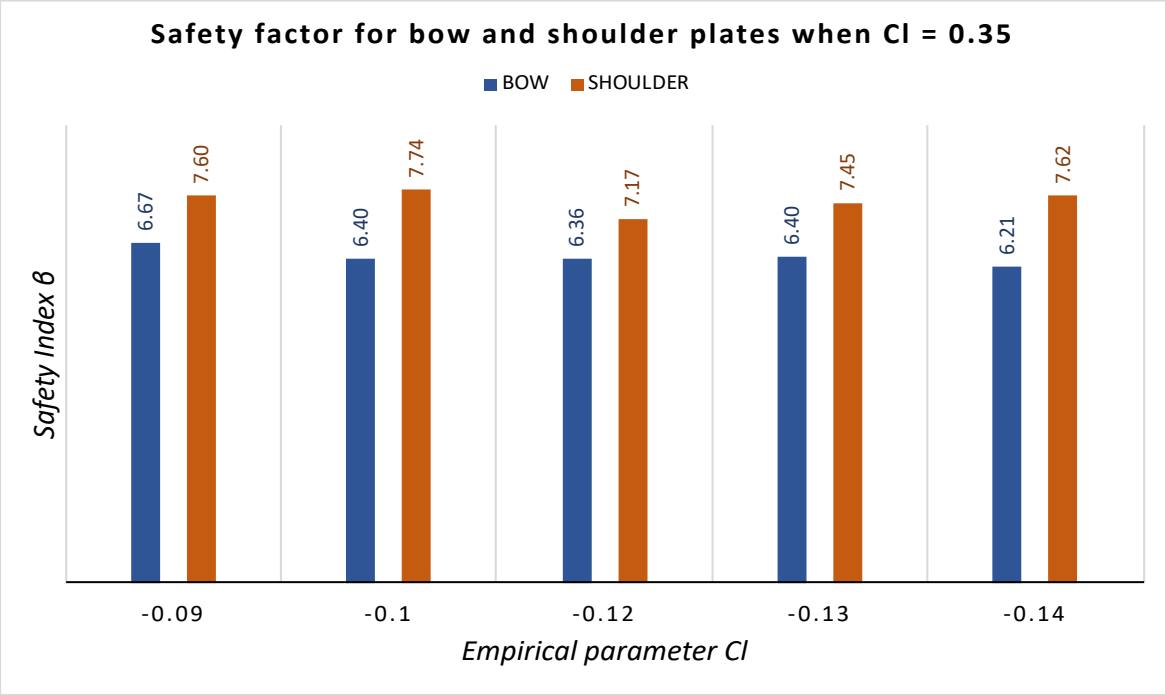

Figure 6. 10 Safety factors for bow and shoulder for C_v values at $C_l = 0.35$

Case 4: *Influence of C_v parameters at $C_l = 0.37$*

The statistical data and reliability indices corresponding to each choice of value for C_v when $C_l = 0.37$ are presented in Table 6.9. According to the simulated result, the number events obtained for

the bow and bow plating were in increasing order as the value of parameter C_v decreases. The simulated maximum ice loads obtained for the bow increases while those corresponding to the shoulder were in random order as the C_v values decrease, only with minimal deviations. Also, the standard deviation and mean values corresponding to the C_v values showed minimal variations as the C_v decreases for both hull sections. The implication of these are reflected in nature of the safety index which are in which there was minimal variations in the magnitudes and less fluctuations in the trends as the C_v values decreases.

Between the results corresponding to the bow and shoulder of the ship hull, same trends were obvious but with more fluctuations shown in the shoulder's result. Also, the greater values obtained for the shoulder proves that the bow plate was more prone to failure than the shoulder across the C_v value.

Table 6. 9 Safety indices and probability of failure for C_v parameters at $C_l = 0.37$

		Bow						
C_l = 0.37		No of peaks	N events	Max (kN/m)	Mean (kN/m)	Std. dev. (kN/N)	β	P_f
C_v	-0.09	777	213675	1032	821.47	248.06	6.41	7.07E-11
	-0.1	862	237050	1065.7	820.05	243.25	6.48	4.53E-11
	-0.12	897	246675	1068.7	817.51	240.34	6.53	3.22E-11
	-0.13	939	258225	1064.8	826.29	242.63	6.46	5.34E-11
	-0.14	960	264000	1086.8	829.84	253.52	6.22	2.47E-10

		Bow shoulder						
C_l = 0.37		No of peaks	N events	Max (kN/m)	Mean (kN/m)	Std. dev. (kN/N)	β	P_f
C_v	-0.09	319	87725	893.29	479.51	194.72	7.78	3.67E-15
	-0.1	219	60225	912.32	515.78	221.46	7.24	2.23E-13
	-0.12	255	70125	870.38	505.53	183.76	8.03	4.72E-16
	-0.13	292	80300	935.96	492.14	228.65	7.04	9.88E-13
	-0.14	341	93775	904.89	486.09	213.06	7.34	1.07E-13

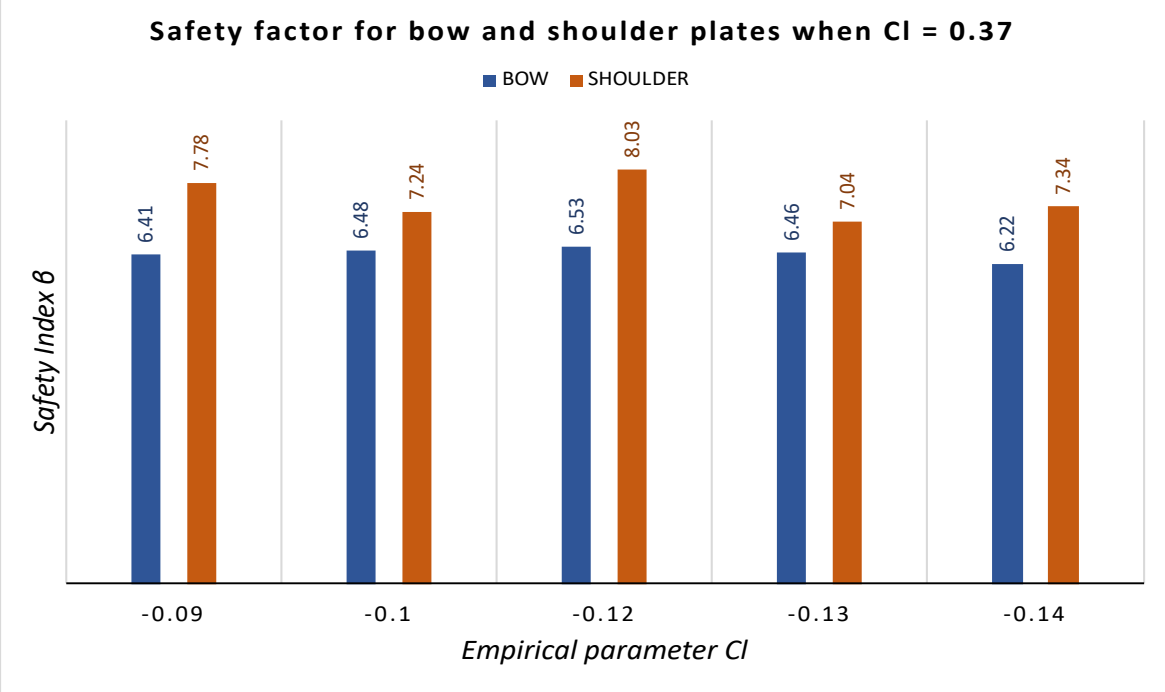

Figure 6. 11 Safety factors for bow and shoulder for C_v values at $C_l = 0.37$

Case 5: *Influence of C_v parameters at $C_l = 0.40$*

Finally, the statistical data and reliability indices obtained from the simulation with C_v values when $C_l = 0.40$ are given in Table 6.10 and Figure 6.12. From the result associated with the bow and shoulder sections of the hull, the number of simulated events increases with decreasing C_v values while the maximum peak loads were in random order relative to the C_v values. Also, the standard deviation and the mean showed gradual variations over the C_v values. The implication of these are reflected in the nature of the safety indices (bow and shoulder) in which the results showed minimal differences across the C_v values. In other words, variations in the C_v values only introduced minimal changes in the resulting safety index for both bow and shoulder of the ship hull. In comparing the results for both sections of the hull as given in Figure 6.12, same trend in the estimated safety index were realized for both hull sections, although with higher fluctuations and greater values obtained at the shoulder. The later simply implied that the bow plating was more susceptible to failure than the corresponding shoulder plating.

Table 6. 10 Safety indices and probability of failure for C_v parameters at $C_l = 0.40$

		Bow						
C_l = 0.40		No of peaks	N events	Max (kN/m)	Mean (kN/m)	Std. dev. (kN/N)	β	P_f
C_v	-0.09	633	174075	1038.8	814.09	250.35	6.45	5.72E-11
	-0.1	685	188375	1008.5	803.16	233.89	6.77	6.34E-12
	-0.12	762	209550	1043.7	831.19	236.69	6.64	1.62E-11
	-0.13	765	210375	1044.3	824.80	246.64	6.44	5.87E-11
	-0.14	808	222200	1039.9	826.33	242.23	6.51	3.70E-11

		Bow shoulder						
C_l = 0.40		No of peaks	N events	Max (kN/m)	Mean (kN/m)	Std. dev. (kN/N)	β	P_f
C_v	-0.09	249	68475	897.88	492.10	213.57	7.41	6.09E-14
	-0.1	224	61600	857.37	493.04	203.31	7.67	8.73E-15
	-0.12	240	66000	910.81	499.83	211.47	7.46	4.41E-14
	-0.13	288	79200	967.78	505.54	226.11	7.07	7.68E-13
	-0.14	287	78925	890.62	468.15	204.22	7.62	1.26E-14

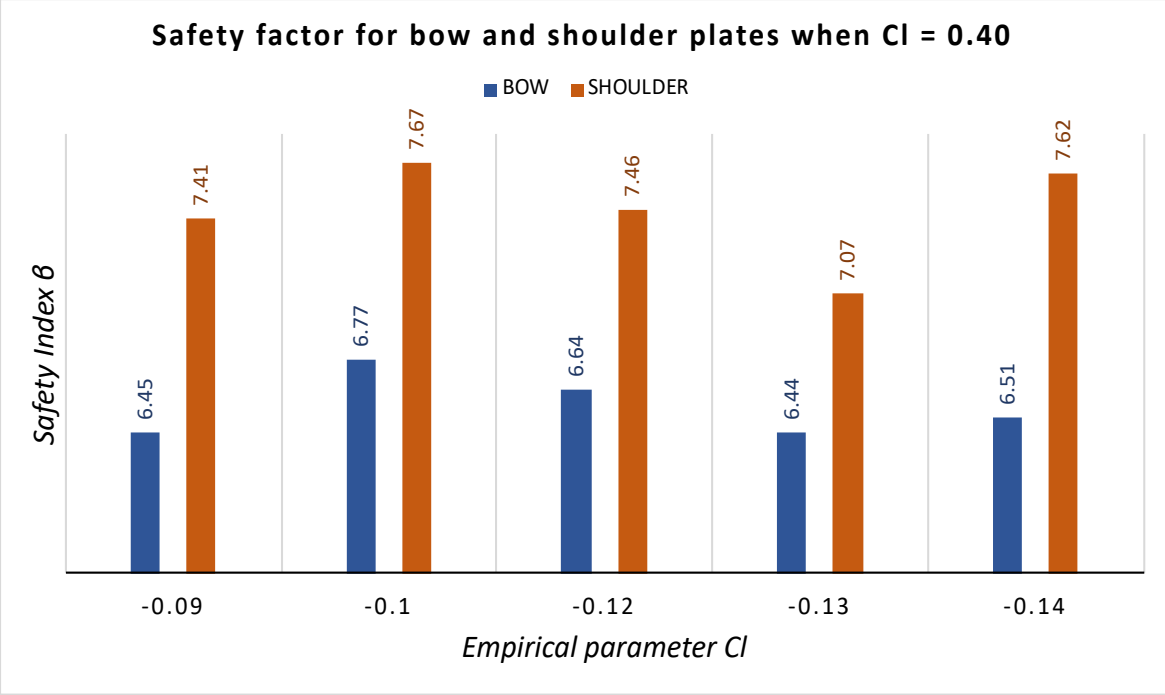

Figure 6. 12 Safety factors for bow and shoulder for C_v values at C_l = 0.40

Summary

From the result obtained in this section, it was obvious that the choice of the C_v values had minimal influences in the estimated reliability and safety index of the ship hull. Across the cases, as the C_v decreases, the number of events rises accordingly while the standard deviations and mean values of the ice loads gradually randomize with minimal variations. The implications of these were observed in the resulting safety index. Across the cases, at the bow and shoulder, the estimated safety index consistently proved to vary minimally as the C_v values changes. In other words, the results showed little sensitivity to the trend of changes in the empirical parameter C_v value. Predictably, the estimated safety index for both hull sections indicated that there is a tendency of convergence in the result if more simulations are carried out since the results resonates some average values.

However, theoretically as expressed in the Equation 2.1, decreasing the value of C_v causes a corresponding decrease in the breaking radius as well as the cusp size resulting from the ice-hull interaction which also causes a corresponding decrease in the value of the imposed ice loads. But a corresponding increase in the number of simulated ice loads eventually minimize the impact of

this changes which then results in a minimal fluctuation in the estimated safety index even as the values of C_v changes. In comparing the results obtained for both hull sections (bow and shoulder), it was obvious that greater numbers of events were continuously realized from the bow simulation than the shoulder. As such the safety indices corresponding to the bow plating were often lower than those of the shoulder; an implication that the bow was more prone to failure than the bow shoulder over the estimated lifetime of the ship.

Finally, across the cases, as we increase the C_l values from 0.30 to 0.40, gradual shift in levels were observed in the corresponding safety indices. As the C_l value changes from 0.30 to 0.40 i.e. case 1 to case 5, there is a predictable shift in the result in the positive direction. This means that the choice of C_l value influences the simulation results in the same order of the C_l value.

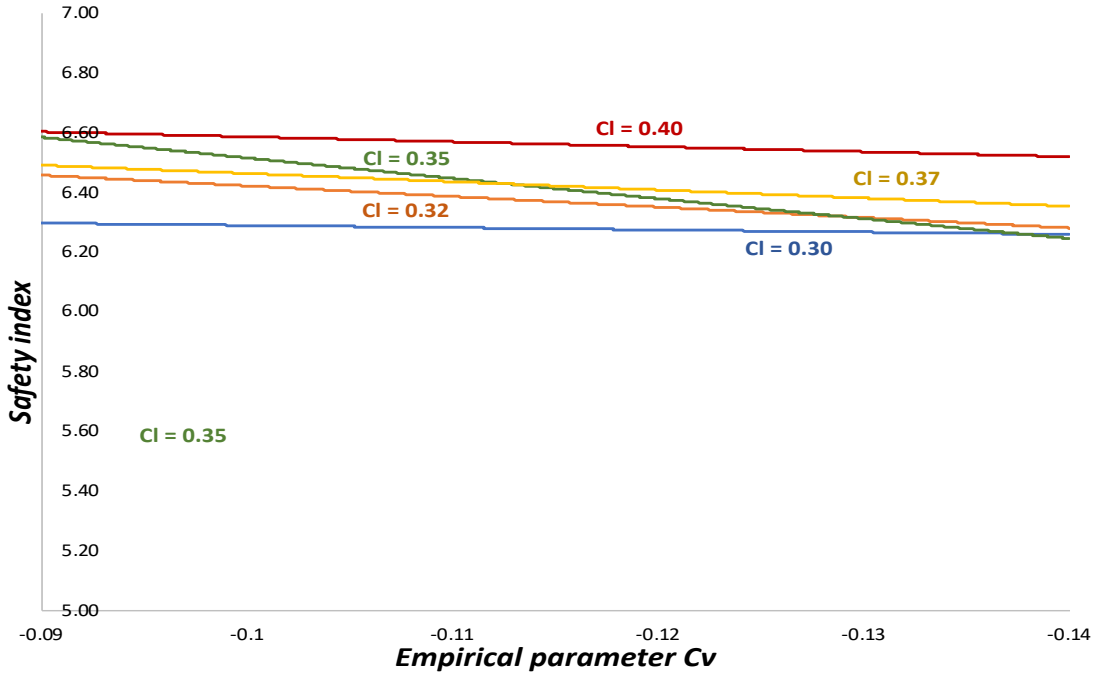

Figure 6. 13 Influence of empirical parameter C_l on the simulation with empirical parameter C_v (Bow)

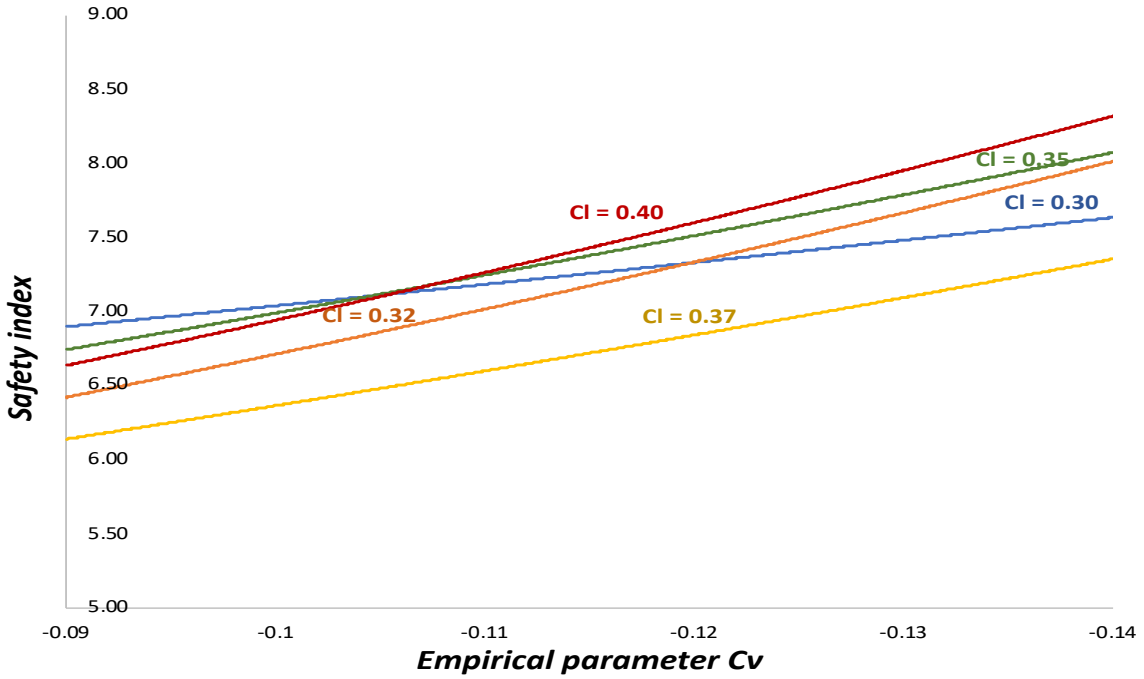

Figure 6. 14 Influence of empirical parameter C_l on the simulation with empirical parameter C_v (Shoulder)

6.1.3 Analysis of safety index and probability of failure for C_f values

This section contains the estimated safety indices and probability of failures obtained from the simulation of selected C_f values. The simulated statistical data and estimated safety indices for the bow and shoulder of the ship hull are given in Table 6.11 – 6.15. In each case, the influence of the C_f values on the simulated number of events as well as the statistical data and reliability indices were analyzed. Also, the observed uncertainties associated with the result are identified as well as the comparison between the bow's and shoulder's result were discussed (Figures 6.15 – 6.19). In addition, the influence of the C_l value, keeping C_v at same level, across the cases was investigated in terms of the nature of safety indices. Finally, the corresponding probability distribution functions for all the cases presented are given in Appendix I-II.

Case 1: *Influence of C_f parameters at $C_l = 0.30$ & $C_v = -0.10$*

The simulated reliability indices and the associated statistical data obtained from the simulation with C_f values when $C_l = 0.30$ and $C_v = -0.10$ are given in Table 6.11. The statistical result generally increases with increasing C_f value. However, with increasing C_f value, the safety index gradually decreases. This simply reflects the influence of the C_f on the ice bending failure as given in Equation 2.18. Since the ice bending failure increases with increasing C_f value then the imposed ice load increases as the C_f rises. As such the safety index of the hull plating drops correspondingly.

Comparing the results, same correlations were realized at the bow and shoulder of the hull with respect to the C_f values with larger safety index obtained at the shoulder (Figure 6.15). Also, the simulated number of events and other statistical data associated with the bow plating were generally higher than those of the shoulder. Again, this associated with the larger ice-hull contact area and larger hull angle at the shoulder which give rise to larger number of ice breaking activities at the bow.

Table 6. 11 Safety index and probability of failure for C_f parameters at $C_l = 0.30$ & $C_v = -0.10$

		Bow						
C_l = 0.30 $C_v = -0.10$		No of peaks	N events	Max (kN/m)	Mean (kN/m)	Std. dev. (kN/N)	β	P_f
C_f	1.5	2087	573925	788.48	483.41	151.32	8.80	6.81E-19
	2	2287	628925	1126.50	632.99	220.51	6.98	1.45E-12
	2.2	2325	639375	1198.20	699.28	242.92	6.38	9.06E-11
	2.5	2526	694650	1288.60	766.35	290.77	5.22	8.91E-08
	3	2371	652025	1632.60	914.65	340.89	4.00	3.14E-05

		Bow shoulder						
C_l = 0.30 $C_v = -0.10$		No of peaks	N events	Max (kN/m)	Mean (kN/m)	Std. dev. (kN/N)	β	P_f
C_f	1.5	1093	300575	803.64	289.48	133.86	9.25	1.08E-20
	2	1474	405350	1119.80	364.71	172.07	8.11	2.55E-16
	2.2	1387	381425	1028.80	413.68	203.28	7.27	1.74E-13
	2.5	1874	515350	1135.40	446.57	237.49	6.30	1.51E-10
	3	1983	545325	1386.20	531.20	268.95	5.39	3.58E-08

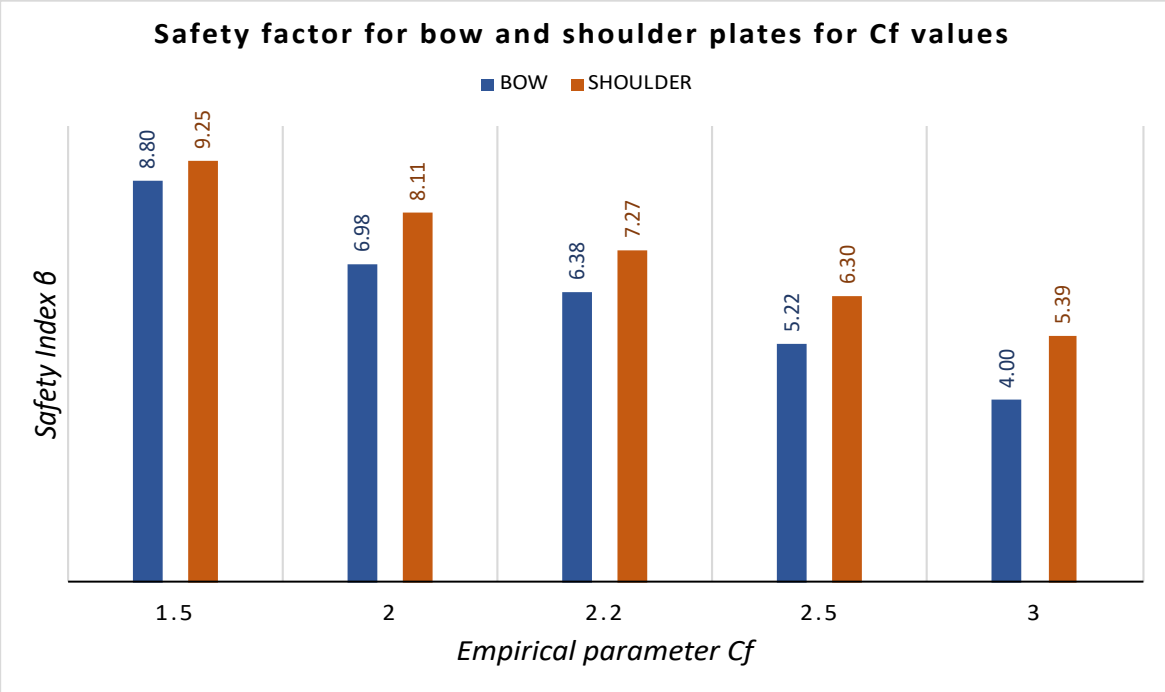

Figure 6. 15 Safety factors for bow and shoulder for C_f values at $C_l = 0.30$ & $C_v = -0.10$

Case 2: *Influence of C_f parameters at $C_l = 0.32$ & $C_v = -0.10$*

Table 6.12 contain the statistical data and reliability indices obtained from the simulation of C_f values when $C_l = 0.32$ and $C_v = -0.10$. The number of events and the estimated statistical data were generally increasing with increasing C_f value. The standard deviation and the mean value showed gradual increase with increasing C_f value. These are reflected in the nature and trend of the corresponding safety index. The estimated safety indices showed clear rise in value as the C_f values rise which simply implies that larger peak loads were imposed on the hull with increasing C_f.

Comparing the results from both sections of the hull, same trends were realized for both the bow and shoulder of the hull but with higher safety index obtained for the shoulder. This indicated that the bow is more susceptible to failure than the shoulder. Obvious reasons for this are the larger number of peak loads generated as well as the larger ice-hull contact area obtainable at the bow compared to the shoulder.

Table 6. 12 Safety index and probability of failure for C_f parameters at $C_l = 0.32$ & $C_v = -0.10$

		Bow						
C_l = 0.32 $C_v = -0.10$		No of peaks	N events	Max (kN/m)	Mean (kN/m)	Std. dev. (kN/N)	β	P_f
C_f	1.5	1938	532950	775.79	488.70	150.47	8.83	5.45E-19
	2	2102	578050	1053.90	647.91	206.37	7.29	1.53E-13
	2.2	2036	559900	1155.20	688.35	245.53	6.38	8.83E-11
	2.5	2197	604175	1266.30	781.77	272.11	5.64	8.71E-09
	3	2399	659725	1592.60	929.18	345.52	3.89	5.11E-05

		Bow shoulder						
C_l = 0.32 $C_v = -0.10$		No of peaks	N events	Max (kN/m)	Mean (kN/m)	Std. dev. (kN/N)	β	P_f
C_f	1.5	952	261800	709.96	285.23	131.57	9.35	4.58E-21
	2	1475	405625	1042.20	382.25	192.59	7.57	1.80E-14
	2.2	1419	390225	989.80	424.37	208.98	7.11	5.79E-13
	2.5	1670	459250	1089.40	452.14	213.12	6.91	2.44E-12
	3	1920	528000	1332.00	528.33	252.16	5.79	3.44E-09

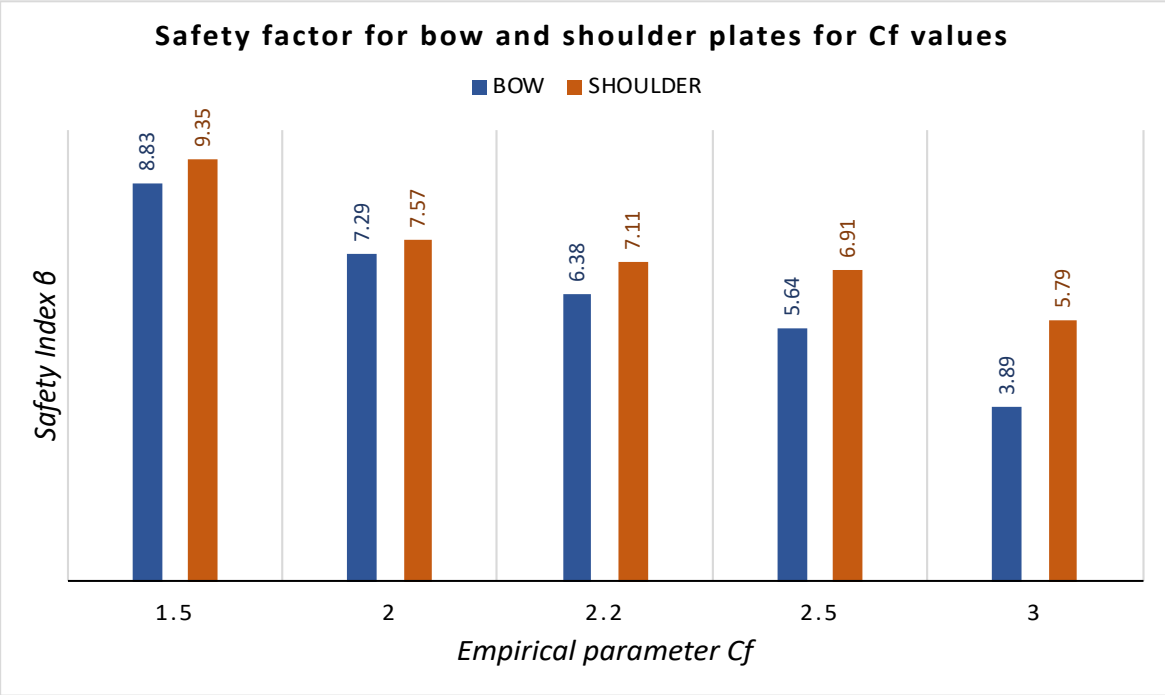

Figure 6. 16 Safety factors for bow and shoulder for C_f values at $C_l = 0.32$ & $C_v = -0.10$

Case 3: *Influence of C_f parameters at $C_l = 0.35$ & $C_v = -0.10$*

Table 6.13 contain the statistical data and reliability indices obtained from the simulation of C_f values when $C_l = 0.35$ and $C_v = -0.10$. According to the result, the number of simulated events as well as the estimated statistical data increases with increasing C_f value. However, the estimated safety index for the bow and shoulder generally decreases with increasing C_f value. The gradual variation in the estimated safety indices at the bow and shoulder were reflections of the gradual rise in the associated standard deviation and mean values. Between the bow and shoulder, more ice-hull interactions were simulated at the bow than the shoulder. The reason for this is as a result of the fact that more ice-hull interactions occurred at the bow than the shoulder due to larger contact area and lower hull angles obtainable at the bow (Su et. al., 2011).

Table 6. 13 Safety index and probability of failure for C_f parameters at $C_l = 0.35$ & $C_v = -0.10$

		Bow						
C_l = 0.35 $C_v = -0.10$		No of peaks	N events	Max (kN/m)	Mean (kN/m)	Std. dev. (kN/N)	β	P_f
C_f	1.5	1570	431750	758.75	486.10	152.82	8.82	5.62E-19
	2	1704	468600	1034.10	635.64	212.10	7.25	2.15E-13
	2.2	1784	490600	1144.50	700.53	233.72	6.66	1.41E-11
	2.5	1936	532400	1365.40	784.62	279.14	5.53	1.61E-08
	3	2077	571175	1608.10	936.24	342.49	3.99	3.27E-05

		Bow shoulder						
C_l = 0.35 $C_v = -0.10$		No of peaks	N events	Max (kN/m)	Mean (kN/m)	Std. dev. (kN/N)	β	P_f
C_f	1.5	916	251900	780.39	315.70	142.56	9.03	8.48E-20
	2	995	273625	817.33	382.25	172.52	8.17	1.60E-16
	2.2	947	260425	962.97	385.88	196.14	7.61	1.38E-14
	2.5	1186	326150	1353.64	466.98	245.96	6.22	2.50E-10
	3	1634	449350	1395.30	600.88	275.78	5.18	1.10E-07

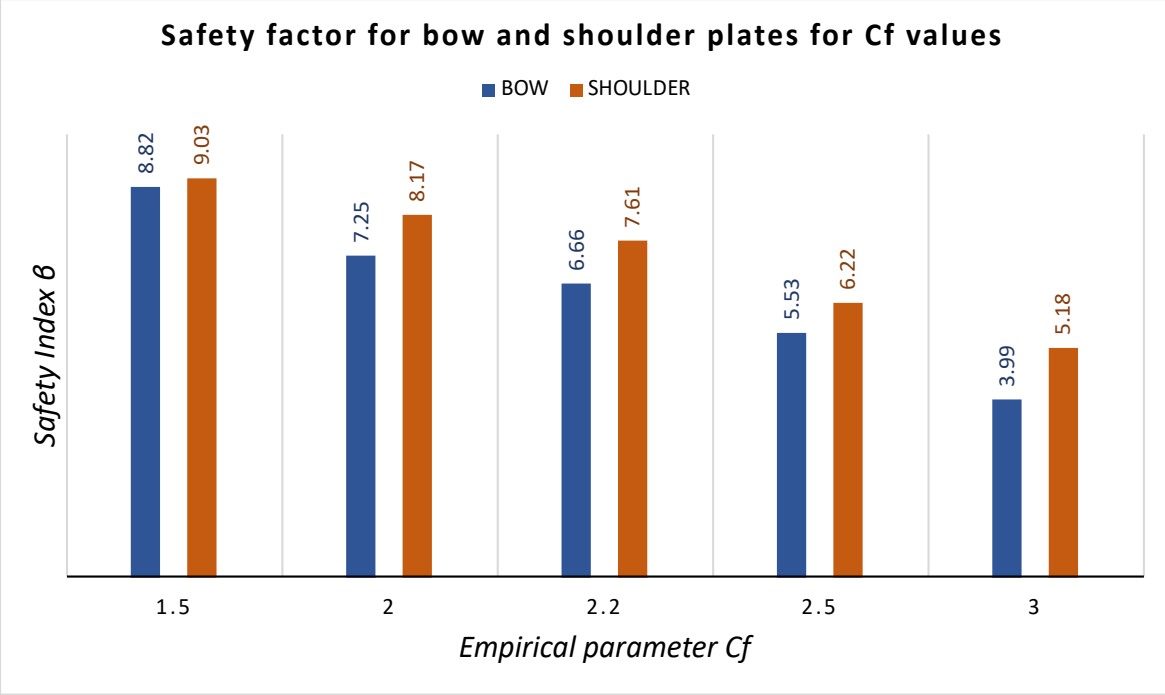

Figure 6. 17 Safety factors for bow and shoulder for C_f values at $C_l = 0.35$ & $C_v = -0.10$

Case 4: *Influence of C_f parameters at $C_l = 0.37$ & $C_v = -0.10$*

Table 6.14 contains the statistical data and reliability indices obtained from the simulation with C_f values when $C_l = 0.37$ and $C_v = -0.10$. Again, the number of events and the corresponding statistical data increase with increasing C_f value while the safety index showed indirect correlations with the rising C_f values. As mentioned in previous cases, the nature of the safety indices were simply the reflections of the influence of the C_f parameter on the ice bearing failure. With increasing C_f, the ice load increases which invariably causes decreasing reliability and safety of the ship hull.

However, the simulated results for the bow were generally higher than those of the shoulder because of the larger contact area and the respective hull angles. According to Figure 6.18, the safety indices obtained from the bow simulation were generally lower than those of the shoulder, implying that the bow plating was more susceptible to failure than the shoulder plating.

Table 6. 14 Safety index and probability of failure for C_f parameters at $C_l = 0.37$ & $C_v = -0.10$

		Bow						
C_l = 0.37 $C_v = -0.10$		No of peaks	N events	Max (kN/m)	Mean (kN/m)	Std. dev. (kN/N)	β	P_f
C_f	1.5	1454	399850	824.66	487.41	152.48	8.84	4.66E-19
	2	1552	426800	1032.10	642.09	206.10	7.39	7.30E-14
	2.2	1619	445225	1134.80	701.46	234.35	6.67	1.28E-11
	2.5	1696	466400	1346.70	782.93	279.64	5.57	1.29E-08
	3	1838	505450	1598.00	924.81	326.49	4.37	6.22E-06

		Bow shoulder						
C_l = 0.37 $C_v = -0.10$		No of peaks	N events	Max (kN/m)	Mean (kN/m)	Std. dev. (kN/N)	β	P_f
C_f	1.5	668	183700	732.19	282.22	143.91	9.13	3.31E-20
	2	902	248050	924.82	414.81	183.13	7.88	1.68E-15
	2.2	1056	290400	973.33	417.18	203.44	7.35	1.03E-13
	2.5	967	265925	1225.80	485.87	241.18	6.37	9.75E-11
	3	1439	395725	1415.20	622.12	302.23	4.61	2.01E-06

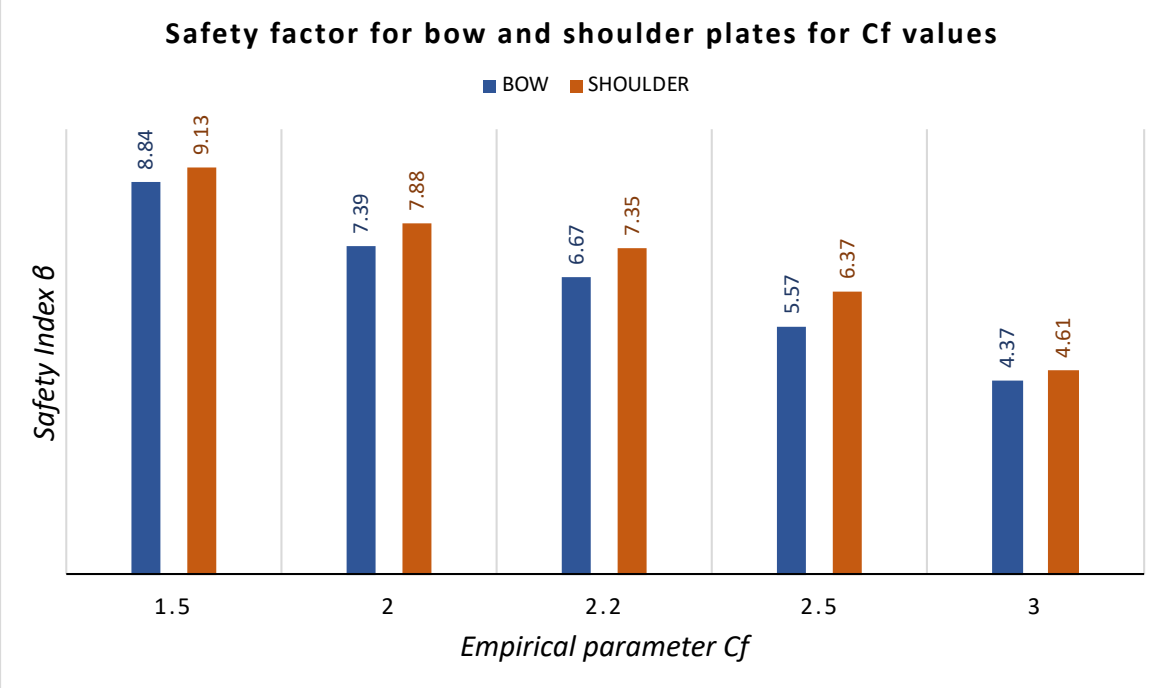

Figure 6. 18 Safety factors for bow and shoulder for C_f values at $C_l = 0.37$ & $C_v = -0.10$

Case 5: *Influence of C_f parameters at $C_l = 0.40$ & $C_v = -0.10$*

Finally, the estimated statistical data and corresponding safety index obtained from the simulation of C_f values when $C_l = 0.40$ and $C_v = -0.10$ are given in table 6.15. Again, the result simply showed that the estimated statistical data increase with increasing C_f while the trend of the safety index showed indirect correlation with parameter C_f. However, between the bow and the shoulder, the simulated results for the bow were much higher than those of the shoulder as more ice-hull interaction occurs at the bow than the shoulder. Also, the safety index obtained for the bow plating were lower than those of the shoulder, implying that the bow was more prone to failure than the shoulder for the period of estimated lifetime of the ship hull.

Table 6. 15 Safety index and probability of failure for C_f parameters at $C_l = 0.40$ & $C_v = -0.10$

		Bow						
C_l = 0.40 $C_v = -0.10$		No of peaks	N events	Max (kN/m)	Mean (kN/m)	Std. dev. (kN/N)	β	P_f
C_f	1.5	1091	300025	775.18	487.76	152.82	8.90	2.91E-19
	2	1264	347600	961.36	647.22	202.64	7.51	2.90E-14
	2.2	1431	393525	1048.3	701.10	235.19	6.69	1.11E-11
	2.5	1387	381425	1219.2	795.26	270.09	5.81	3.04E-09
	3	1625	446875	1444.1	918.13	330.97	4.34	7.05E-06

		Bow Shoulder						
C_l = 0.40 $C_v = -0.10$		No of peaks	N events	Max (kN/m)	Mean (kN/m)	Std. dev. (kN/N)	β	P_f
C_f	1.5	464	127600	737.28	277.25	125.11	9.65	2.38E-22
	2	777	213675	871.56	367.85	172.57	8.26	7.51E-17
	2.2	788	216700	1009.4	416.32	186.68	7.83	2.49E-15
	2.5	806	221650	1021.3	452.92	229.08	6.76	6.68E-12
	3	1237	340175	1425.9	581.04	290.28	5.00	2.83E-07

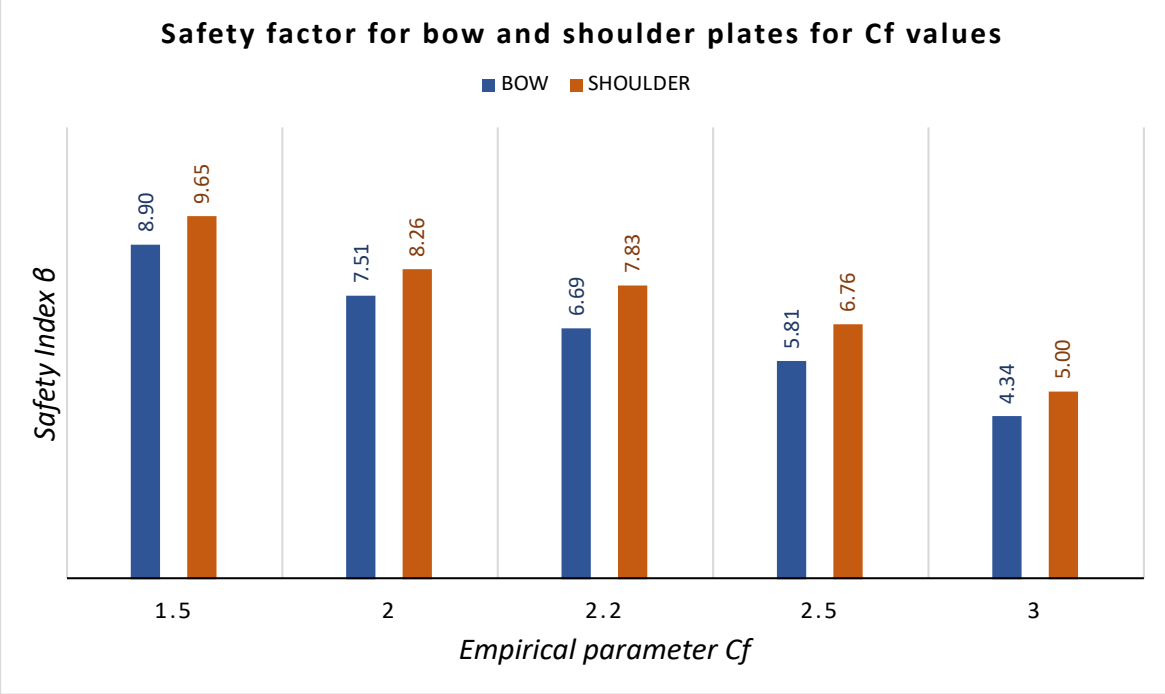

Figure 6. 19 Safety factors for bow and shoulder for C_f values at $C_l = 0.40$ & $C_v = -0.10$

Summary

From the result obtained from this section, it was obvious that the choice of the C_f value influences the estimated reliability and safety of the ship since the coefficient C_f affects the bending failure of the ice. As C_f increases, it was obvious that the number of ice-hull interactions obtained for each simulation case also increases. Also, the statistical data such as the mean and standard deviation increases with increasing C_f value. The implication of this is that the higher the C_f value the higher the variation in the simulated ice bending failure which invariable means larger ice loads are imposed on the hull. As such, the safety and reliability of the hull correspondingly decreases.

Furthermore, the comparison between the bow and shoulder results proved that greater number of events and relatively larger ice loads were realized from the bow simulation with respect to the shoulder. But the safety index associated with the bow were mostly lower than those of the shoulder, which implied that the bow plating was more prone to failure than the corresponding shoulder plating. As we change the C_l value across the cases (Figures 6.20 – 6.21), there was a clear shift in the resulting safety index towards the positive direction at the bow while for the shoulder, same trend was initially realized but a random trend evolved later with higher C_f value.

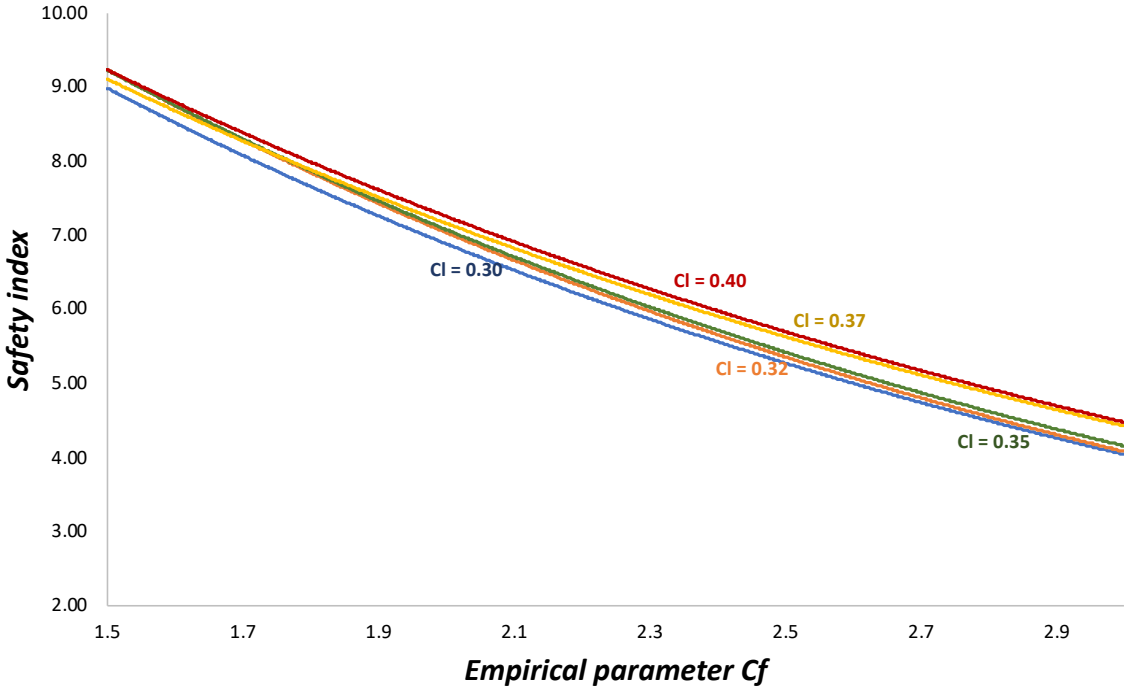

Figure 6. 20 Influence of empirical parameter C_l on the simulation with empirical parameter C_f (Bow)

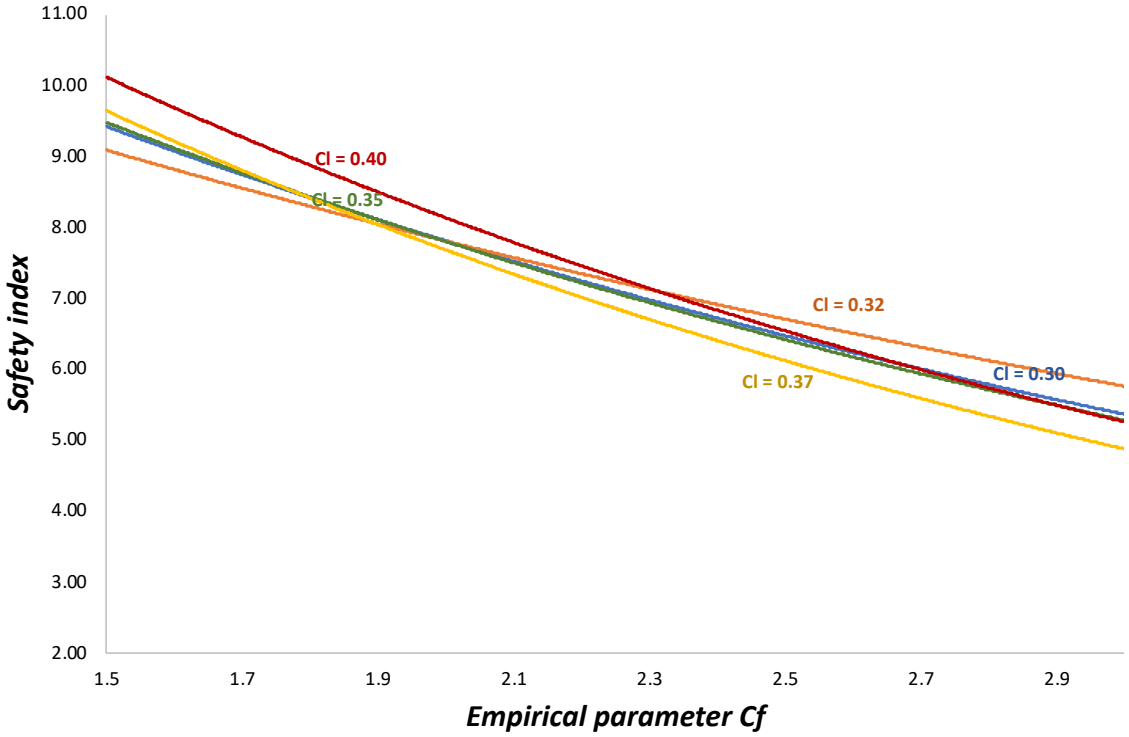

Figure 6. 21 Influence of empirical parameter C_l on the simulation with empirical parameter C_f (Shoulder)

7 Uncertainty Analysis

In the previous chapter, the influence of the empirical parameters on the reliability and safety analysis of the ship hull have been studied under various cases. Also, the resulting statistical data obtained from each simulation were presented and analyzed with respect to the choice of empirical parameter value. In all cases, the results obtained for the bow plate of the hull are often higher than those of the shoulder due to the more frequent event occurring at the bow. As such the safety indices are always lower for the bow than the bow shoulder which established the fact that the bow plating was more prone to failure than the shoulder of the ship hull under same condition.

In general, majority of the results agrees with the breaking radius expression given in Equation 2.1 of Chapter two. According to the expression, increase in the C_l value should cause a corresponding increase in the breaking radius which will in turn results into higher ice loads. The implication of this was decreasing number events. However, these imposed minimal impact on the estimated safety index which showed minimal variation in value and trend across the selected C_l values. An obvious reason been that the impact of the increasing breaking radius and peak loads were simply minimized by the corresponding decrease in the number of ice loads, as clearly shown in the nature and trend of the mean and standard deviations in which minimal variations were obvious.

The results presented in Figure 6.1 – 6.5 validates this relationship. The estimated safety index for the bow and shoulder gradually and consistently randomize with minimal variations as the C_l value increases from 0.30 to 0.40. Also, with respect to same expression (Equation 2.1), the influence of decreasing C_{v} caused a corresponding decrease in the ice breaking radius which invariably resulted in the continuous rise in the number of events and the corresponding imposed ice loads. Again, this caused minimal impact of the resulting safety index. The influence of the reduction in the breaking radius which invariable reduces the imposed ice load was minimized by the rise in the number simulated of peak loads. This is reflected in the minimal variation observed with the mean and standard deviation results. The eventual implication is reflected in the minimal variations observed in the estimated safety index obtained for the bow and shoulder. Finally, the influence of the C_{f} value on the ice bending failure (Equation 2.18) is expressed in the results given in Figure 6.15 – 6.19. Increasing C_{f} value causes a corresponding increase in the ice bending failure which invariably means higher imposed ice loads on the hull plating. Therefore, there will be a corresponding decrease in the safety index value as shown by the declining trend of the safety index for both the bow and shoulder of the ship hull as the C_{f} value increases.

However, in spite of the trend shown by the simulation results with respect to the empirical parameter values, there were some random responses observed in the results. For instance, in the simulation with the C_l and C_v, there were continuous randomness, though at minimal level, in the estimated safety index. Also, the trends in the statistical data were not always smooth but characterized with some deviation, although mostly minimal. These observed variations were indications of the presence of uncertainties suspected to characterize the simulation model performance in predicting ice loads. In addition, it was obvious that there were better predictions at the bow than the shoulder. In most cases, the bow simulation showed good correlations with the empirical parameter while the shoulder sometimes reflects random correlation.

To further establish the suspected uncertainties in the simulation model, we provide a quantitative analysis of the inherent uncertainty based on the coefficient of variation. The uncertainties inherent in each of the parameter cases are quantified based on the magnitude of uncertainty (Suominen, 2018). As mentioned in chapter four, the uncertainties are classified into two categories (Equation 7.1). We start by quantifying the uncertainties associated with the measured data. Table 7.1 contains the estimated coefficient of variation for the estimated safety index for the full-scale

analysis. From the result, it was obvious that the uncertainty associated with the bow is of *high variance* ($\delta_X = 1.12 > 1$) while that of the bow shoulder is of *low variance* uncertainty. In other words, the confidence level for the estimated safety index for the bow shoulder plating was higher than that of the bow plating. Having established and quantified the uncertainties associated with the measured data, we now estimate the corresponding uncertainties for the model data.

$$\begin{cases} \widehat{\delta_X} < 1 & Low\ variance \\ \widehat{\delta_X} > 1 & high\ variance \end{cases} \qquad (7.\ 1)$$

Table 7. 1 COV for estimated safety index associated with full-scale measurement

	Bow	**Shoulder**
Mean	2,41	5,89
Std	2,55	1,72
$\boldsymbol{\delta_X}$	1,06	0,29

7.1 Uncertainty associated with empirical parameter C_l

According to Table 7.2, there were varying uncertainties characterizing the safety index estimations for the bow and bow shoulder across the C_l values. In this section, the uncertainties characterizing each value for the parameter C_l over the selected values of C_v is estimated in terms of COV. For both hull sections, the *COV* were random in trend and magnitude with minimal variations. Based on the result, it was obvious that the simulation with C_l parameter was characterized with low variance uncertainties since $\delta_X < 1$. From Figure 7.1 – 7.2, the safety index across the cases shift randomly with decreasing C_v value for both the bow and shoulder of the ship hull. However, the shoulder is characterized with higher uncertainties relative to the bow.

Table 7. 2 Coefficient of variation for safety index with respect to empirical parameter C_l

C_v		-0.09	-0.10	-0.12	-0.13	-0.14
		Coefficient of variation (Bow)				
C_l	0.3	*0.29*	*0.30*	*0.30*	*0.30*	*0.30*
	0.32	*0.28*	*0.29*	*0.30*	*0.29*	*0.29*
	0.35	*0.28*	*0.29*	*0.29*	*0.29*	*0.31*
	0.37	*0.30*	*0.30*	*0.29*	*0.29*	*0.31*
	0.4	*0.31*	*0.29*	*0.28*	*0.30*	*0.29*

C_v		-0.09	-0.10	-0.12	-0.13	-0.14
		Coefficient of variation (Shoulder)				
C_l	0.3	*0.49*	*0.44*	*0.45*	*0.43*	*0.47*
	0.32	*0.44*	*0.43*	*0.41*	*0.45*	*0.43*
	0.35	*0.42*	*0.37*	*0.43*	*0.42*	*0.43*
	0.37	*0.38*	*0.43*	*0.36*	*0.46*	*0.44*
	0.4	*0.43*	*0.41*	*0.42*	*0.45*	*0.44*

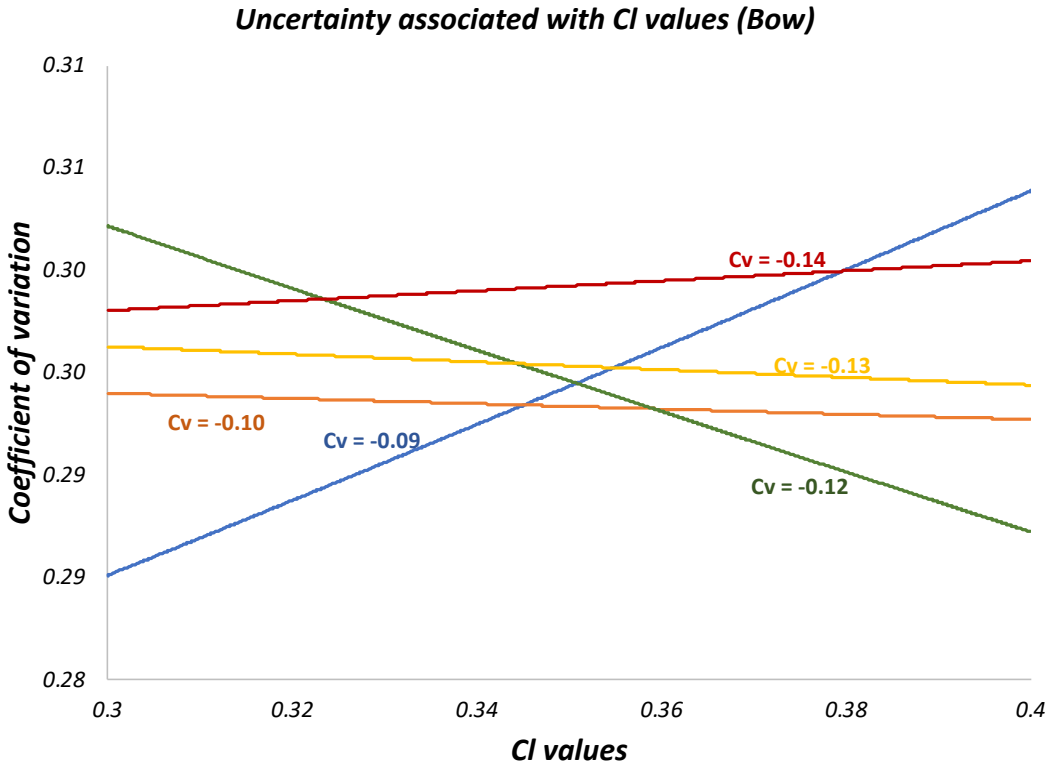

Figure 7. 1 Uncertainties in empirical parameter Cl simulation (Bow)

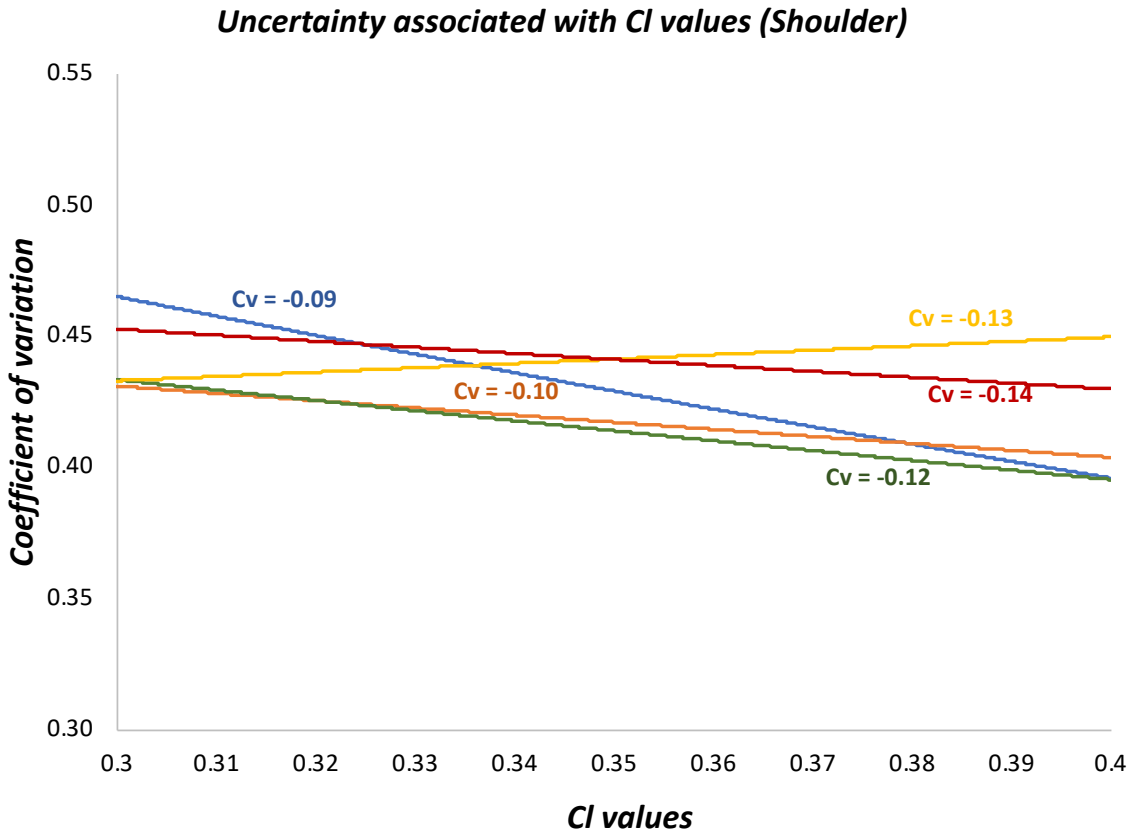

Figure 7. 2 Uncertainties in empirical parameter Cl simulation (Shoulder)

7.2 Uncertainty associated with empirical parameter C_v

The uncertainties characterizing each of C_v value estimated in terms of their coefficient of variation are given in Table 7.3. According to Table 7.3, the COVs estimated for the Bow and shoulder reflects *low variance uncertainty* as the coefficient of variation was generally less than one i.e. $\delta_X < 1$. Also, the results showed mostly direct correlations with the C_v value at the bow but at the shoulder, random correlations with the C_v values were obvious. However, as the value of the parameter C_l increases across the cases (Figure 7.3 – 7.4), the uncertainties shift randomly for both hull sections. In addition, between the bow and the shoulder, the uncertainties characterizing the shoulder were obviously higher than those of the bow in terms their respective coefficient of variation. As such, the model's prediction with the bow showed better results than the shoulder.

Table 7. 3 Coefficient of variation for safety index with respect to empirical parameter C_v

C_l		0.30	0.32	0.35	0.37	0.40
		Coefficient of variation (Bow)				
C_v	-0.09	*0.29*	*0.28*	*0.28*	*0.30*	*0.31*
	-0.1	*0.30*	*0.29*	*0.29*	*0.30*	*0.29*
	-0.12	*0.30*	*0.30*	*0.29*	*0.29*	*0.28*
	-0.13	*0.30*	*0.29*	*0.29*	*0.29*	*0.30*
	-0.14	*0.30*	*0.29*	*0.31*	*0.31*	*0.29*

C_l		0.30	0.32	0.35	0.37	0.40
		Coefficient of variation (Bow)				
C_v	-0.09	*0.44*	*0.47*	*0.42*	*0.41*	*0.43*
	-0.1	*0.44*	*0.43*	*0.37*	*0.43*	*0.41*
	-0.12	*0.45*	*0.41*	*0.43*	*0.36*	*0.42*
	-0.13	*0.43*	*0.45*	*0.42*	*0.46*	*0.45*
	-0.14	*0.47*	*0.43*	*0.43*	*0.44*	*0.44*

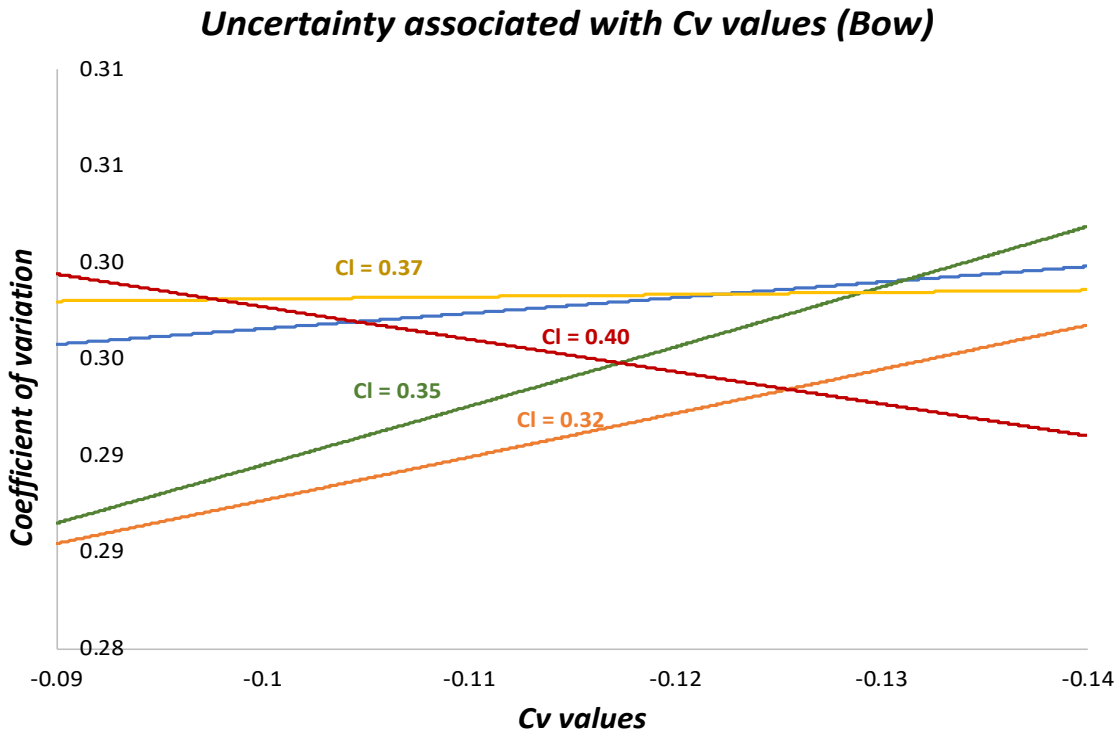

Figure 7. 3 Uncertainties in empirical parameter Cl simulation (Bow)

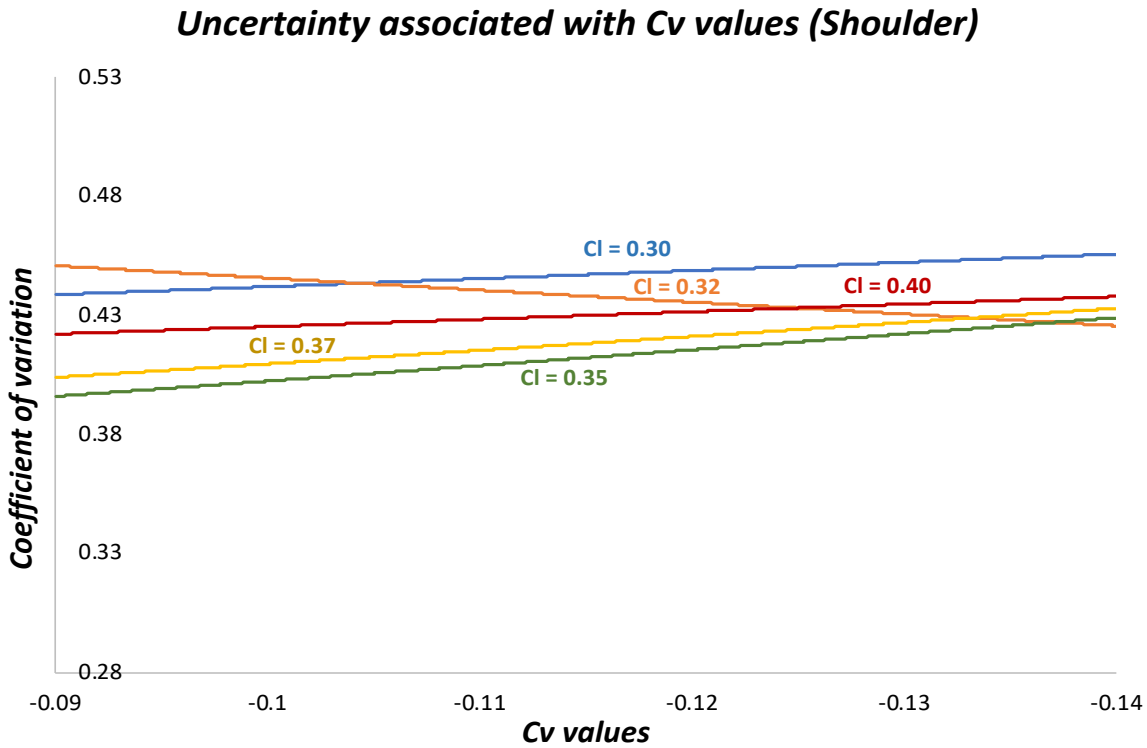

Figure 7. 4 Uncertainties in empirical parameter Cl simulation (Shoulder)

7.3 Uncertainty associated with empirical parameter C_f

The coefficient of variations estimated for the bow and shoulder simulation for the empirical parameter C_f values are presented in Table 7.4. The result obtained for the bow reflects direct correlation between the uncertainties and the C_f values, although with minimal deviations. On the

other hand, the shoulder results showed random correlations with the C_f values. Also, it was obvious that the uncertainties associated with shoulder were higher compared to those of the bow. However, low variance uncertainties were realized in all the cases considered i.e. $\delta_X < 1$ which simply means that the uncertainties were within acceptable domain. Furthermore, according to Figure 7.5 – 7.6, the estimated uncertainties for the bow shifted in a diminishing manner as the C_l value rises but random order were obtained for the shoulder, although with minimal variations.

Table 7. 4 Coefficient of variation for safety index with respect to empirical parameter C_f

C_l		0.30	0.32	0.35	0.37	0.40
$C_v = -0.10$		*Coefficient of variation (Bow)*				
C_f	1.5	*0.31*	*0.31*	*0.31*	*0.31*	*0.31*
	2	*0.35*	*0.32*	*0.33*	*0.32*	*0.31*
	2.2	*0.35*	*0.36*	*0.33*	*0.33*	*0.34*
	2.5	*0.38*	*0.35*	*0.36*	*0.36*	*0.34*
	3	*0.37*	*0.37*	*0.37*	*0.35*	*0.36*

C_l		0.30	0.32	0.35	0.37	0.40
$C_v = -0.10$		*Coefficient of variation (Shoulder)*				
C_f	1.5	*0.46*	*0.46*	*0.45*	*0.51*	*0.45*
	2	*0.47*	*0.50*	*0.45*	*0.44*	*0.47*
	2.2	*0.49*	*0.49*	*0.51*	*0.49*	*0.45*
	2.5	*0.53*	*0.47*	*0.53*	*0.50*	*0.51*
	3	*0.51*	*0.48*	*0.46*	*0.49*	*0.50*

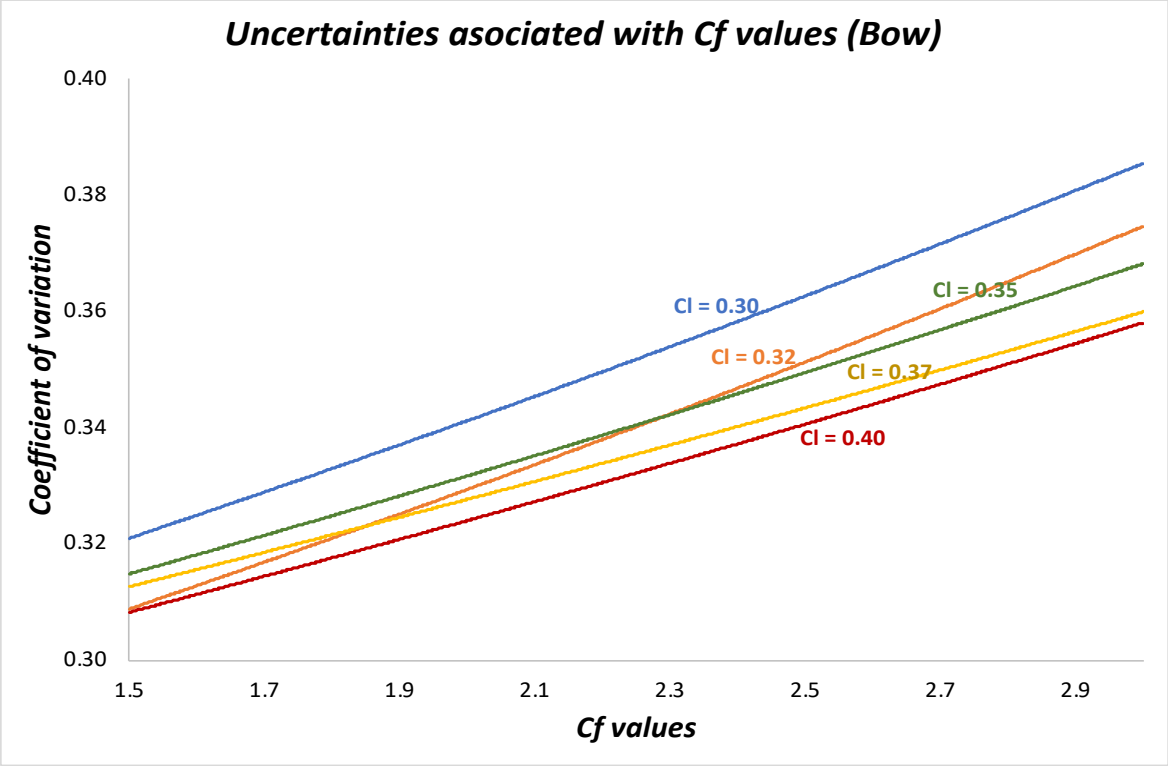

Figure 7. 5 Uncertainties in empirical parameter Cl simulation (Bow)

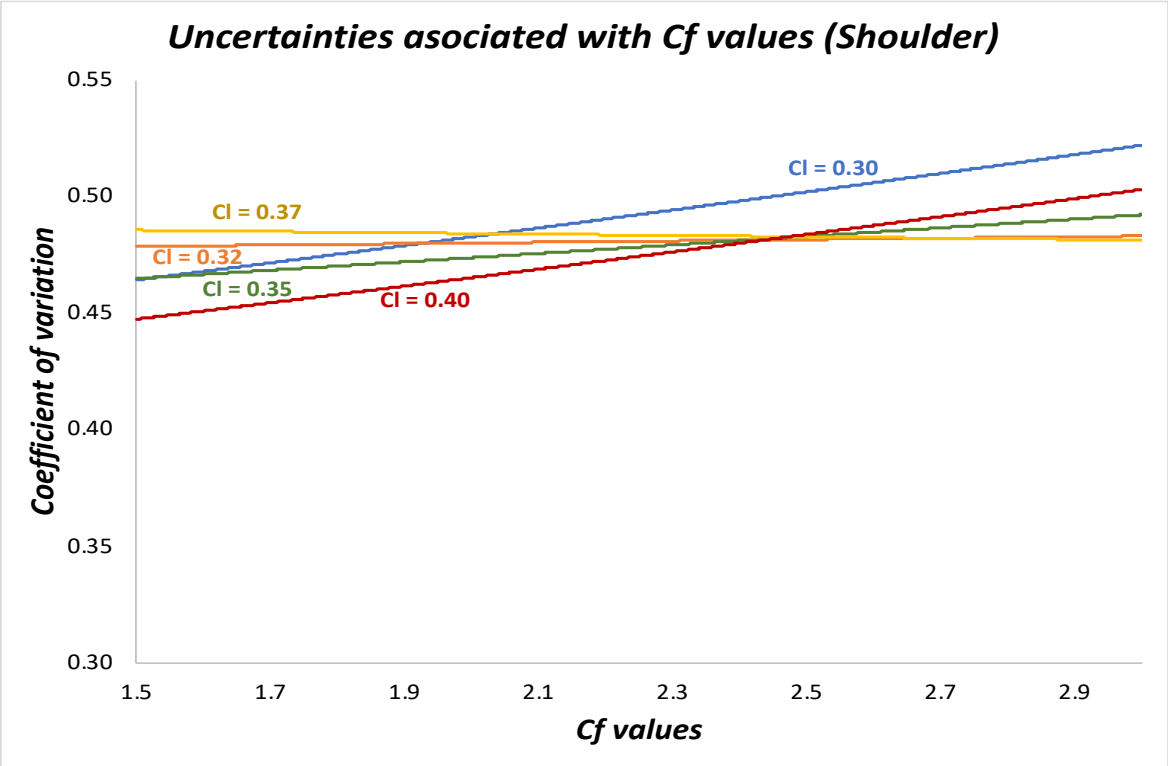

Figure 7. 6 Uncertainties in empirical parameter Cf simulation (Shoulder)

7.4 Discussion

In this chapter, the inherent parameter uncertainties estimated in terms of the coefficient of variation *COV* were discussed. According to the results obtained for all the cases, it was established that there were obviously existing uncertainties in the ice model's predictions, although with minimal variations. The suspected uncertainties associated with the model parameters were estimated about the local average of the simulated ice loads for each parameter cases. The results were categorized as either low variance or high variance uncertainty depending on whether the resulting COVs were lesser or greater than 1. For the cases investigated for the C_l and C_v, the estimated uncertainties showed random order correlations with respect to the empirical parameter values while for the C_f case, the uncertainties evaluated showed an increasing order of magnitude with increasing C_f value. However, across the cases studied for the empirical parameters C_l and C_v, there was random shift in results as the fixed empirical parameter value (C_v and C_l respectively) changes while in the C_f case, a diminishing order was obtained for the bow and a random order for the shoulder as the C_l value rises.

In general, low variance uncertainties were obtained across all the cases considered for the empirical parameter simulation. As shown in section 7.1 – 7.3, the coefficient of variation estimated for empirical parameter values corresponded to low variance values i.e. $\delta_X < 1$, which implied that the uncertainties inherent in the model simulations were minimal. In addition, the bow simulation consistently showed lower uncertainties compared to the shoulder's simulation which also proved that better predictions were realized at the bow. Furthermore, the influence of the fixed parameters when estimating uncertainty for one parameter were also investigated. For the C_l cases, the influence of C_v showed that the uncertainties simply shifted in a random order as the C_v value decreases for the bow and shoulder. Likewise, for the C_v cases, the observed trend simply reflected a random order of magnitude as the value of C_l increases across the cases, while for the C_f cases, the evaluated uncertainties increase with increasing C_l value for the bow but in a random order for the shoulder.

8 Conclusion and recommendation

The study presented in this thesis is a risk-based approach in establishing the influence of parameter uncertainties in a typical ice prediction model performance with respect to the predicted ice loads. The model considered in this thesis was designed in line with the S.A. Agulhas II ship hull. The ice prediction model estimates the ice loads emerging from the ice-hull interaction in an idealized ice field (Su, et al., 2010). Series of ice loads resulting from such interactions over a set period were simulated for various analysis. However, based on the model design which consists of three major empirical parameters (C_l, C_v & C_f) representing certain phenomenon, there was suspicion for inherent uncertainties in the model performance.

In light of this, this study aimed to establish the presence of the uncertainties characterizing the model with respect to the applied empirical parameters and to quantify the extent of their influence on the model's predictions with respect to the long-term reliability and safety analysis of the ship hull. For confidence of application, it was necessary to quantify the inherent uncertainties and their respective influence on the model performances when predicting ice loads. For this reason, the uncertainties were numerically quantified in terms of coefficient of variation so as to determine the extent of how much they influence the performance of the model with respect to long-term reliability and safety estimation of the ship hull.

For this study, the plastic structural design method developed by Hayward (Hayward, 2001) was applied to determine the structural responses of the ship hull with plate deflection as the serviceability limit. The imposed deflection was determined from an accident database gathered during the winters between 1984 to 1987 for ships navigating regularly in the Baltic Sea (Kujala, 2015). Also, since the model design was based on the S. A. Agulhas II ship hull configuration, the polar code PC5 plate requirements were used in determining the necessary hull response distribution. For the bow and bow shoulder, the steel grade for the plate were of extra high strength steel with thicknesses of 28mm and 26mm respectively. Also, traversely framed structure was idealized such that the plate sections considered at the bow and bow shoulder were located between specific frames. In addition, second level reliability analysis approach (Sipes, 1990) was applied in this study. The safety index and corresponding probability of failure were estimated as the difference in the long term probability distributions of the ice loads and the corresponding hull responses. The safety indices estimated for all the cases studied formed the basis for the uncertainty analysis in this thesis.

In each case study, the nature of the estimated safety indices with respect to the choice of empirical parameter values reflected the relationship expressed in the fundamental principles given by Equations 2.1 and 2.18. As depicted in Equation 2.1, the influence of the empirical parameters C_l and C_v on the ice breaking radius R were studied in sections 6.1.1 & 6.1.2. The performance of the model as the C_l and C_v changes were studied for the bow and shoulder of the idealized ship hull. Also, the influence of the C_f parameter on the ice bending failure was investigated for five carefully selected values (Section 6.1.3) in the vicinity of literature values (Quan, et al., 2015). Although the results obtained for the parameters showed very close agreement with the underlying ice-hull interaction processes but few variations observed in the results indicated the presence of uncertainties. Since visual observations of these variations were not sufficient, further uncertainty analysis were carried out to quantify the magnitude of such variations and to establish the extent of their influence on the model's performance in terms of the ice loads for various parameter values.

In the first stage of the analysis, the reliability and safety index obtained for the bow and bow shoulder plates were estimated. Next, the uncertainties inherent in the estimated safety indices

were quantified in terms of the coefficient of variations. The simulated statistical data, mean and standard variation, obtained in each case were applied in evaluating the coefficient of variations in accordance with Equation 3.14. The coefficient of variations evaluated for the cases reveals the presence and quantity of uncertainties in the ice model performance. Across the cases, the result showed that low variance uncertainties were dominant. Also, the influence of other parameters when investigating a single parameter revealed how the uncertainty changes from case to case.

In general, there were some agreements between the results from this thesis and some existing results in terms of the nature of the ice breaking process and the predicted ice loads (Su, 2011) (Quan, 2015). In all the cases studied for each empirical parameter, the trend of estimated safety indices showed good correlations with the empirical parameter values. Although some randomness was observed in the result but there were minimal variations in the safety index results. In most cases, random correlations between the estimated safety indices and the applied parameter values occurred except for the cases for parameter C_f in which there was obvious indirect correlations with the C_f values. In addition, the estimated safety indices for the bow plating were in most cases lower compared to the shoulder which simply implied that the shoulder plating were less prone to failure than the bow plating for a given estimated period. Clearly, this justified the presence of higher and more peak loads at the bow than at the shoulder due to the larger number of simulated events and greater ice-hull contact area (Su, et al., 2014).

Based on these results, the suspicion that the model's performance could be affected by the inherent uncertainties emerging from the choice of applied empirical parameters ($C_l, C_v\ and\ C_f$) values was established. Although the uncertainties were within acceptable range (mostly of low variance), it is believed that better or improved performance can be achieved from the model's prediction if the influences of the empirical parameters were minimized or totally eliminated by replacing them with appropriate and provable mathematical expressions. The inclusion of mathematical expressions or development of improved ice prediction approaches will help to create uniformity in research results and minimize the emerging variations irrespective of the application areas. However, the study revealed that increasing the simulation time could introduce further improvement in the results. With longer simulation time, a greater number of events will be simulated, and more ice loads obtained. This is expected to minimize the variation in the results and provide a reliable average peak load which is important in estimating the safety index. In this study, improved simulation time was achieved by simply increasing the ice field until satisfactory results was obtained and this brought about considerable improvements in the entire results.

Finally, the result obtained in this study has been very informative and revealing. The study established the presence of inherent uncertainties characterizing the model's performance in relation with the empirical parameters. However, further study on this topic is highly recommended for improved results. For future studies, it is recommended that varying ice conditions i.e. ice thickness, be considered for more robust analysis. In this study, only a single ice condition was selected for analysis. Ice thickness $h_i = 0.5m$ offered better simulation and stability for the model based on preliminary analysis on various ice conditions. Also, only a forward motion was considered with no form of turning or maneuverability. As such, only the bow and the bow shoulder area of the hull were realistic for this study leaving out the stern since no feasible ice breaking is expected at the stern.

Furthermore, large amount of ice loads will be necessary to minimize other possible uncertainties that could emerge as a result of insufficient simulation time or even computing errors. In this regard, more simulation time should be ensured to generate more ice loads sufficient enough to minimize other possible sources of errors. Finally, the amount of safety indices data analyzed for

uncertainties were considered less sufficient for such a sensitive analysis as this, therefore more parameter values should be considered which will invariably increase the safety index and failure probabilities in numbers and in turn add more improvements to the results (Suominen, et al., 2016).

References

Andres, K. (2016). *Analysis of Structural Safety of Ice-going Vessels in the Arctic and Antarctic.* Espoo: Aalto University.

Bertram, H., Schneekluth, V., (1998). *Ship Design for Efficiency and Economy.* Great britain: Butterworth-Heinemann, Linacre House, Jordan Hill, Oxford OX2 8DP, 225 Wildwood Avenue, Woburn, MA 01801-2041.

Brown, A. J. (2001). Collision scenarios and probabilistic collision damage. *Marine Structures*, 335-364.

Cesnauskis, V. (2006). Estimation of expected cargo oil outflow from tanker involved in casualty. *Transportation, XXI*, 293-300.

Daley, C., Jukka, T., Riska, K., (1998). The role of discrete failures in local ice loads. *Cold Region Science and Technology, 27*(3), 197-211.

Enkvist, Ernst. (1972). *On the Ice Resistance Encountered by Ships Operating in The Continuous Mode of Icebreaking.* Helsinki, Finland: The Swedish Academy of Engineering Science in Finland.

Faber, M. H. (2009). *Risk and Safety in Engineering.* Zurich: Swiss Federal Institute of Technology, Zurich.

Goerlandt, Floris. (2017). *Marine risk and safety (Lesson note).* Espoo: Aalto University.

Goerlandt, F., Montewka, J., (2015). A framework for risk analysis of maritime transportation systems: A case study for oil spill from tankers in a ship–ship collision. *Safety science*, 42-66.

Hayward, R. C., (2001). *Plastic Response of Ship Shell Plating Subjected to Loads of Finite Height.* Hamburg: National Library of Canada.

Jian, H., Li, Zhou., (2014). *Experimental and numerical study on ice resistance for ice breaking vessels. Aker Solutions, Fornebu, Norway.* China: 1College of Shipbuilding Engineering, Harbin Engineering University, Harbin, China.

Kotisalo, K., Kujala, P., (1998). *Ice load measurements onboard MT Uikku.* Espoo, Finland: Helsinki University of Technology, Ship.

Kristensen, H. O., (September 2010). *Determination of Regression Formulas for Main Dimensions of Tankers and Bulk Carriers based on IHS Fairplay data.* Denmark: Technical University of Denmark.

Kujala, P., (1994). *On the Statistics of Ice Loads on Ship Hull in the Baltic.* Espoo: Helsinki University of Technology.

Kujala, P., (2008). Reliability of ice-strengthened shell structures of ships navigating in the Baltic Sea. *Journal of Structural Mechanics, 41*(2008), 108-118.

Kujala, P., (2015). Maximum ice induced loads on ships in the Baltic. (2015).

Kujala, P. S. (2009). Statistics of Ice Loads Measured on MT Uikku in the Baltic. Luleå, Sweden: Helsinki University of Technology.

Kuuliala, L., (2015). *Feasibility study of a semi-empirical simulation model for level ice breaking.* Espoo Finland: Aalto University.

Laracy, J. R. (2006). A systems-theoretic accident model applied to biodefense. *Defense & Security Analysis, 22*, 301-310.

Leveson, N. (2012). *Engineering a safer world - Systems theory applied to safety.* Cambridge, MA: MIT Press.

Li, F. (2016). *Evaluation of a semi-empirical numerical method for level ice breaking.* Espoo Finland: Aalto University.

Li, F., Goerlandt, F., Kujala, P., Lehtiranta, J., & Lensu, M. (2018). *Evaluation of selected state-of-the-art methods for ship transit simulation in various ice conditions based on full-scale measurement*. Cold Regions Science and Technology, 151, 94-108.

Lindqvist, G. (1989). A straightforward method for calculation of ice resistance of ships. *Proceedings of POAC*, 722-735.

Liu, J., Lau, M., Williams, F. M., (2008). Numerical Implementation and Benchmark of Ice-Hull Interaction Model for Ship Manoeuvring Simulations. Vancouver, British Columbia, Canada: NRC Publications Record / Notice d'Archives des publications de CNRC.

Michael L., Jian, C. L., Ahmed, D., Mary, W. F., (2004). Preliminary results of ship maneuvering in ice experiments using a planar motion mechanism. Proceedings of the 17th International IAHR Symposium on Ice. Saint Petersburg, Russia: International Association of Hydraulic Engineering and Research.

Nguyen, D. T., Sorbo, A. H., Sorensen, A. J., (2009). Modeling and control of dynamic positioned vessels in level ice. . *Proceedings of 8th Conference of Manoeuvering and Control of Marine Craft (MCMC'2009).*

Pluta, P. J. (2003). *Evaluation of accidental oil spills from bunker tanks (PHASE I).* United State: Ship structure committee.

Quan, Z., Heather, P., (2015). Numerical investigations of ship-ice interaction and maneuvering performance in level ice. *Cold Region Science and Technology*(2015), 36-49.

Riska, K. (1987). On the Mechanics of Ramming interaction between a ship and a massive ice Floe. *Technical research center of Finland*, 86.

Robert, R. S., James, F. R., (2013). The principles and practice of statistics in biological research. *Biometry, 41*, 776.

Sipes, J. D., Haller, H. T., Liu, D., (1990). *An Introduction to Structural Reliability Theory.* United state: Ship structural committee.

Sodhi, D. (1988). Ice-induced Vibration of Structures. *Proc IAHR Ice Symposium*, (pp. 625-657). Sapporo, Japan.

Su, B. (2011). *Numerical Pridiction of Global and Local Ice Loads on Ships.* Norwegian University of Science and Technology.

Su, B., Riska, K., Moan, T., (2010). A numerical method for the prediction of ship performance in level ice. *Cold Region Science and Technology, 60*(2010), 177-188.

Su, B., Riska, K., Moan, T., (2011). Numerical Simulation of local ice loads in uniform and randomly varying ice condition. *Cold Region Science and Technology, 65*(2011), 145-159.

Su, B., Roger, S., Tor, B., (2014). Numerical assessment of a double.acting offshore vessel's performance in level ice with experimental comparison. *Cold Regions science and Technology*(2014), 96-109.

Tan, X. Riska, K., Moan, T., (2014). Effect of dynamic bending of level ice on ship's continuous-mode icebreaking. *Cold Regions Science and Technology.*

Timco, G. (1986). Indentation and Penetration of Edge-based Freshwater Ice Sheet in Brittle Range. *International Offshore Mechanics and Arctic Engineering Symposium. IV*, pp. 444-452. New York: ASME.

Vainio, J., Lumiaro, R., (2014). *ILMATIETEEN LAITOS*. Retrieved April 4, 2018, from http://portal.liikennevirasto.fi/sivu/www/f/liikenneverkko/liikennejarjestelma/tavaraliikenne

Wang, S., (2001). *A Dynamic Model for Breaking Pattern of Level Ice by Conical Structures* (1st ed.). Espoo: Finnish Academy of Technology.

Weeks, W., (2010). *On sea ice.* Fairbanks: Alaska, University of Alaska Press.

APPENDIX I Probability distributions for reliability and safety analysis of S.A. Agulhas II ship hull model (Bow)

A. Pdf for selected C_l values

a) C_l values simulation with $C_v = -0.09$

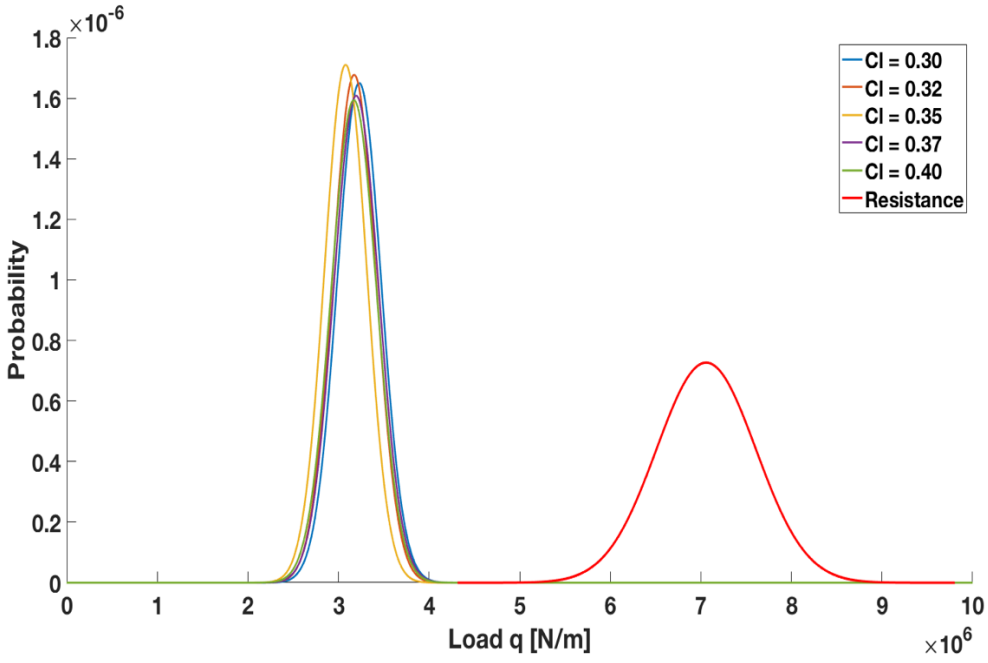

b) C_l values simulation with $C_v = -0.10$

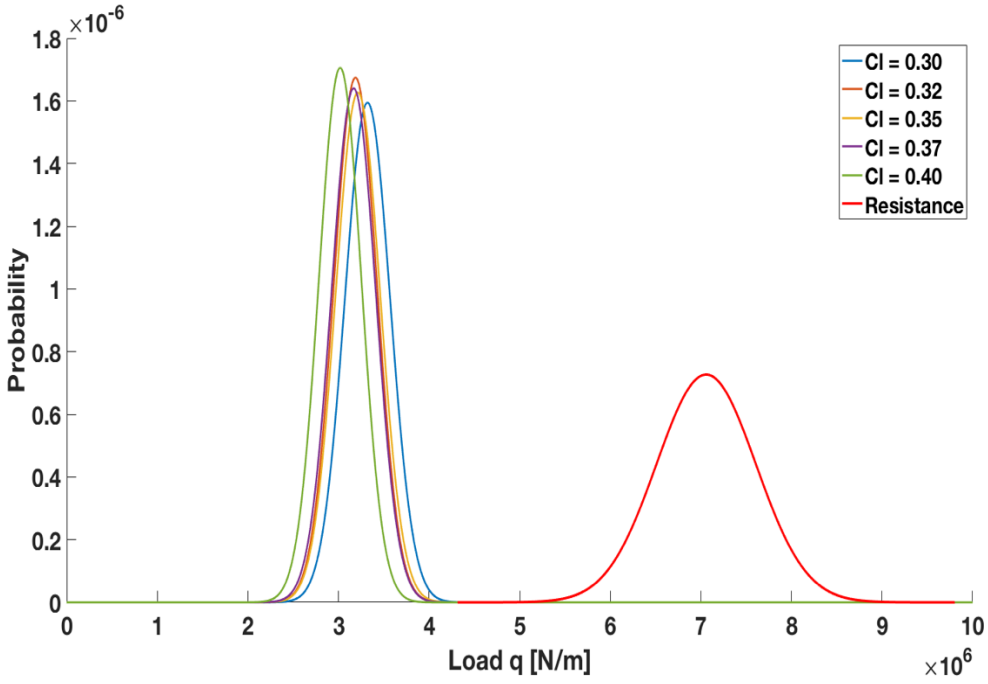

c) C_l values simulation with $C_v = -0.12$

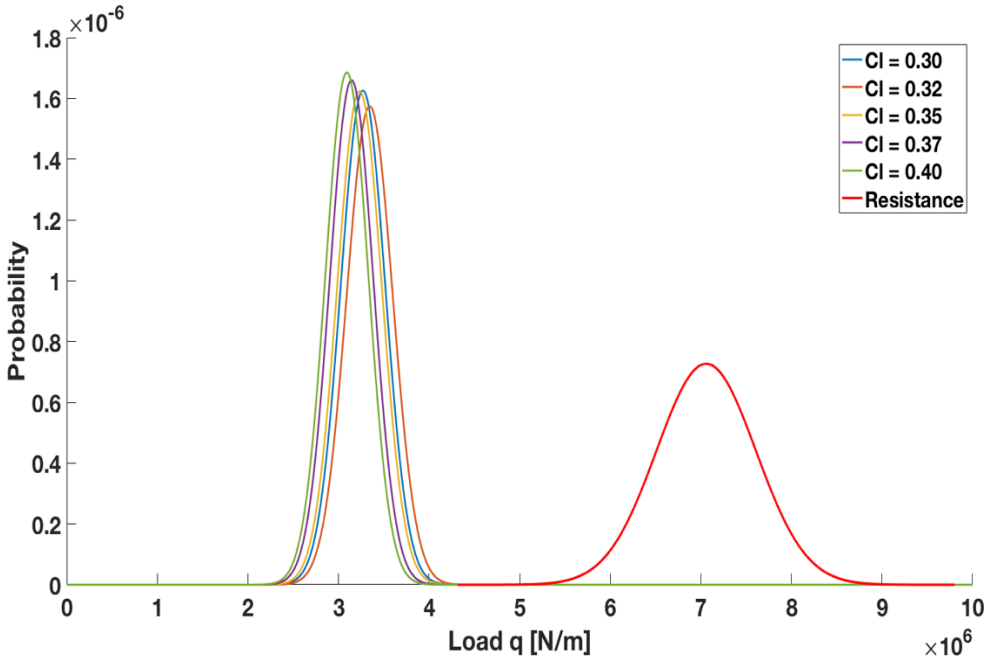

d) C_l values simulation with $C_v = -0.13$

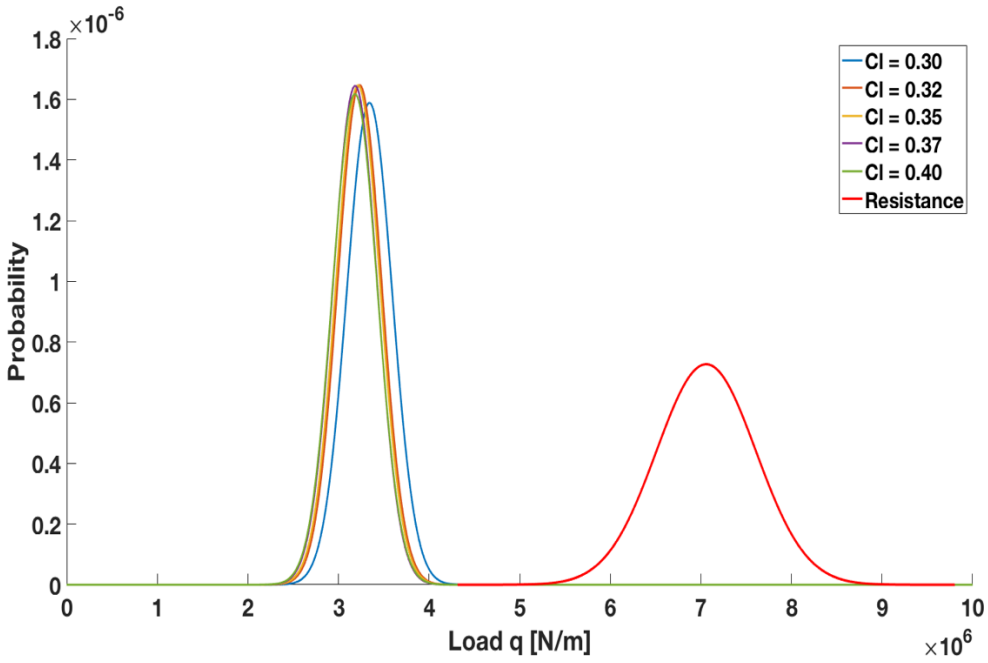

e) C_l values simulation with $C_v = -0.14$

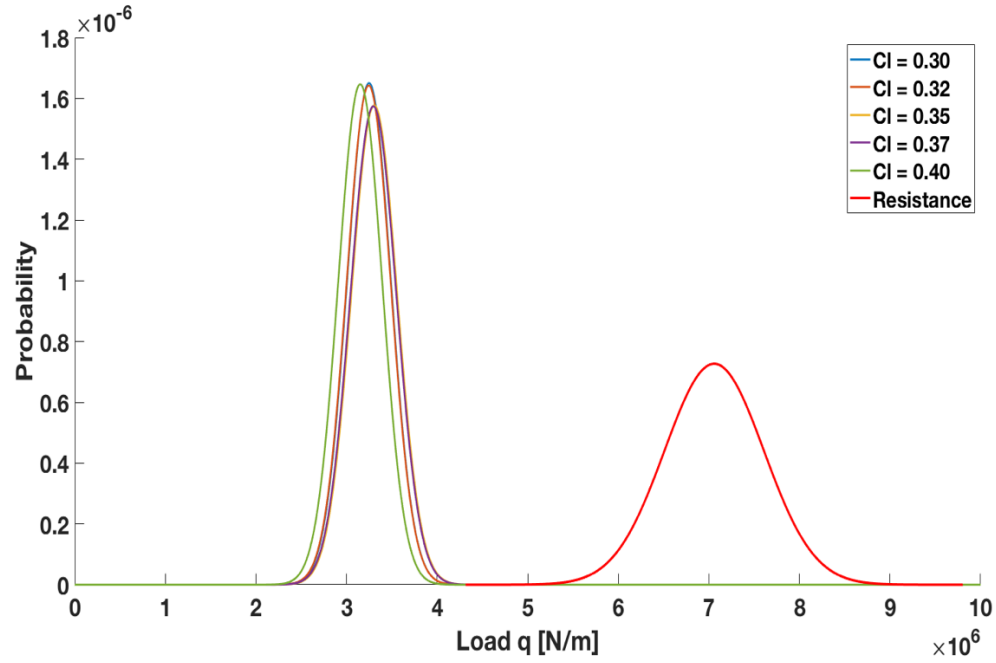

B. Pdf for selected C_v values

a) C_v values simulation with $C_l = 0.30$

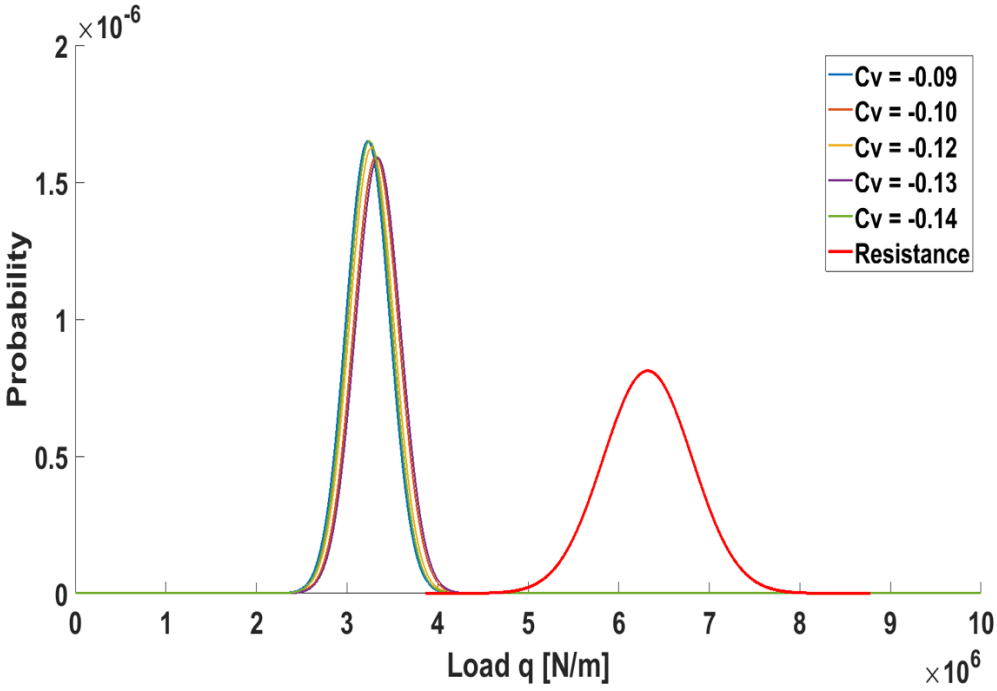

b) C_v values simulation with $C_l = 0.32$

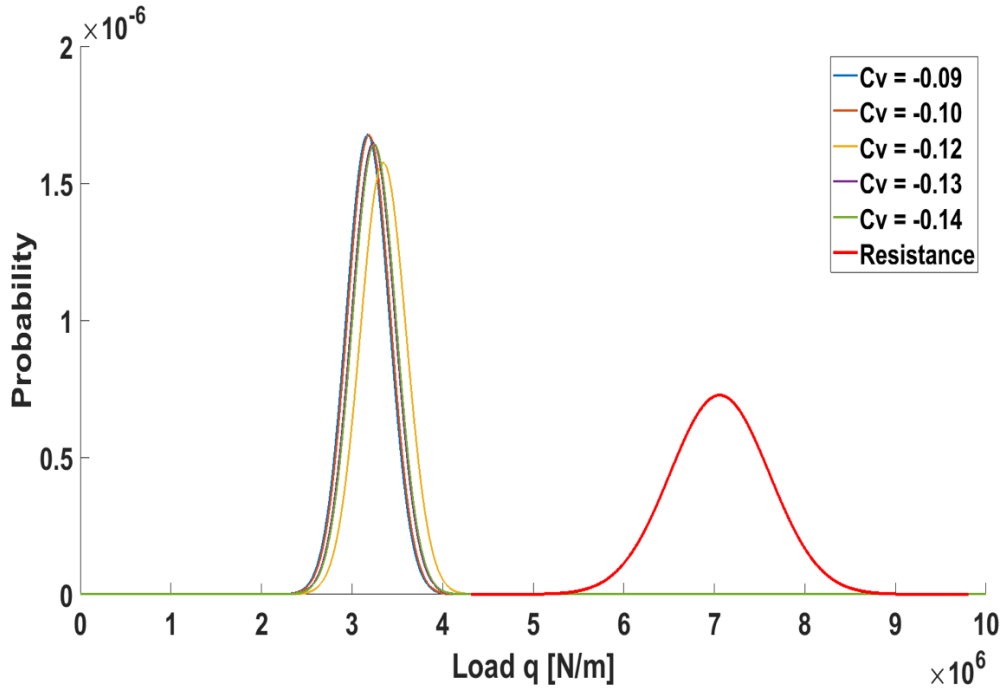

c) C_v values simulation with $C_l = 0.35$

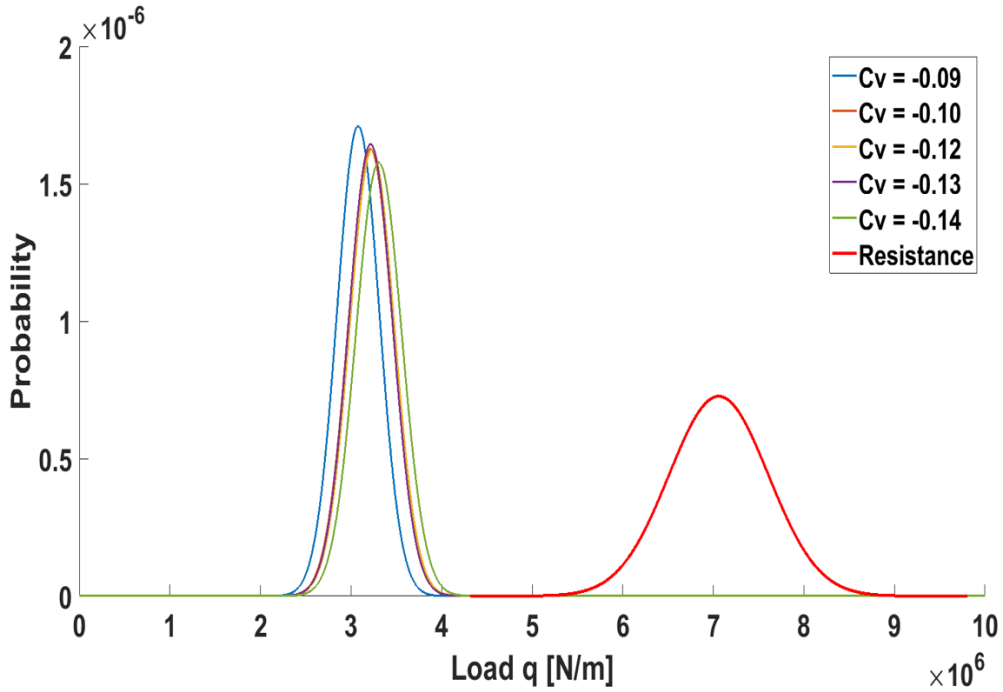

d) C_v values simulation with $C_l = 0.37$

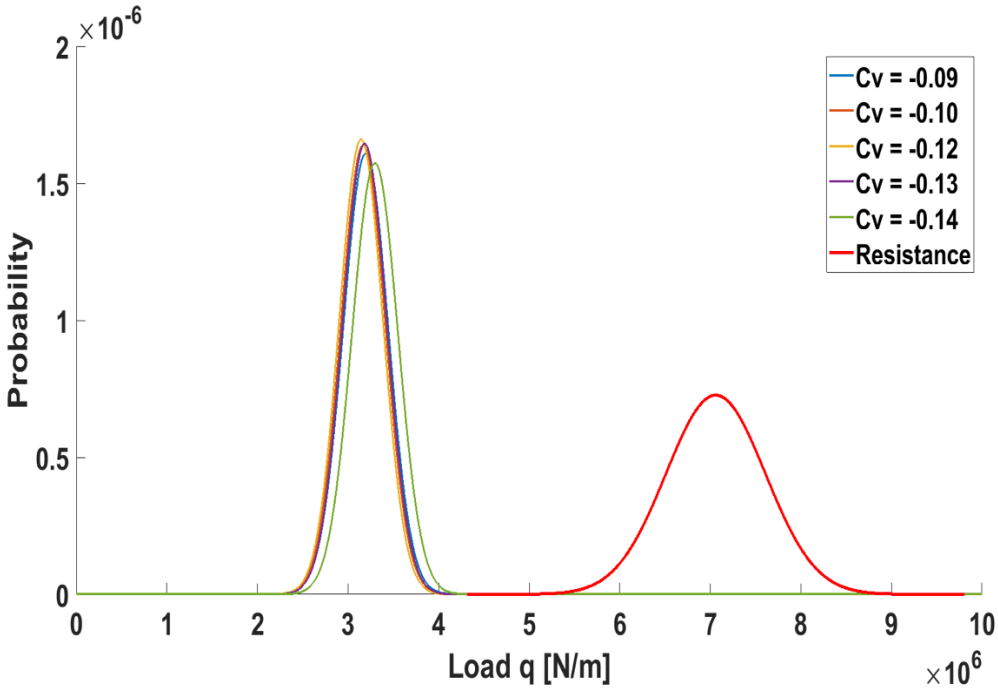

e) C_v values simulation with $C_l = 0.40$

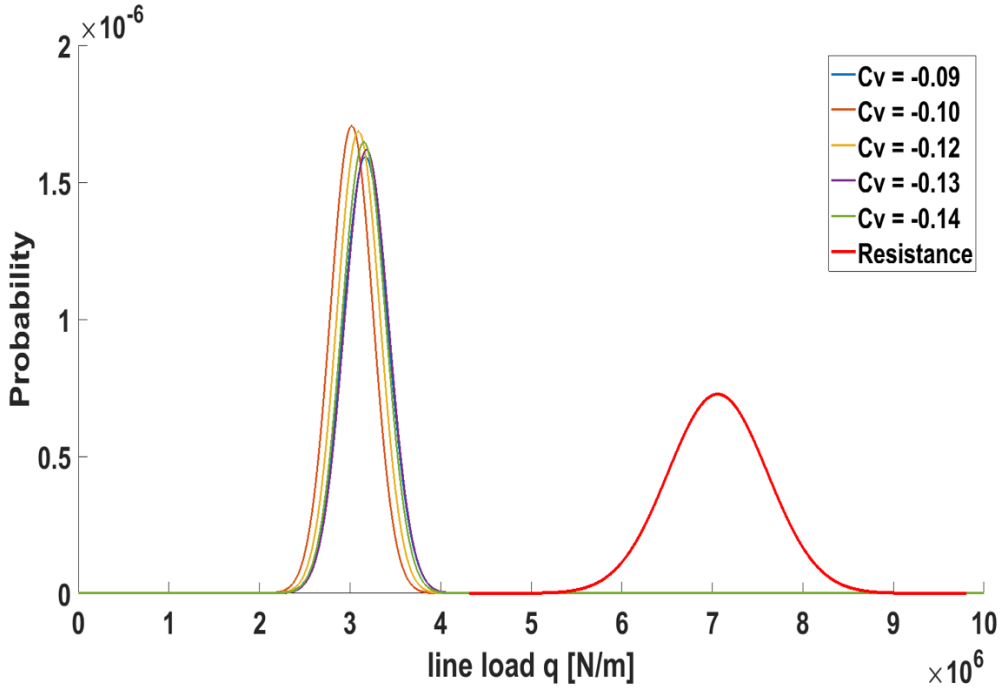

C. Pdf for selected C_f values

a) C_f values simulation at $C_l = 0.30$ & $C_v = -0.10$

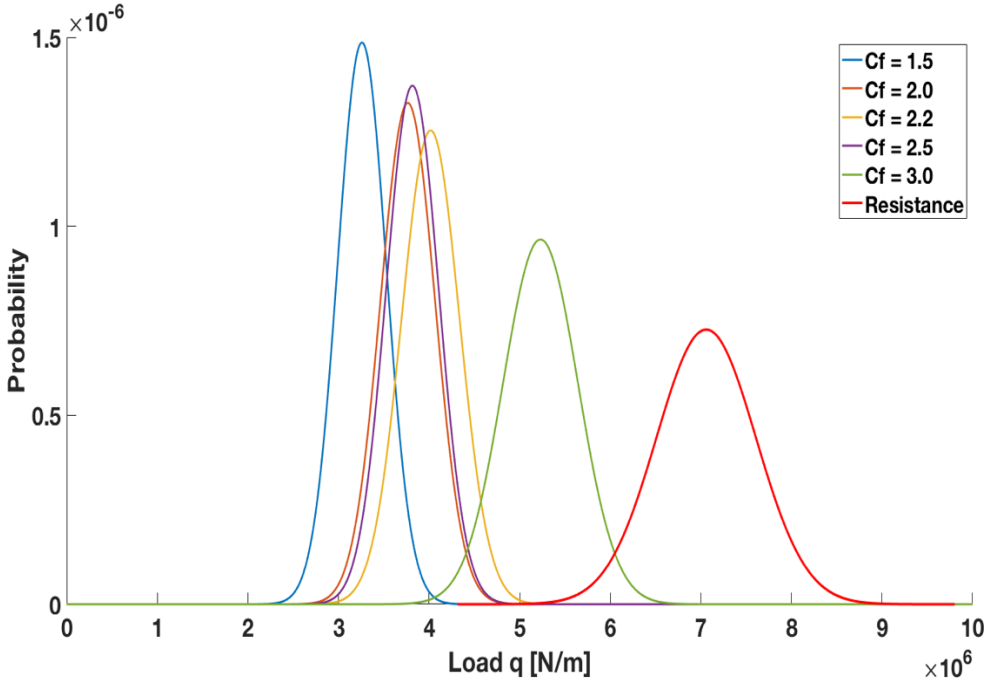

b) C_f values simulation at $C_l = 0.32$ & $C_v = -0.10$

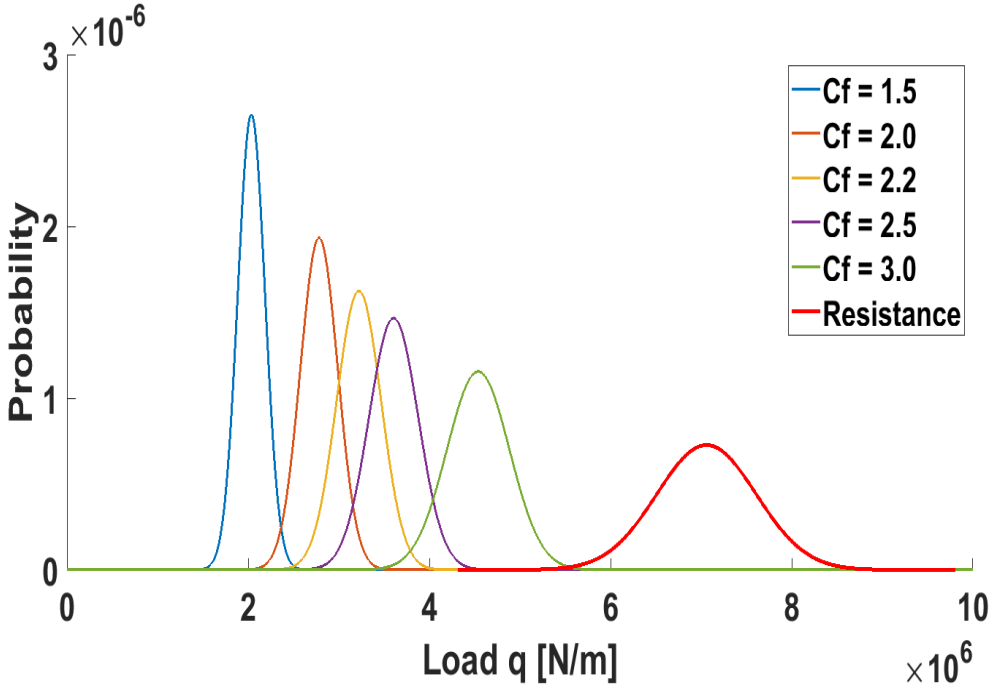

c) C_f values simulation at $C_l = 0.35$ & $C_v = -0.10$

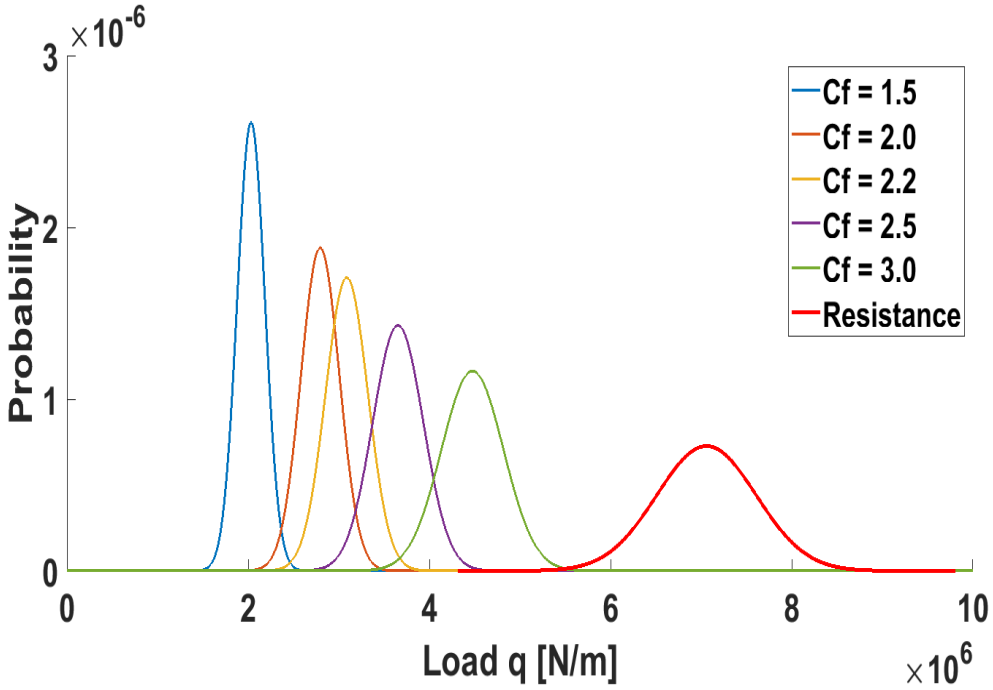

d) C_f values simulation at $C_l = 0.37$ & $C_v = -0.10$

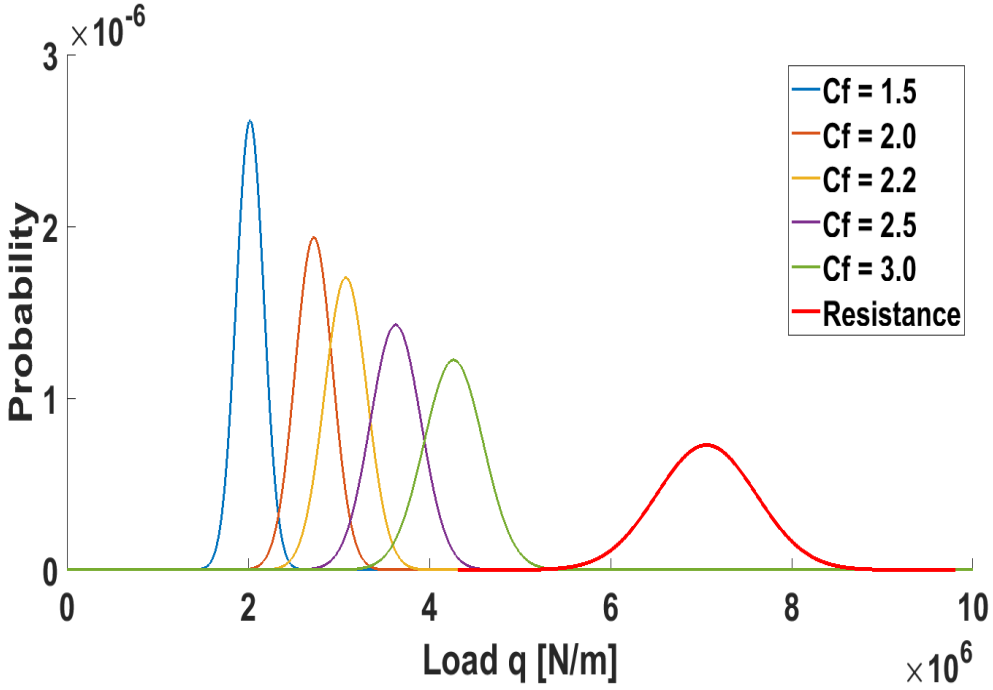

e) C_f values simulation at $C_l = 0.40$ & $C_v = -0.10$

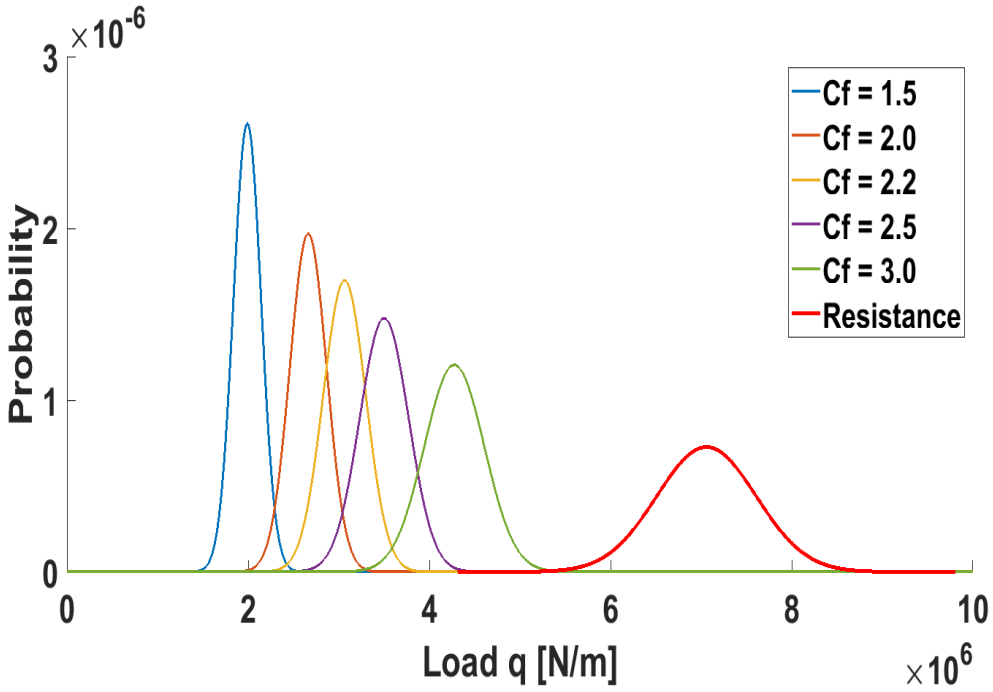

APPENDIX II Probability distributions for reliability and safety analysis of S.A. Agulhas II ship hull model (Bow shoulder)

A. Pdf for selected C_l values

a) Pdf for C_l values when $C_v = -0.09$

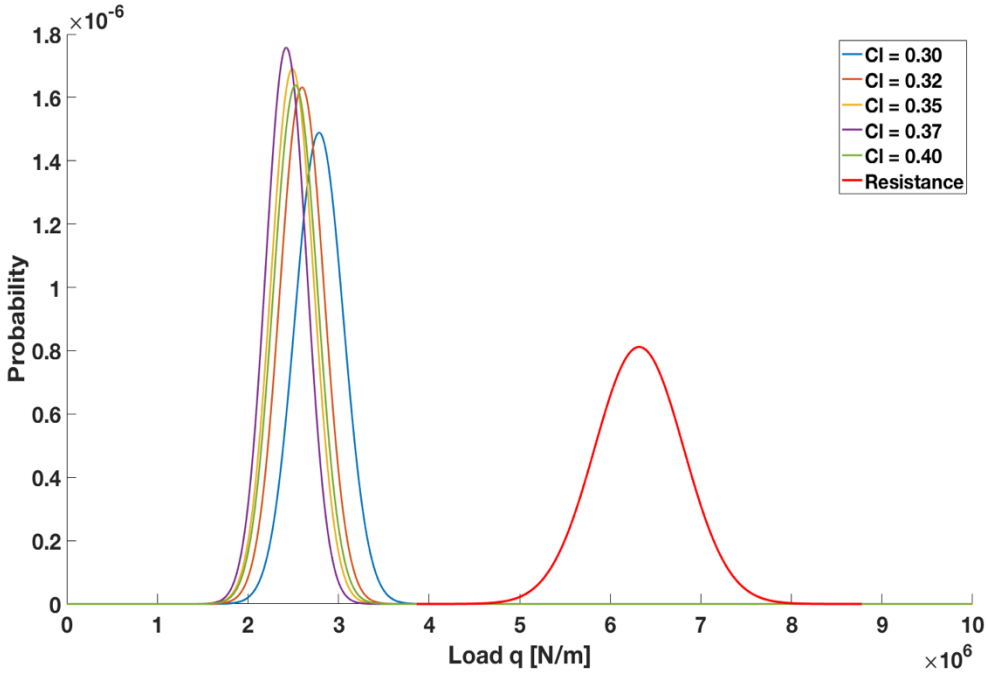

b) Pdf for C_l values when $C_v = -0.10$

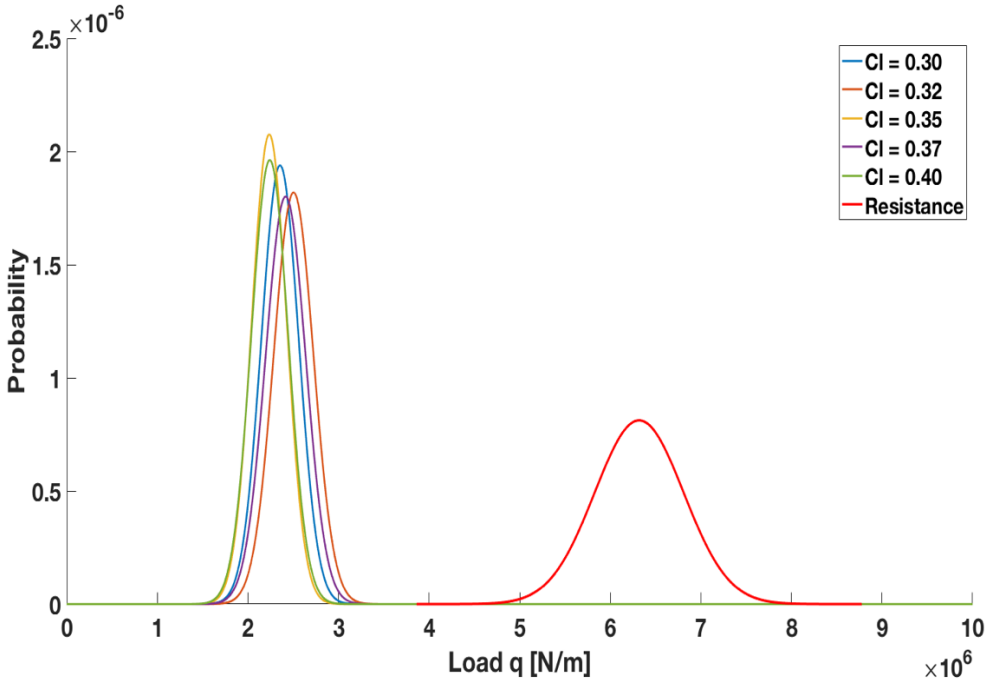

c) **Pdf for C_l values when $C_v = -0.12$**

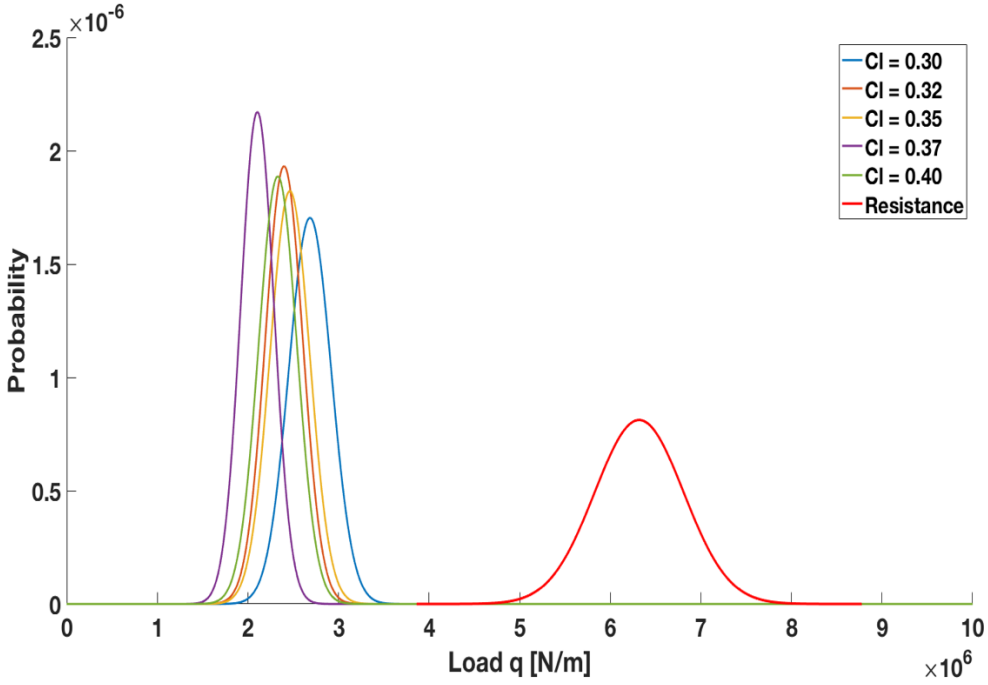

d) **Pdf for C_l values when $C_v = -0.13$**

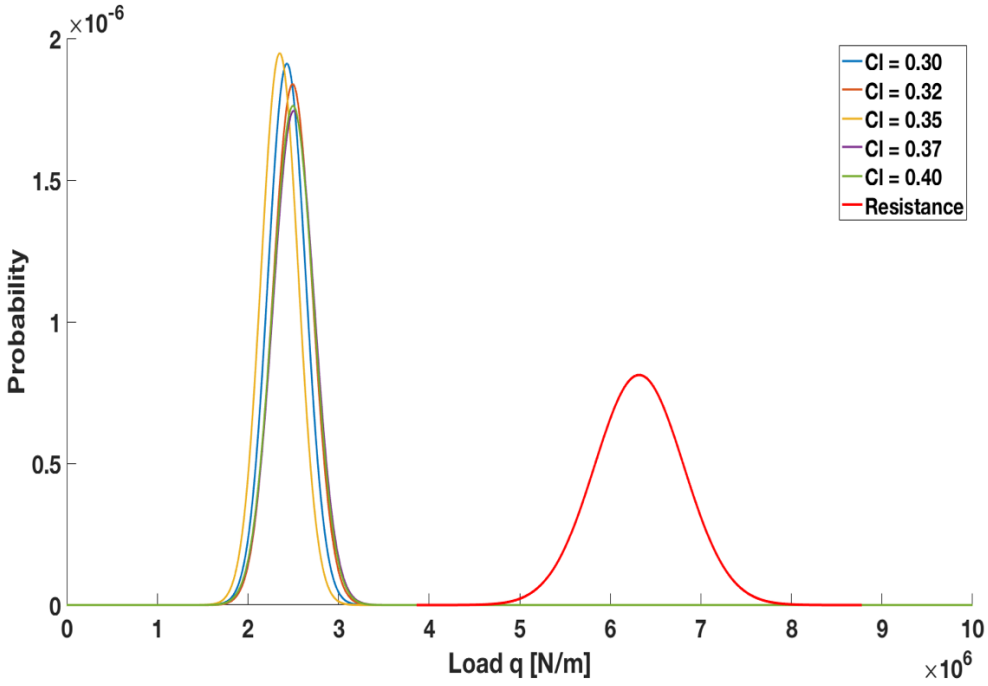

e) Pdf for C_l values when $C_v = -0.14$

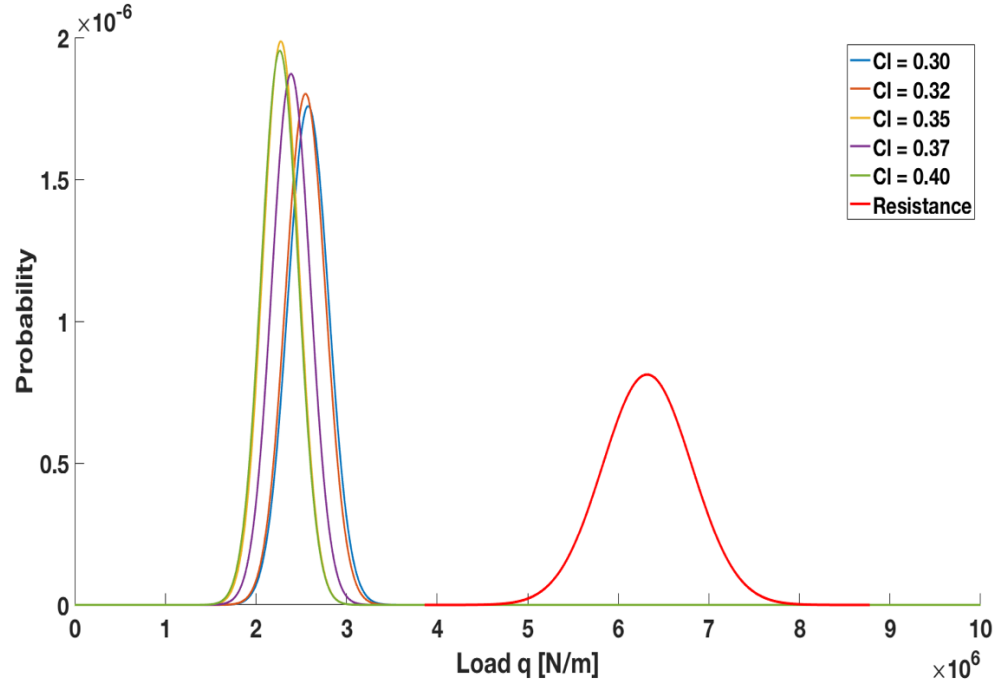

B. Pdf for selected C_v values

a) Pdf for C_v values when $C_l = 0.30$

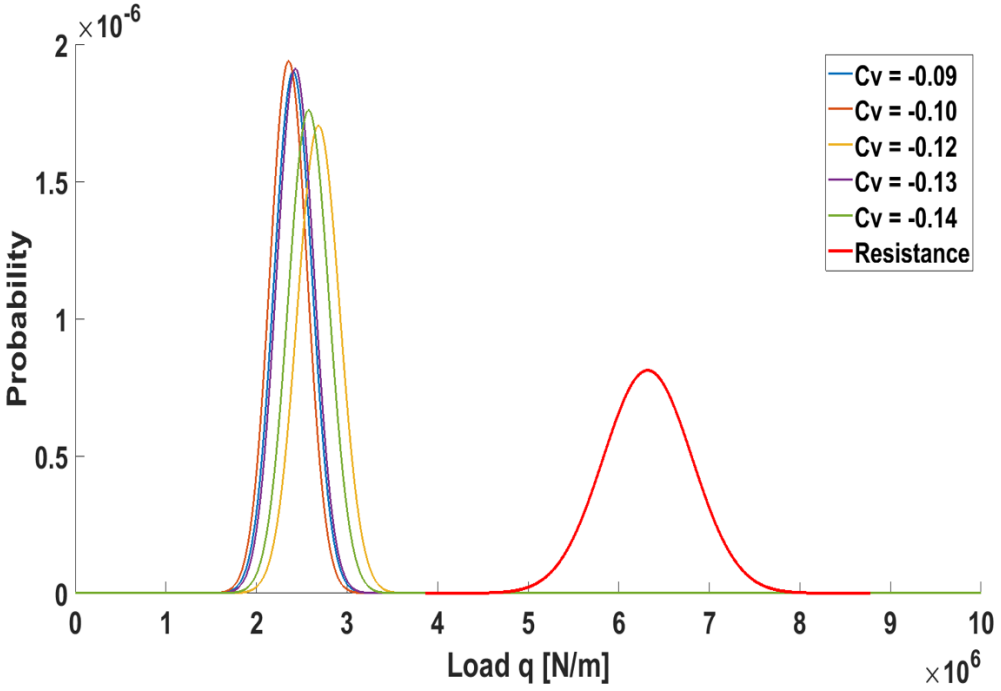

b) Pdf for C_v values when $C_l = 0.32$

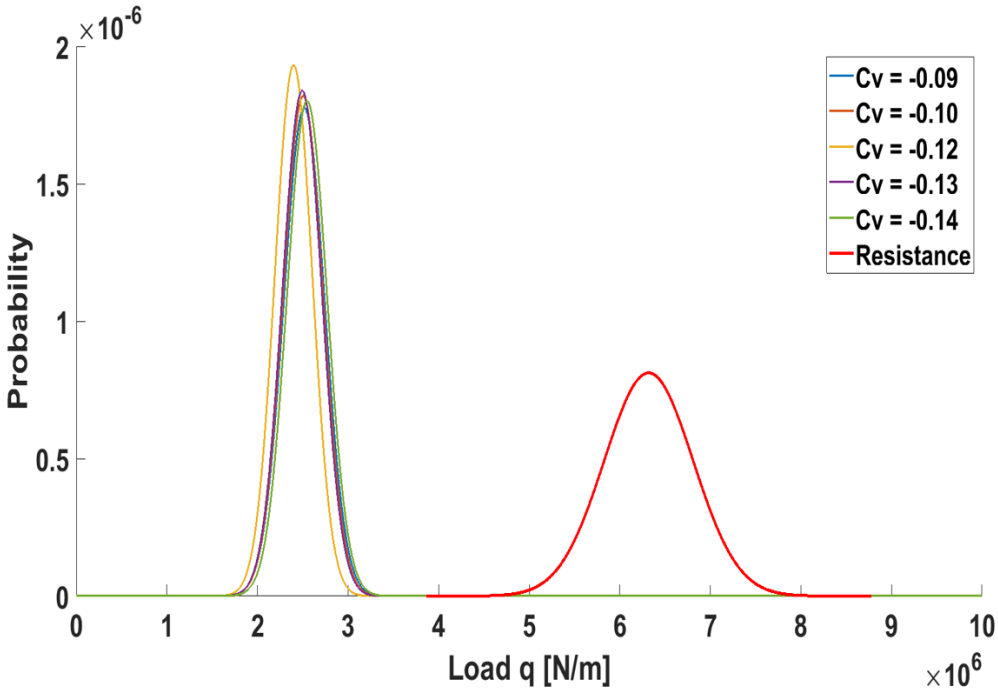

c) Pdf for C_v values when $C_l = 0.35$

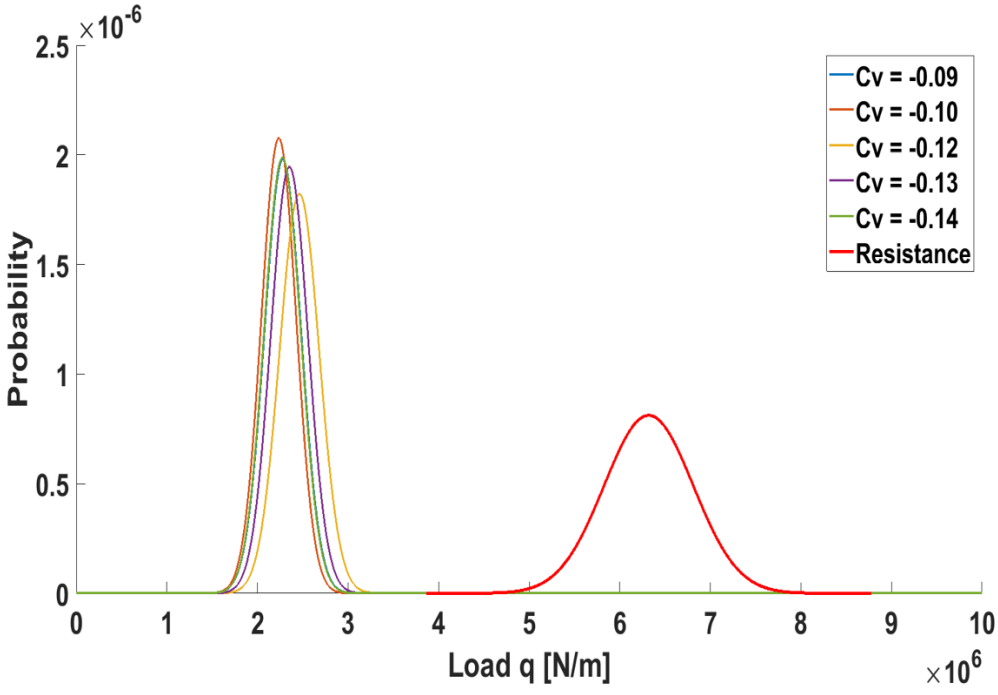

d) Pdf for C_v values when $C_l = 0.37$

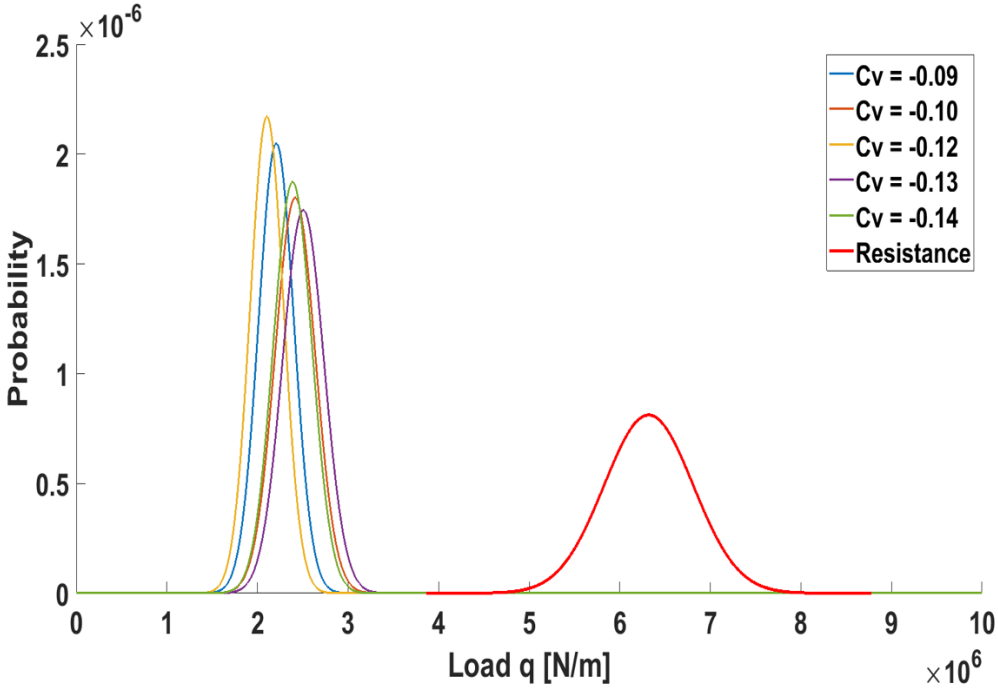

e) Pdf for C_v values when $C_l = 0.40$

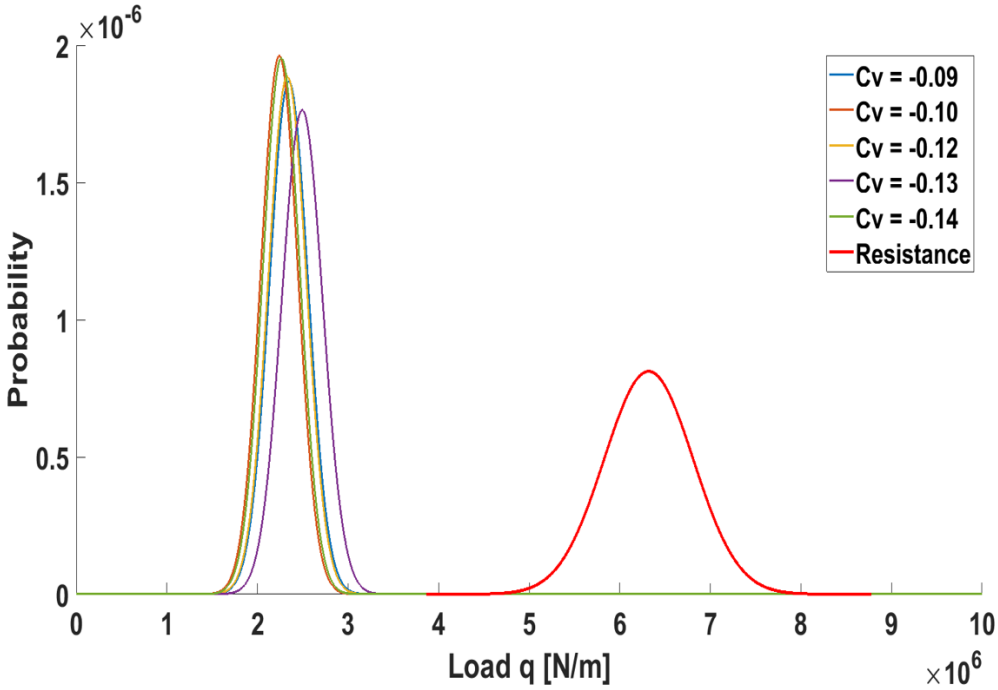

C. Pdf for selected C_f values

a) Pdf for C_f values when $C_l = 0.30$ and C_v = -0.10

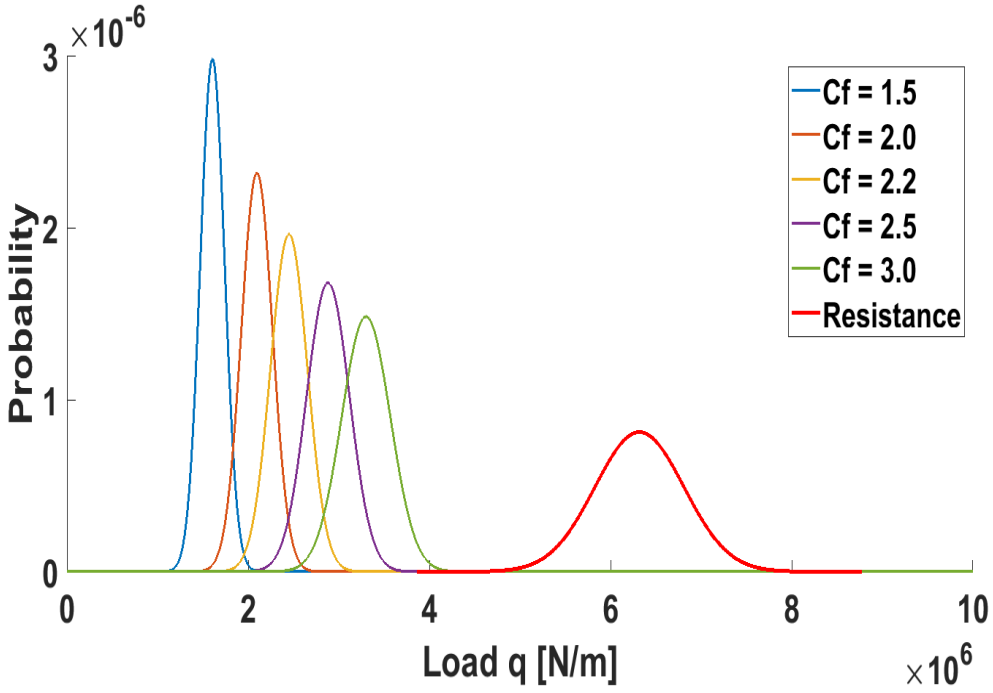

b) Pdf for C_f values when $C_l = 0.32$ and C_v = -0.10

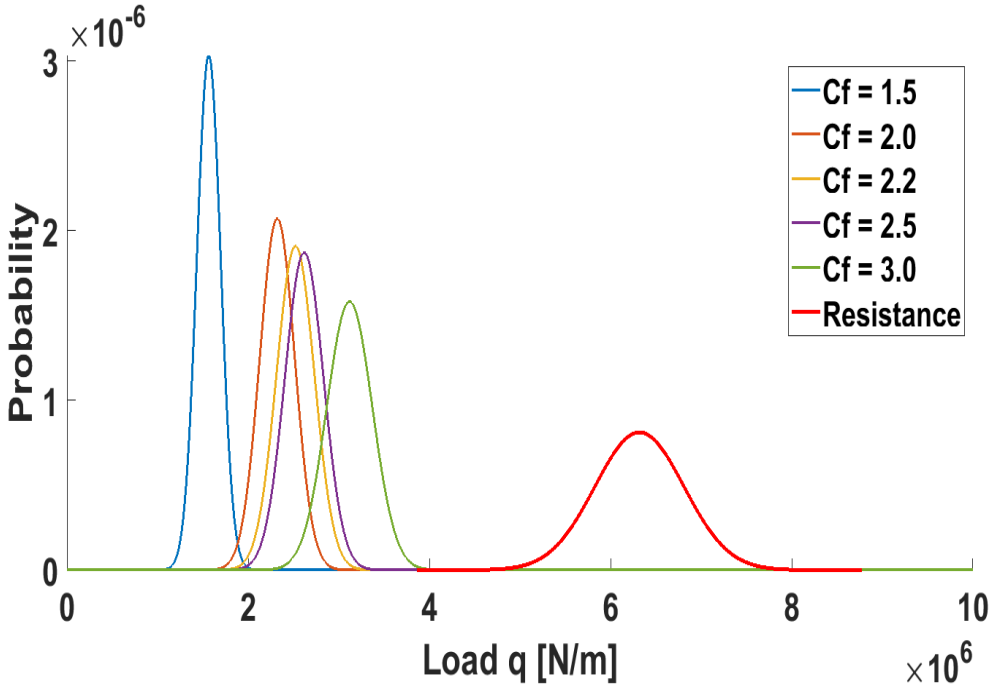

c) Pdf for C_f values when $C_l = 0.35$ and C_v = -0.10

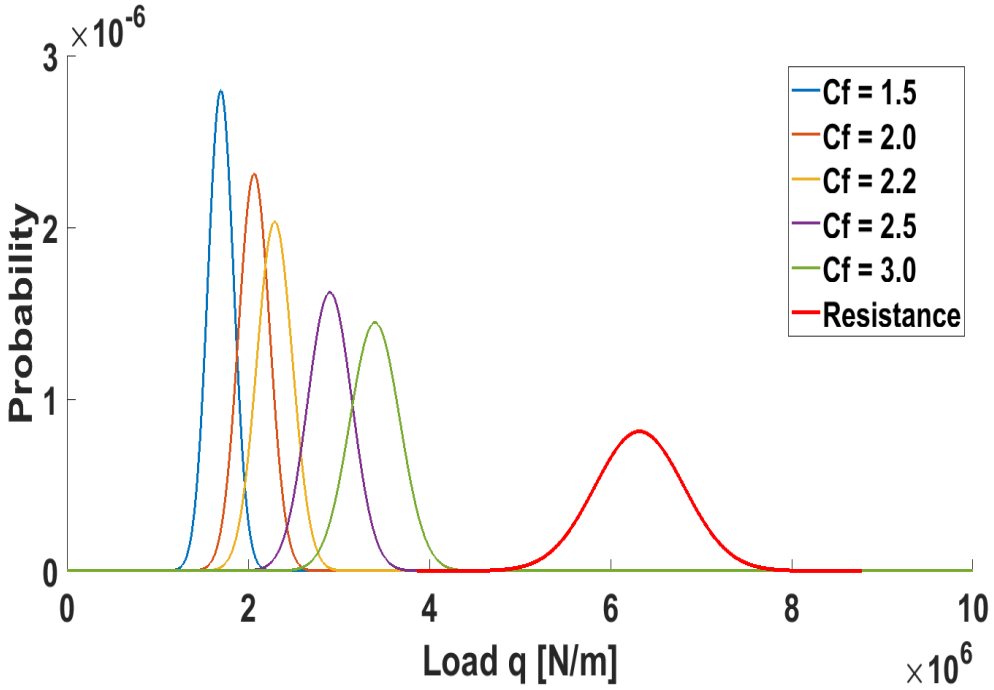

d) Pdf for C_f values when $C_l = 0.37$ and C_v = -0.10

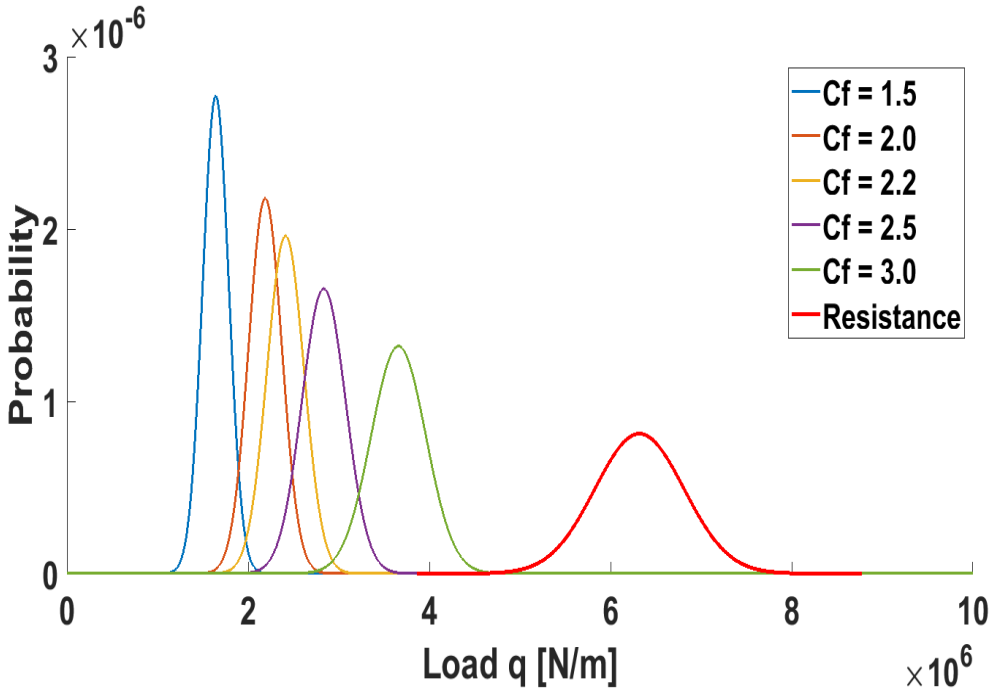

e) Pdf for C_f values when $C_l = 0.40$ and C_v = -0.10

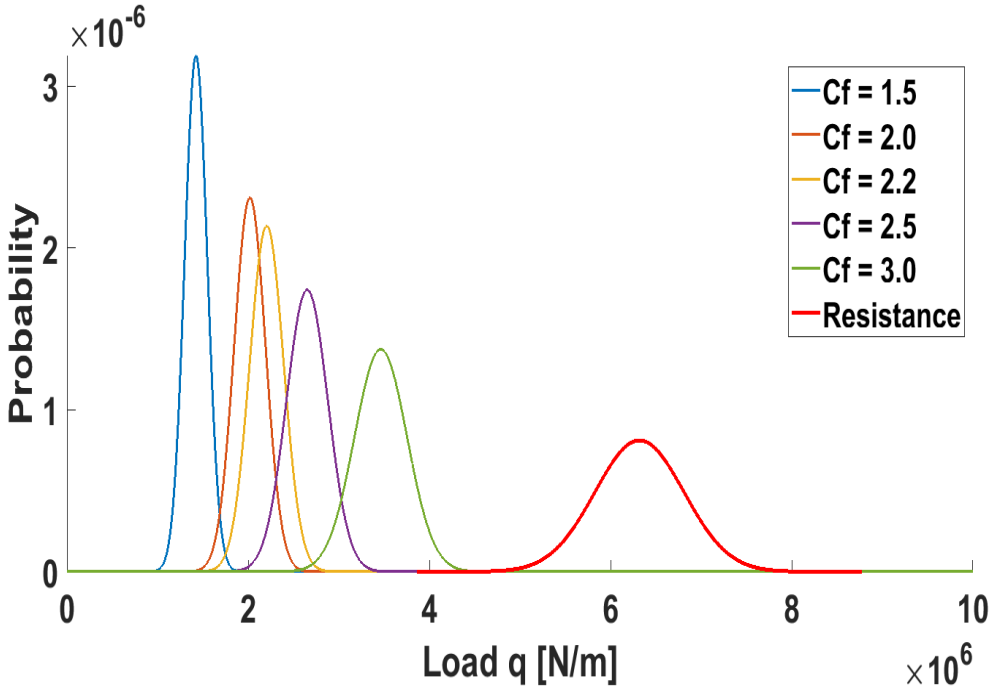

APPENDIX III Observed maximum permanent deflection for transversely framed plating (mm)

Ship no.	Frame spacing	Frame span	Plate thickness	Maximum deflection
4	450	3000	19	20
7	380	3000	16.5	10
13	350	3200	16	20
	700	3200	10	15
14	350	2375	14	15
	700	2375	13	25
16	350	3500	10	25
21	400	2200	19.5	10
	800	2200	19.5	15
	400	2200	13.5	10
	800	2200	13.5	15
35	350	2500	15.5	15
43	400	1750	17	25
44	400	1750	9.5	30
51	350	2100	15.5	15

APPENDIX IV Locations of strain gauges on board S.A. Agulhas II ship